



FACULTY OF ENGINEERING AND SURVEYING

# **Flexural Behaviour of Sandwich Panels under Elevated Temperature**

A dissertation submission by

**Swetha Surendar**

In fulfilment of the requirements of

**Courses ENG 8411 and 8412 Research Project**

Towards the degree of

**Master of Engineering Sciences – Structural Engineering**

Submitted on: 30<sup>th</sup> October 2014

## Abstract

The objective of this work was to experimentally determine the flexural behaviour of composite sandwich panels under elevated temperatures from 21°C to 180°C. The new generation sandwich beams were fabricated using top and bottom skins made of two plies of bi-axial glass fibre/resin and an innovative phenol-formaldehyde core. The composite sandwich beams and the skins were subjected to flexure test under 3-point static bending test to determine the strength and the stiffness. The elevated temperature effects were applied using an environment chamber. The peak load, strength and the Young's modulus of each specimen under each temperature was recorded. Prior to this, the skin and the core materials were also subjected to Dynamic Mechanical Analysis (DMA) in order to determine the material properties at elevated temperatures.

The glass transition temperatures of the skin and the core were obtained through the DMA as 125.06°C and 136.11°C respectively. A rapid loss in the storage modulus was observed in the core specimens as the temperature increased and the specimens began to decompose beyond the glass transition temperature. The testing of the skin specimens revealed that the storage modulus decreases steadily with the increase in temperature until the glass transition temperature and beyond the transition temperature the storage modulus begins to increase.

The flexure test of the skin revealed that the Young's modulus of the specimens decrease steadily with the increase in the temperature before increasing beyond 120°C. The strength of the skin decreases rapidly until 120°C and shows a slight increase in strength beyond this temperature. The flexure test of the sandwich panels revealed that the Young's modulus of the sandwich panels decreases steadily as the temperature increases. The strength of the sandwich panels was found to increase with the increase in temperature until 50°C and starts to decrease beyond this temperature before showing a slight increase in the flexural strength at 180°C.

A theoretical equation was developed which predicted the behaviour of the sandwich panels under elevated temperature. The theoretical equation revealed that the Young's Modulus of the sandwich panel predicted through the theoretical equation correlated well with the experimental values until 100°C. From 120°C, the experimental values were lower than the values obtained from the prediction equation due to the partial loss in the composite action of the sandwich panel.

**University of Southern Queensland**

**Faculty of Health, Engineering and Science**

**ENG8411/ENG8412 Masters Dissertation Project**

## **Limitations of Use**

The Council of the University of Southern Queensland, its Faculty of Health, Engineering and Science, and the staff of the University of Southern Queensland, do not accept any responsibility for the truth, accuracy or completeness of material contained within or associated with this dissertation.

Persons using all or any part of this material do so at their own risk, and not at the risk of the Council of the University of Southern Queensland, its Faculty of Health, Engineering and Science or the staff of the University of Southern Queensland.

This dissertation reports an educational exercise and has no purpose or validity beyond this exercise. The sole purpose of this dissertation project is to contribute to the overall education within the student's chosen degree program. This document, the associated hardware, software, drawings, and other material set out in the associated appendices should not be used for any other purpose: if they are so used, it is entirely at the risk of the user.

**Professor Frank Bullen**

Dean

Faculty of Engineering and Surveying

# Certification

I certify that the ideas, designs and experimental work, results, analyses and conclusions set out in this dissertation are entirely my own effort, except where otherwise indicated and acknowledged.

I further certify that the work is original and has not been previously submitted for assessment in any other course or institution, except where specifically stated.

**Student Name:** SwethaSurendar

**Student Number:** 0061044210

---

Signature

---

Date

## **Acknowledgements**

I would like to take this opportunity thank my supervisor Dr. Allan Manalo for his guidance and support throughout this project. I also wish to extend my thanks to the Centre for Excellence in Engineered Fibre Composites (CEEFC) and the University of Southern Queensland for sponsoring my project. I would also like to thank LOC Composites, Pty Ltd for providing the necessary equipment and testing materials for this project.

Finally I would like to thank my parents and my husband Mr. Prasad Pendlimarry for their patience and support throughout this endeavour.

# Table of Contents

|                                      |      |
|--------------------------------------|------|
| <b>Abstract</b>                      | i    |
| <b>Limitations of Use</b>            | ii   |
| <b>Certification</b>                 | iii  |
| <b>Acknowledgements</b>              | iv   |
| <b>List of Figures</b>               | xi   |
| <b>List of Tables</b>                | xvi  |
| <b>Glossary of Terms</b>             | xvii |
| <b>Chapter 1 – Introduction</b>      | 1    |
| 1.1. Introduction                    | 1    |
| 1.2. Project Background              | 2    |
| 1.3. Research Aims                   | 2    |
| 1.4. Justification                   | 3    |
| 1.5. Scope                           | 3    |
| 1.6. Summary                         | 4    |
| <b>Chapter 2 – Literature Review</b> | 5    |
| 2.1. Introduction                    | 5    |

|   |           |
|---|-----------|
| 2.2. History of Composites                                  | 5         |
| 2.2.1. Types of Fibres                                      | 5         |
| 2.2.2. Types of Resins                                      | 6         |
| 2.3. Limitations of the Composites                          | 7         |
| 2.4. Background on Sandwich Panels                          | 7         |
| 2.4.1. Background on Skin                                   | 8         |
| 2.4.2. Background on Core                                   | 9         |
| 2.4.3. Structural Applications of the Sandwich Panels       | 10        |
| 2.5. Behaviour of Sandwich Panels under Ambient Temperature | 11        |
| 2.6. Effect of Elevated Temperature on Composites           | 14        |
| 2.7. Effect of Elevated Temperature on Sandwich Panels      | 16        |
| 2.8. Research Gaps from Previous Works                      | 17        |
| 2.9. Summary  | 17        |
| <b>Chapter 3 – Project Methodology</b>                      | <b>18</b> |
| 3.1. Introduction   | 18        |
| 3.2. Materials  | 18        |
| 3.3. Test Specimen  | 19        |

|   |           |
|---|-----------|
| 3.4. Specimen Preparation                   | 20        |
| 3.5. Experimental Procedure                 | 20        |
| 3.5.1. Dynamic Mechanical Analysis (DMA)    | 20        |
| 3.5.2. Flexure Test                         | 21        |
| 3.6. Summary                                | 23        |
| <b>Chapter 4 – Results and Observation</b>  | <b>24</b> |
| 4.1. Introduction                           | 24        |
| 4.2. Dynamic Mechanical Analysis            | 24        |
| 4.2.1. Skin                                 | 25        |
| 4.2.2. Core                                 | 27        |
| 4.3. Behaviour of the Skin                  | 28        |
| 4.3.1. Load – Deflection Relation           | 28        |
| 4.4. Failure Modes of the Skin              | 37        |
| 4.4.1. Failure Mode at 21°C                 | 37        |
| 4.4.2. Failure Mode at 35°C                 | 39        |
| 4.4.3. Failure Modes at 50°C, 65°C and 80°C | 40        |
| 4.4.4. Failure Modes at 100°C and 120°C     | 43        |



|   |    |
|---|----|
| 4.4.5. Failure Modes at 150°C and 180°C   | 45 |
| 4.5. Behaviour of the Sandwich Panel  | 47 |
| 4.5.1. Load – Deflection Relation   | 47 |
| 4.6. Failure Modes of the Sandwich Panels   | 55 |
| 4.6.1. Failure Modes at 21°C and 35°C   | 55 |
| 4.6.2. Failure Modes at 50°C, 65°C and 80°C   | 56 |
| 4.6.3. Failure Modes at 100°C and 120°C   | 58 |
| 4.6.4. Failure Modes at 150°C and 180°C   | 60 |
| 4.7. Summary  | 62 |
| <b>Chapter 5 – Discussion</b>   | 63 |
| 5.1. Mechanical Properties of the Skin and the Core under Dynamic Mechanical Analysis (DMA) | 63 |
| 5.2. Load – Displacement Diagram of the Skin under Three Point Bending Test                 | 65 |
| 5.3. Load – Displacement Diagram of the Sandwich Panel under Three Point Bending Test       | 67 |
| 5.4. Effect of Elevated Temperature on the Strength of the Skin                             | 68 |
| 5.5. Effect of Elevated Temperature on the Modulus of the Skin                              | 69 |
| 5.6. Effect of Elevated Temperature on the Strength of the                                  | 70 |

|  |           |
|--|-----------|
| Sandwich Panel   |           |
| 5.7. Effect of Elevated Temperature on the Modulus of the Sandwich Panel                                 | 71        |
| 5.8. Summary   | 72        |
| <b>Chapter 6 – Theoretical Prediction of the Composite Sandwich Behaviour under Elevated Temperature</b> | <b>74</b> |
| 6.1. Introduction  | 74        |
| 6.2. Assumptions made for the Theoretical Prediction Equation  | 74        |
| 6.3. Prediction of the Strength and the Modulus of the Skin and the Core of the Sandwich Panel           | 74        |
| 6.3.1. Prediction Equation for the Flexural Modulus of the Skin  | 75        |
| 6.3.2. Prediction Equation for the Flexural Strength of the Skin   | 76        |
| 6.3.3. Prediction Equation for the Flexural Strength and the Flexural Modulus of the Core                | 77        |
| 6.4. Empirical Equations   | 78        |
| 6.4.1. Prediction of the Theoretical Young's Modulus (E <sub>sw</sub> )                                  | 78        |
| 6.4.2. Prediction of the Strength of the Skin and the Core   | 80        |

|   |     |
|---|-----|
| 6.5. Comparison of the Results  | 81  |
| 6.5.1. Comparison of the Theoretical Modulus with the<br>Experimental Modulus   | 82  |
| 6.5.2. Comparison of the Theoretical Strength of the Skin<br>and the Core of the Sandwich Panel with the Experimental<br>Strength | 83  |
| 6.6. Summary  | 85  |
| <b>Chapter 7 – Conclusion and Recommendation</b>  | 86  |
| 7.1. Conclusion   | 86  |
| 7.2. Recommendations for Future Work  | 89  |
| <b>References</b>   | 90  |
| <b>Appendix A - Project Specification</b>   | 94  |
| <b>Appendix B</b>   | 95  |
| <b>Appendix C</b>   | 102 |

## List of figures

|  |    |
|--|----|
| Figure 1.1. Composite fibre bridge in Tasmania, Australia  | 1  |
| Figure 2.1. Illustration explaining sandwich panel concept | 8  |
| Figure 2.2. Fibre Composite Laminate                       | 9  |
| Figure 2.3. Honeycomb and Foam cores                       | 9  |
| Figure 2.4. Structural Applications of Sandwich Panels     | 11 |
| Figure 3.1. Carbon LOC <sup>®</sup> Panels                 | 19 |
| Figure 3.2. DMA Testing Equipment                          | 21 |
| Figure 3.3. DMA Test Set-Up                                | 21 |
| Figure 3.4. Schematic Diagram of Three Point Bending Test  | 22 |
| Figure 3.5. Flexure Test Equipment                         | 22 |
| Figure 3.6. Flexure Test Set-Up                            | 23 |
| Figure 4.1. DMA Result of the Skin                         | 25 |
| Figure 4.2. DMA results of the Core                        | 27 |
| Figure 4.3. Load – Deflection diagram for the skin at 21°C | 28 |
| Figure 4.4. Load – Deflection diagram for the skin at 35°C | 29 |
| Figure 4.5. Load – Deflection diagram for the skin at 50°C | 30 |

|  |    |
|--|----|
| Figure 4.6. Load – Deflection Diagram for the skin at 65°C           | 31 |
| Figure 4.7. Load – Deflection Diagram for the skin at 80°C           | 32 |
| Figure 4.8. Load – Deflection Diagram for the skin at 100°C          | 33 |
| Figure 4.9. Load – Deflection Diagram for the skin at 120°C          | 34 |
| Figure 4.10. Load – Deflection Diagram for the skin at 150°C         | 35 |
| Figure 4.11. Load – Deflection Diagram for the skin at 180°C         | 36 |
| Figure 4.12. Failure of the specimen at 21°C                         | 37 |
| Figure 4.13. Cracks on the compression side of the specimens at 21°C | 38 |
| Figure 4.14. Failure of the specimen at 35°C                         | 39 |
| Figure 4.15. Cracks on the tension side of the skin at 35°C          | 39 |
| Figure 4.16. Failure of the specimen at 50°C                         | 40 |
| Figure 4.17. Compression and tension cracks on the specimen at 50°C  | 40 |
| Figure 4.18. Failure of the specimen at 65°C                         | 41 |
| Figure 4.19. Compression and tension cracks on the specimen at 65°C  | 41 |
| Figure 4.20. Failure of the specimen at 80°C                         | 42 |
| Figure 4.21. Compression and tension cracks on the specimen at 80°C  | 42 |
| Figure 4.22. Failure of the specimen at 100°C                        | 43 |

|  |    |
|--|----|
| Figure 4.23. Compression and tension cracks on the specimen at 100°C   | 43 |
| Figure 4.24. Failure of the specimen at 120°C                          | 44 |
| Figure 4.25. Compression and tension cracks on the specimen at 120°C   | 44 |
| Figure 4.26. Compression cracks on the specimen at 150°C               | 45 |
| Figure 4.27. Failure of the specimen at 180°C                          | 45 |
| Figure 4.28. Failure on the compression side of the specimen at 180°C  | 46 |
| Figure 4.29. Load – Deflection diagram for the sandwich panel at 21°C  | 47 |
| Figure 4.30. Load – Deflection diagram for the sandwich panel at 35°C  | 48 |
| Figure 4.31. Load – Deflection diagram for the sandwich panel at 50°C  | 48 |
| Figure 4.32. Load – Deflection diagram for the sandwich panel at 65°C  | 49 |
| Figure 4.33. Load – Deflection diagram for the sandwich panel at 80°C  | 50 |
| Figure 4.34. Load – Deflection diagram for the sandwich panel at 100°C | 51 |
| Figure 4.35. Load – Deflection diagram for the sandwich panel at 120°C | 52 |
| Figure 4.36. Load – Deflection diagram for the sandwich panel at 150°C | 53 |
| Figure 4.37. Load – Deflection diagram for the sandwich panel at 180°C | 54 |
| Figure 4.38. Failure modes at 21°C and 35°C                            | 55 |
| Figure 4.39. Delamination failures at 21°C and 35°C                    | 55 |

|   |    |
|---|----|
| Figure 4.40. Failure modes at 50°C and 65°C   | 56 |
| Figure 4.41. Delamination failures at 50°C and 65°C                                     | 56 |
| Figure 4.42. Failure mode of the specimen at 80°C                                       | 57 |
| Figure 4.43. Delamination of the plies at 80°C  | 57 |
| Figure 4.44. Failure mode of the specimen at 100°C                                      | 58 |
| Figure 4.45 Failure mode of the specimen at 120°C                                       | 59 |
| Figure 4.46. Delamination of the core at 100°C and 120°C                                | 59 |
| Figure 4.47. Failure of the specimen at 150°C   | 60 |
| Figure 4.48. Failure of the specimen at 180°C   | 61 |
| Figure 4.49. Delamination of the core at 150°C and 180°C                                | 61 |
| Figure 5.1. Skin specimens before and after the DMA                                     | 64 |
| Figure 5.2. DMA result of the skin  | 64 |
| Figure 5.3. Load – Displacement Diagram of the skin specimens at different temperatures | 65 |
| Figure 5.4. Load – Deflection diagram of the sandwich panel at different temperatures   | 67 |
| Figure 5.5. Strength Vs Temperature of the skin   | 68 |
| Figure 5.6. Modulus Vs Temperature of the Skin  | 69 |

|  |    |
|--|----|
| Figure 5.7. Strength Vs Temperature of the sandwich panel                                | 70 |
| Figure 5.8. Modulus Vs Temperature of the sandwich panel                                 | 71 |
| Figure 6.1 Prediction Equation for the modulus of the skin                               | 75 |
| Figure 6.2. Prediction Equation for the strength of the skin                             | 76 |
| Figure 6.3. Prediction equation for the modulus of the core                              | 77 |
| Figure 6.4. Prediction equation for the strength of the core                             | 77 |
| Figure 6.5. Normalised data of the skin  | 79 |
| Figure 6.6. Dimensions of the sandwich panel   | 80 |
| Figure 6.7. Comparison of the theoretical and experimental modulus of the skin           | 82 |
| Figure 6.8. Comparison of the theoretical strength and experimental strength of the skin | 83 |
| Figure 6.9. Comparison of the theoretical and experimental Strengths of the core         | 84 |



## List of Tables

|  |    |
|--|----|
| Table 3.1 Test Specimen Dimensions       | 19 |
| Table 3.2. Dimensions of the DMA samples | 20 |

## Glossary of Terms

|            |   |
|------------|---|
| T          | Temperature in °C                       |
| S          | Storage Modulus in MPa                  |
| P          | Peak Load in N                          |
| $\epsilon$ | Peak Strain                             |
| $\Delta$   | Deflection in mm                        |
| I          | Inertia in mm <sup>4</sup>              |
| M          | Moment of inertia in KNm                |
| L          | Length in mm                            |
| $\sigma_s$ | Flexural Strength of the skin           |
| $\sigma_c$ | Flexural Strength of the Core           |
| $E_s$      | Young's modulus of the Skin             |
| $E_c$      | Young's modulus of the Core             |
| $E_{sw}$   | Young's modulus of the Sandwich Panel   |
| $I_s$      | Moment of Inertia of the Skin           |
| $I_c$      | Moment of Inertia of the Core           |
| $I_{sw}$   | Moment of Inertia of the Sandwich panel |

|             |  |
|-------------|--|
| $(EI)_{sw}$ | Effective Equivalent Stiffness of the Sandwich Panel |
| $b$         | Width of the sandwich panel                          |
| $t_s$       | Thickness of the skin                                |
| $t_c$       | Thickness of the core                                |
| $y$         | Distance from the neutral axis                       |
| DMA         | Dynamic Mechanical Analysis                          |
| CEEFC       | Centre for Excellence in Engineered Fibre Composites |

# Chapter 1 - Introduction

## 1.1. Introduction

A recent trend in the arena of civil engineering is to employ the use of light weight, smart materials for the construction of residential, commercial and industrial structures. Fibre reinforced composites are found to be one of the best light weight construction materials to be employed in the building material systems. There are a number of naturally occurring composites in the nature such as the wood and bone.

The fibre reinforced polymer composites are a class of engineering materials which consists of two or more constituent materials. The major constituent materials are the reinforcement fibres and the matrix. The reinforcement fibres are generally in a dispersed phase and the matrix is in a continuous phase. The matrix is often commonly referred to as the resin. The primary purpose of the fibres is to provide the necessary strength and the stiffness to the composite and to carry the primary loads to which the composite is subjected. The purpose of the resin/matrix system is to bind the fibres as a cohesive unit. The resin also performs other functions such as ensure the transfer of loads between the fibres and the plies, carry the shear loads, support fibres against buckling and to protect the fibres from mechanical and chemical damage.



Figure 1.1: Composite fibre bridge in Tasmania, Australia

The use of sandwich structures is increasing at a rapid rate in the engineering and manufacturing world. This material has been widely used in the automotive, aerospace, marine and other industrial applications due to its many advantages (Manalo et al, 2012)(Manalo, A., Aravinthan, T. & Karunasena, W. 2012). There is especially substantial growth in this area, in applications where weight saving is a major advantage. (Mujika et al. 2011).The light weight of the sandwich panels facilitates the ease of handling during the manufacturing, assembling, and installation and also reduces the manufacturing costs. In addition, composite sandwich structures are preferred over conventional materials because of its high corrosion resistance (Manalo et al, 2012).

## **1.2. Project Background**

The sandwich panels which have already found their applications in the other fields due to their many advantages are now being researched for their structural applications in the field of civil engineering. The concept of sandwich panels provides an efficient structural system suitable for a variety of applications, including floor and roof panels, pedestrian bridge decks and cladding walls for buildings(Fam & Sharaf 2010).When the composite sandwich panels are used as structural components in the field of structural engineering, they will be exposed to a variety of operating environments and the effect of elevated temperature is considered to be one among them. However, there is very limited studies conducted investigating the effect of elevated temperature, which is the main motivation of this project.

## **1.3. Research Aims**

The aim of this research is to understand and analyse the effect of elevated temperature on the flexural behaviour of the fibre reinforced sandwich panels through experimental investigation and analytical studies.

The specific objectives of the project are as follows:

- To understand and analyse the behavioural characteristics of the core and the skin materials under elevated temperature.
- To determine the flexural behaviour of the FRP panels under elevated temperature
- To establish an empirical equation describing the behaviour of the sandwich panels.

#### **1.4. Justification**

The fibre composite sandwich panels are currently being researched for their applications in the field of civil engineering. Any structure will be subjected to a variety of operating environments and the effect of elevated temperature is one among them. This kind of scenario is more common in the mining industry. Although, there is extensive research conducted on the behaviour of the fibre composites under elevated temperatures, the past research on the composite sandwich panels is limited to those conducted under ambient temperatures to predict their behaviour. There is very limited literature available for behaviour of sandwich panels under elevated temperatures. Hence, this research fulfils the gap in the literature by investigating the behaviour of the composite sandwich panels under elevated temperatures.

#### **1.5. Scope**

This project has focussed on the flexural behaviour of the fibre reinforced sandwich panels under elevated temperature. The structural behaviour of the sandwich panels subjected to the effect of temperature and three point static bending was investigated in this study. The effect of temperature on the structural properties such as the strength and stiffness was studied in detail for each temperature range. Through the experimental investigation load-deflection, stress-strain, strength-temperature and young's modulus-temperature relation was established for each specimen under each temperature. A theoretical equation describing the behaviour of the sandwich panels was developed which predicts the behaviour of the sandwich panels under elevated temperature. The results from the theoretical equation were compared with the experimental results for correlation.

## **1.6. Summary**

This research has studied and analysed the flexural behaviour of the fibre composite sandwich panels under elevated temperature. Since there are very limited resources available on the behaviour of the sandwich panels under elevated temperature, the material properties and the behaviour of the panels under elevated temperature are experimentally investigated followed by developing an empirical relation describing the behaviour of the sandwich panels under elevated temperatures. The results from this prediction were compared with experimental results in order to understand the effect of the temperature on the sandwich panels.

# Chapter 2 – Literature Review

## 2.1. Introduction

The history of composites, constituent materials and their structural application pertaining to civil engineering will be discussed in this chapter. A detailed discussion on the sandwich panels, their composition and their applications is presented in this section. Further the past studies conducted on the composites under elevated temperature, sandwich panels under ambient and elevated temperatures are discussed in detail. Finally the research gaps from the previous works are discussed briefly.

## 2.2. History of Composites

The fibre reinforced polymer composites appear to be a relatively new concept, but however the basics of these composites are age-old concepts dating back to the early 18<sup>th</sup> century. The first structural application was through the development of the Adobe bricks, which are straw- reinforced clay bricks. The first patent for the synthetic composites was obtained in the year 1899 which was developed using the phenol-formaldehyde resin (Bakelite). The commonly used reinforcements during the early periods were linen cloth, asbestos and wood. However, they had a number of pitfalls such as the brittle behaviour of the reinforcement fibres, low tensile strength and the high cost of production and fabrication. The break-through to these problems were achieved in the 1940's through the release of the first commercial glass fibre cloth by the Owens-Corning's and the commercial release of the unsaturated polymer resins. From this point there was a number of consecutive researches conducted in-order to aid the development of the composite materials.

### 2.2.1. Types of Fibres

The reinforcement fibres are classified into two types namely:

- Natural Fibres
- Synthetic Fibres

The natural fibres are those fibres which are obtained from naturally available materials. They are further classified into the plant which is derived from plants such as the hemp,



flax, jute, coir etc., and animal fibres such as the fur and wool which are obtained from animals. On the other hand artificially manufactured fibres through certain mechanical processes are called synthetic fibres such as the glass, carbon, aramid/Kevlar, ceramic, and so on. The glass, carbon and the Kevlar fibres are commonly used due to their advantages.

### **2.2.2. Types of resins:**

The resin/matrix system is classified into two types namely:

- Thermoplastic polymers
- Thermoset Polymers

Thermoplastics are polymeric materials with a series of long chain polymers without any covalent bonds connecting them. At room temperatures these polymers tend to behave like a solid due to the entanglement of the long chained molecules, but under heat and high pressure these molecules tend to slip under each other resulting in new shapes. It is found that upon cooling these polymers possess the ability to restore back to its original shape due to the restriction in the relative movement between the individual molecules. At this juncture of time, it is found that the thermoplastic molecules find a very limited application in the structural fibre composites from the civil/structural engineering perspective due to their disadvantages such as high processing and production costs. It was also found that thermoplastic polymers possess a poor compressive strength and a poorer resistance towards solvents in comparison to the thermosetting polymers. Some of the commonly used thermoplastic polymers from the perspective of composites are polyphenylene-sulphide (PPS), polyether ether ketone (PEEK), polyether imide (PEI) and polyamide-imide (PAI)

The thermoset polymers are materials in which the low molecular weight, reactive compounds are cross-linked to each other via covalent bonds to form a single three dimensional polymeric network. Unlike the thermoplastic polymers, the shape of the thermosetting polymers cannot be altered by the application of heat as this would involve the sliding of initial chain and would result in the breaking of the bonds. It is observed that upon heating there is an increase in the strength of the bonds resulting in a more rigid material. The thermoset polymers are widely used as the composite matrices due to their advantages such as they can be formulated at ambient temperatures and can

be processed without the application of high pressures. They also offer increased resistance to chemicals such as acids, bases and solvents. Some of the examples of the thermosetting polymers are polyesters, vinyl esters, epoxies, phenols and polyurethanes.

### **2.3. Limitations of the Composites**

Although the composite sandwich structures have a number of advantages, they possess some constraints such as limited performance history, lack of design codes and standards. Apart from this the major limitation was that the design of the composite laminates is governed by stiffness rather than the strength which results in greater deflection. This limitation of increased deflection led to the innovation of the novel composite sandwich structures.

### **2.4. Background on Sandwich Panels**

Typically, a low density core, which could also have excellent insulation characteristics, is sandwiched between high strength and stiffness thin skins bonded to the core. The system provides very high strength- and stiffness-to-weight ratios(Fam & Sharaf 2010). The skin and the core are generally bonded together by either adhesives or by co-curing. The top and the bottom skins carry the in-plane and the bending stresses (compression at the top and tension at the bottom), while the cores carry the shear loads and the normal loads.

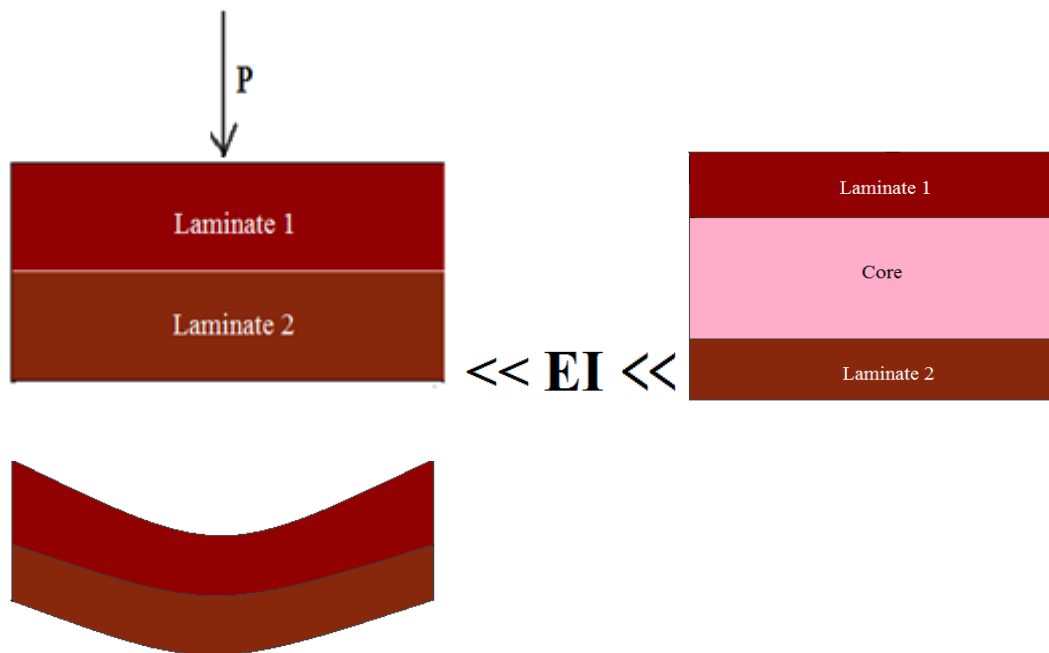


Figure 2.1: Illustration explaining sandwich panel concept

#### 2.4.1 Background on Skin

The main purpose of the skin is to provide the flexural strength and rigidity to the sandwich panels by carrying the tensile and compressive forces. In the most weight-critical applications, composite materials are used for the skins; cheaper alternatives such as aluminium alloy, steel or plywood are also commonly used (Petras & Sutcliffe 1999). The skin generally comprises of two components namely the fibres and the resin matrix. The fibres are in a dispersed phase and the matrix is in a continuous phase. The fibres carry the load and the resin binds the fibres as a single cohesive unit. Laminates of glass, Kevlar/aramid or carbon fibres are generally used as the skins. The commonly used resin systems for the engineering applications are vinyl-esters, epoxies, phenols and poly-urethanes. The sandwich panel under study has the skins made of laminates of glass fibres and a phenol-formaldehyde resin system.

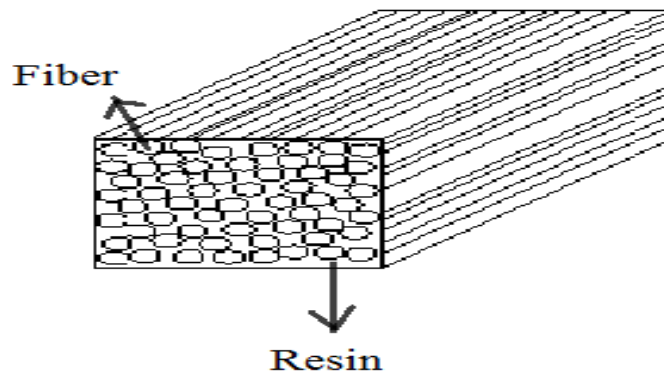


Figure 2.2: Fibre composite laminate

### 2.4.2 Background on Core

The core of a sandwich beam behaves in a manner similar to that of the web portion in an I-beam. The major purpose of the core is to carry the shear loads. Materials used for cores include polymers, aluminium, wood and composites. To minimise weight these are used in the form of foams, honeycombs or with a corrugated construction (Petras & Sutcliffe 1999).

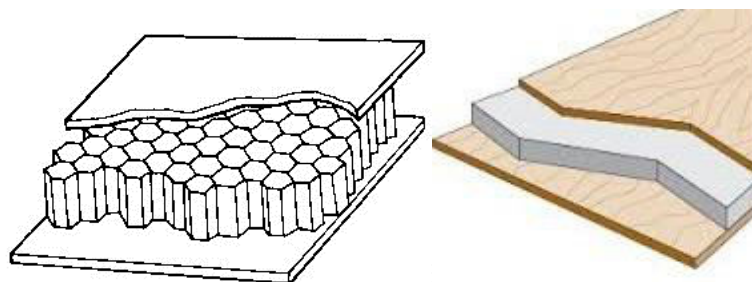


Figure 2.3: Honeycomb and Foam cores

The application of the sandwich panel in field of civil engineering is limited due to the core materials used in the construction of sandwich panels. The main reason for this could be that most of the currently used core is not appropriate for this type of

application. Foam core and balsa wood are soft and will crush under high compressive loads. Honeycomb and trussed-core structures have high compressive strength but the presence of cavities in these core materials reduces their capacity to hold mechanical connections. The evolution of a sandwich structure with lightweight, high strength core and with good holding capacity for mechanical connections provides an opportunity to develop this material for structural beams (Manalo et al, 2012).

### **2.4.3 Structural Applications of the Sandwich Panels**

Their usage is mainly in the aerospace, aircraft and marine industries because of their fuel efficiency in transportation vehicles, but at present, there is a strong interest in the development and applications of sandwich structures for civil and building material systems(Manalo 2013). These materials are now commonly used as structural panel for roofs, floors, walls, and bridge decks(Manalo et al, 2012).The fibre reinforced sandwich panels are being investigated for their applications in the field of civil/structural engineering.



Figure 2.4: Structural Applications of Sandwich Panels

Source: [www.usq.edu.au/CEEFC](http://www.usq.edu.au/CEEFC)

## 2.5. Behaviour of Sandwich Panels under Ambient Temperatures

**Manalo (2013)** studied the behaviour of structural fibre composite sandwich beams made up of glass fibre composite skins and phenolic core material under three-point short beam and asymmetrical beam shear tests. The study focussed on the effect of the shear span-to-depth ratio ( $a/D$ ) on the strength and failure behaviour of the composite sandwich beams. The test results showed that with an increase in the  $a/D$  ratio, there was a decrease in the failure load of the sandwich beam. Further it was found that, the coupling effect of flexural stresses increased with an increasing  $a/D$  ratio. It was to be noted that, the fibre composite sandwich beams tested under asymmetrical beam shear test exhibited higher failure load in comparison with the beams tested under short beam shear test. Numerical analysis showed that the shear stress in the core is more dominant than flexural stress when the  $a/D$  ratio is 1 for the sandwich beams under short beam test and 1–3 for the sandwich beams tested under asymmetrical beams shear test. A suitable prediction equation was developed based on the results obtained, which accounts for the combined effect of shear and flexural stresses due to the changing  $a/D$  ratio,

presented a good agreement with the experimental results, showing that it can reasonably estimate the failure load of structural fibre composite sandwich beams.

**Awad et al., (2011)**, studied the geometry effect on the behaviour of single and glue-laminated glass fibre reinforced polymer composite sandwich beams loaded in four-point bending. The purpose of this research was to investigate the behaviour of single and glue laminated glass fibre reinforced polymer (GFRP) composite sandwich beams considering different spans and beam cross sections. The composite sandwich beams with different thicknesses 1, 2, 3, 4, and 5 sandwich layers were tested using the four-point static flexural test with different shear span to depth ratio ( $a/D$ ). From the experimental results, it was found that the  $a/D$  ratios had a direct effect on the flexural and shear behaviour of the sandwich beams. It was also found that the capacity of the beam decreased with an increasing  $a/D$  ratio. Several failure modes such as the core crushing, core shear, and top skin compression failure were observed during the testing of the beams. The failure mode map which was developed based on the experimental findings and the analytical prediction indicated that the failure mode is affected by the  $a/D$  with the number of glue laminated panels.

**Manalo et al., (2012)** conducted a research on the Prediction of the Flexural Behaviour of Fibre Composite Sandwich Beams. A simplified Fibre Model Analysis (FMA) to describe the approximate behaviour and the governing failure mechanisms of composite sandwich structures under flexural load was developed in this research. The fundamental design methodology was based on several key parameters such as the sectional equilibrium, strain compatibility, and the constitutive material behaviour which employed the use of a layer-by-layer approach to evaluate the sectional forces and for the calculation of the nominal flexural capacity of a composite sandwich section. A major merit of the proposed model was found to be its accountability for the nonlinear behaviour of the core in compression, the effect of core cracking in tension and the linear elastic behaviour of the fibre composite skins. Through this method, the analysis of the composite sandwich structures with non-symmetric sections could be carried out. The efficiency and practical application of the developed prediction equation was demonstrated by analysis of the behaviour of the individual and glue-laminated composite sandwich beam structures made from the glass fibre composite skins and phenolic core material and through the comparison of the results from the numerical simulation with the results of experimental investigation. This method was

found to reasonably describe the behaviour of the fibre composite sandwich structures in flexure.

**Manalo et al., (2012)**, studied the geometry and restraint effects on the bending behaviour of the glass fibre reinforced polymer sandwich slabs under point load. The study investigated the flexural behaviour of a new generation composite sandwich beams made up of glass fibre reinforced polymer skins and modified phenolic core material. 4-point static bending test was used to determine their strength and failure mechanisms in the composite sandwich beams in the flatwise and the edgewise positions. The results of the experimental investigation revealed that the composite sandwich beams tested in the edgewise position failed at a higher load with less deflection compared to specimens tested in the flatwise position. Under flexural loading, the composite sandwich beams in the edgewise position failed due to progressive failure of the skin while failure in the flatwise position is in a brittle manner due to either shear failure of the core or compressive failure of the skin followed by debonding between the skin and the core. Analytical predictions and numerical simulations were developed and compared with the experimental results. It was found that the results of the analytical predictions and numerical simulations agreed with the experimental results

**Fam and Sharaf.,(2010)**, studied the Flexural performance of sandwich panels comprising polyurethane core and GFRP skins and ribs of various configurations. The feasibility of fabrication and flexural performance of panels composed of lowdensitypolyurethane foam core sandwiched between two GFRP skins were studied. From the study it was found that, through the integration of the ribs, strength and stiffness of the panels increased, by 44–140%, depending on the configuration of the ribs. The maximum gain in strength was equivalent to the effect of doubling the core density in a panel without ribs. Shear deformation of the core contributed over 50% of mid-span deflection in the panel without ribs. Through the addition of ribs, the flexure became more dominant and shear deformations of the ribs contributed only 15–20% of the total deflection.



## **2.6. Effect of Elevated Temperature on Composites**

**Yu Bai and Thomas Kellar., (2011)** investigated the delamination and kink band failure of pultruded GFRP laminates under elevated temperature and compression. Pultruded glass fibre composite laminates of width 48 mm, thickness 12 mm and 500 mm length were mechanical properties. The glass transition temperature was determined by the dynamic mechanical analysis and the decomposition temperature was determined by thermogravimetric analysis. The specimens were tested for their axial compression under elevated temperature range of 20°C and 220°C at an interval of 40°C. The DMA test revealed that the storage modulus decreased with increasing temperatures and the leathery state was reached at 220°C. At lower temperature range the load displacement curves revealed a clear bifurcation of the maximum and the post-buckling load but as the temperature increased this bifurcation was less obvious and disappeared beyond 180°C. At temperature below 180°C the delamination caused by the second-order bending of the slender specimen was observed which was absent in case of the specimens tested at temperatures above 180°C.’

**Alsayed et al., (2012)** investigated the performance of glass reinforced polymer bars at elevated temperatures. E-glass/vinyl ester specimens of 12 mm diameter were used for the study. The specimens were divided into two sets with one set of the specimen covered in 40 mm concrete. All the specimens were exposed to the temperatures 100°C, 200°C and 300°C for a period of 1, 2 and 3 hours and tested for their mechanical properties. Physical examination of the bars after the temperature exposure revealed distinct dis-colouration which was observed for the temperatures 200 and 300°C. The stress strain relationship was similar for all the specimens and the failure mode was brittle in nature. The test revealed that the losses in tensile strength at elevated temperatures were 3.1-35.1 % for concrete covered GRFP bars and 4.7-41.9 % for the bare GRPF bars.’

**Wong et al., (2004)** ‘Studied the behaviour of pultruded GFRP short columns under elevated temperature. The specimen under study was 100 x 30x 4 mm E-glass/ polyester columns tested for their compressive strengths at 20, 60, 90, 120, 150, 200 and 250°C. Two sets of specimens of lengths 30 mm and 400 mm were tested. The experimental tests of the 30mm specimen revealed that at lower temperature of 20, 60 and 90°C the specimens failed along the mid-length in a brittle manner and at elevated temperature greater than 90°C the specimen failure was due to the resin softening phenomenon.

Distinct discolouration was observed at a temperature of 250°C. The results of the column test conducted on the 400 mm specimen revealed that the column strengths of the 60 and 90 °C specimens were reduced by about 65% of the ambient temperature results and the specimens tested at 120°C and above revealed a quarter of the strength of that under ambient temperatures. The failure mode at lower and elevated temperatures was characterized by local buckling deformation.'

**Gibson et al., (2010)** 'Studied the high temperature and fire behaviour of the glass fibre/polypropylene laminates. Samples of width 20 mm and span 150 mm were tested for their mechanical properties under three point bending and the flexural moduli was measured in terms of creep applying dead loads to the centre of the samples at 1, 10, 100, 1000's. From the experimental study it was found that the flexural modulus from room temperature just before of melting point varies linearly. The compressive strength of the specimens was substantially lower than their tensile strengths. The tensile stress-strain curves were found to be non-linear which is attributed to the resin-fibre debonding combined with resin creep and fibre misalignment. It was found that the properties of glass/pp composites decline gradually with temperature unlike the thermoset polymers and the glass transition temperature influenced its behaviour from 20°C to 250°C.'

**Lauobi et al., (2014)** 'Studied the thermal behaviour of E glass fibre reinforced unsaturated polyester composites. The test materials under study are polyester resin and glass/polyester composites. The specimens were heated at a temperature of 100°C, 200°C and 280°C for 1 hour and were cooled under ambient temperatures before the commencement of the testing. The results of the thermogravimetric analysis of the resin revealed that the decomposition of the resin takes place at two temperatures namely 130°C and 400°C. In case of the composite the decomposition was just below 180°C. The glass transition temperature for the resin was found to be 64.20°C and 81.66°C for the composites. The mechanical properties of the resin and the composite were tested using the tensile and the three point bending tests. The physical examination of the specimens after the thermal exposure reveal no apparent change in their appearance until 100°C however, on exposure to 200°C they undergo degradation at the fibre-matrix interface and apparent de-lamination at 280°C. The stress-strain curve obtained for the tensile tests reveal that the curve is linear at the beginning and non-linear at the end but for 280°C which tends to follow a brittle behaviour. It was found that above 200°C the resin was more vulnerable than the composite. The three point bending test

revealed that the tensile strength slightly increases before 100°C and decreases thereafter. The modulus of elasticity increases strongly at 100 °C and 200°C and decreases thereafter. The displacement of the specimen gradually decreases with the increase in the temperature.’

## **2.7. Effect of Elevated Temperature on Sandwich Panels**

**Liu et al.,(2011)** ‘Investigated the temperature effects on the strength and crushing behaviour of carbon fibre composite truss sandwich cores. In this project the sandwich panels under study were made from carbon/epoxy prepreg face sheets and unidirectional carbon rods were used for the truss cores. The specimens of composite rods were tested for their mechanical strengths at cryogenic and elevated temperatures in the following temperature range: -60°C, -30°C, -10°C, 20°C, 50°C, 80°C, 110°C, 140°C, 160°C, 200°C, and 260°C. The specimens of sandwich panels were tested at -60°C, 20°C, 70°C, 100°C, 140°C, and 160°C. The results from the experimental test revealed that at elevated temperatures the strength and the stiffness of the sandwich panels decreased which is attributed to the softening of the polymer matrix. Delamination failure was observed throughout the operating temperature range, while the failure above the glass transition temperature was characterised by the plastic kinking of the truss members.’

**Liu et al, (2013)** ‘Investigated the mechanical behaviour and failure mechanisms of carbon fibre composite sandwich panel after thermal exposure. The sandwich panel specimens were made from carbon/epoxy prepreg by molding hot-press method. The composite sandwich panels were tested for their mechanical properties on exposure to temperatures of 20, 100, 150, 200, 250, 300°C for 6 hours. The thermogravimetric analysis revealed that the epoxy resin matrix decomposed in two stages namely the first stage of rapid degradation from 250°C until a pseudo-plateau and the second stage leading to the complete degradation. A distinct decolouration of the sandwich panels were observed on exposure to temperatures beyond 150°C. It was observed that the carbon sandwich panels failed due to core shear buckling and node rupture for the specimens exposed from 100 - 200°C and face sheet crushing was observed for the specimens exposed to 250 and 300°C which may be attributed to the severe heat damage caused to the face sheet during the thermal exposure of the specimens.

## **2.8. Research Gaps from Previous Works**

On reviewing the current literature it is found that the research on the sandwich panels at elevated temperature is limited to the carbon fibre composite with a truss core (**Liu et al., 2011**). It is also found that the sandwich panels are tested only for the compression at higher temperature range and no significant information is found to explain the flexural behaviour of the glass fibre composites. Therefore, it is identified that there exists a research gap in current knowledge which explains the flexural behaviour of glass fibre reinforced sandwich panels under elevated temperature.

Thus the flexural behaviour of the sandwich panels at elevated temperature under three point static bending is investigated in this research in order to fill the gap in the literature. Further an empirical equation describing the behaviour of the sandwich panels under elevated temperature is also proposed in this study. The methodology, results and the observations from the testing of the panels are discussed in the following sections. It is believed that this research will increase the application of the sandwich panels as structural elements in the field of civil engineering.

## **2.9. Summary**

The history of composites, their constituent materials and the types of the constituent materials of a composite were briefly studied in this chapter. The limitations of the composite materials were also briefly highlighted. Further, a brief background on the sandwich panels and its constituent materials and their structural applications were provided following which the past literature on the sandwich panels under ambient temperature, composites under elevated temperature and sandwich panels under elevated temperature was reviewed. Finally, the gaps from the previous works were discussed thereby justifying the need for this research.

## **Chapter 3 – Project Methodology**

### **3.1. Introduction**

This chapter outlines the experimental methodology adopted in this project. The materials used for the testing are discussed briefly in this chapter. The testing specimens and the equipment used for the purpose of testing the specimens are also discussed and outlined in this chapter. Finally the experimental set-up and the testing procedure adopted are discussed in detail in this chapter.

### **3.2. Materials**

The composite sandwich panel used in this study is made up of glass fibre composite skins co-cured onto the modified phenolic core material using a toughened phenol formaldehyde resin. The top and the bottom skins of the sandwich panels is made up of 2 plies of stitched bi-axial (0/90) E-CR glass fabrics with a chopped strand mat and a toughened phenol formaldehyde resin is used as the laminate matrix. The skin has a fibre fraction of 45% by weight and an average density of 1365 kg/m<sup>3</sup>. The phenolic core material is a proprietary formulation by LOC Composites Pty Ltd, Australia. This material comes from natural plant products derived from vegetable oils and plant extracts and chemically bonded within the polymer resin. It has an average density of 855 kg/m<sup>3</sup>. Further information on the core is unavailable due to the commercial nature of the product.

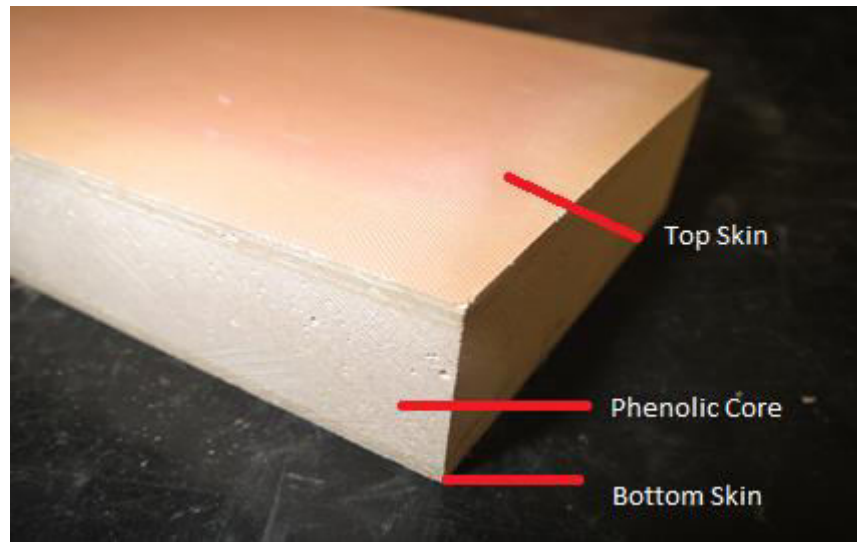


Figure 3.1: Carbon LOC<sup>®</sup> Panels

### 3.3. Test Specimen

The skin and the sandwich panels were tested for their flexure under three point static bending test. The sandwich panels are 50 mm wide and 220 mm in length. The thickness of the core is measured to be 10 mm. The Table 3.1 gives a detailed description about the test specimens.

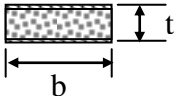
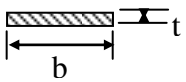
| Specimen type | Illustration  | No. of specimens | Thickness, $t$ (mm) | Width, $b$ (mm) | Total length, $L_T$ (mm) | Support span, $L$ (mm) |
|---------------|---|------------------|---------------------|-----------------|--------------------------|------------------------|
| Sandwich beam |  | 60               | Actual              | <b>50</b>       | <b>220</b>               | 180                    |
| Skin only     |  | 60               | actual              | <b>50</b>       | <b>220</b>               | 120                    |

Table 3.1: Test Specimen Dimensions

The skin and the core materials were subjected to dynamic mechanical analysis in order to determine their material properties. The details of the specimens used are given in the Table 2.

| <b>Specimen Type</b> | <b>Thickness, t (mm)</b> | <b>Width, b (mm)</b> |
|----------------------|--------------------------|----------------------|
| Skin                 | 5                        | 10                   |
| Core                 | 5                        | 10                   |

Table 3.2: Dimensions of DMA samples

### **3.4. Specimen Preparation**

The test specimens were made to order from the CarbonLOC Pvt Ltd, Australia. The specimens were manufactured at the manufacturing facility in USQ, Toowoomba.

### **3.5. Experimental Procedure**

#### **3.5.1. Dynamic Mechanical Analysis (DMA)**

The DMA test is a thermo-mechanical test which is performed to identify and measure the visco-elastic properties of the constituent materials. The test was carried out according to ASTM D 4065-2001 testing standards. The responses of the material as it is subjected to the periodical forces are called as the Dynamic Mechanical Properties of the material. The DMA applies an oscillating force in the form of stress and records the oscillating responses of the sample. The modulus of the specimen tested is calculated from the elastic responses and the damping is calculated from the viscous responses. The mechanical properties are displayed in the form of sinusoidal oscillations as a function of time and temperature. The green curve of the resulting graph represents the storage modulus ( $E'$ ) and the blue curve represents the tan delta. According to the ASTM D 4065-2001 specifications the maximum of the curve representing the Tan delta (Tan delta) represents the glass transition temperature. The glass transition temperature ( $T_g$ ) of the material is defined which helps in predicting the behaviour of the materials when subjected to both mechanical and thermal stresses.

A specimen of  $35 \times 10 \times 5 \text{ mm}^3$  is placed in the equipment and a small deformation is applied to the specimen in a cyclic manner. Through this test the response of the specimen to various parameters such as the temperature, stresses and the modulus are studied.

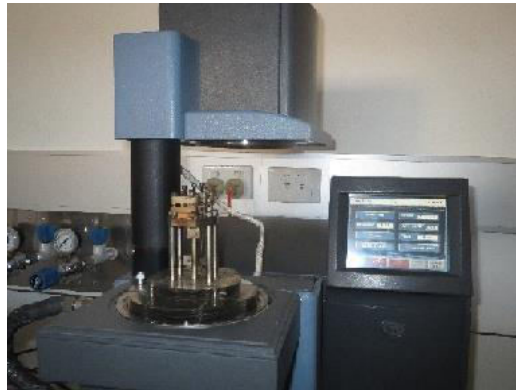


Figure 3.2: DMA Testing Equipment



Figure 3.3: DMA Test Set-Up

### 3.5.2. Flexure Test

In order to analyse the mechanical behaviour of the sandwich panels under elevated temperature the skin and the sandwich panels were subjected to flexure test by three point static bending tests (Figure 6) at elevated temperature under nine different temperature ranges from  $21^\circ\text{C}$  to  $180^\circ\text{C}$  namely  $21^\circ\text{C}$ ,  $35^\circ\text{C}$ ,  $50^\circ\text{C}$ ,  $65^\circ\text{C}$ ,  $80^\circ\text{C}$ ,  $100^\circ\text{C}$ ,  $120^\circ\text{C}$ ,  $150^\circ\text{C}$ ,  $180^\circ\text{C}$ . A test specimen of  $220 \times 50 \times 20 \text{ mm}^3$  is simply supported on



two ends and the load is applied at the mid-point through a 100kN servo-hydraulic loading machine. The effects of temperature are applied through an environmental chamber. The maximum temperature capacity of the chamber is 350°C. The specimens were separated by a span of 180 mm for the sandwich panels and 120 mm for the skin panels. The rate of loading was 5 mm/min. A set of 5 specimens were tested for each temperature range.

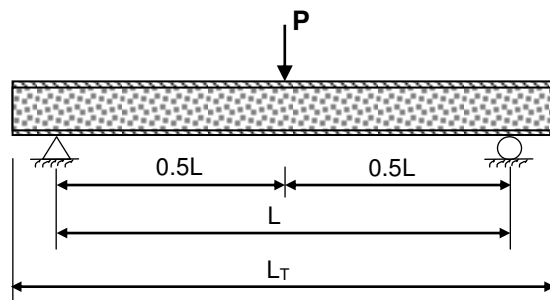


Figure 3.4: Schematic Diagram of Three Point Bending Test



Figure 3.5: Flexure Test Equipment



Figure 3.6: Flexure Test Set-Up

### **3.6. Summary**

The constituent materials, equipment used for the testing and the various procedures adopted for the testing of the sandwich panels have been described in this section. A detailed description about the CarbonLOC® panels has been discussed in this section. The dimensions of the specimens involved in the project were discussed in detail. The relevant standards pertaining to each test is given. Finally, the testing procedure involved in each test is discussed in detail.

# Chapter 4 - Results and Observation

## 4.1. Introduction

The experimental results of the DMA test and the 3 point bending test will be discussed in this section. The failure modes, stress-strain relation, load-deflection and the strength-temperature relationship will be discussed in this section.

## 4.2 Dynamic Mechanical Analysis

The results obtained from the Dynamic Mechanical Analysis of the composite skin and the resin core specimens reveal that the mechanical properties of the skin and the core vary with the temperature. This variation in temperature is explained by behaviour exhibited in the three different phases observed in the composite skin and the resin core. The different phases exhibited by the specimens may be explained by the effect of temperature on the polymeric bonds. From the results of the Dynamic Mechanical Analysis of the glass transition temperature ( $T_g$ ) of the composite skin and the resin core were found to be  $125^{\circ}\text{C}$  and  $136^{\circ}\text{C}$  respectively.

There are two types of polymeric bonds namely the primary and the secondary bonds. The primary bonds are the strong covalent bonds in the polymeric chains and the cross-links of the thermosets while the secondary bonds are the much weaker bonds. At lower temperatures the primary and the secondary bonds remain relatively intact without being affected by the temperature changes which explains the steady trend in the graphs. This state is referred as the **Glassy State**.

As the temperature increases towards the glass transition temperature ( $T_g$ ), the weaker secondary bonds are affected by temperature and are consequently broken while the primary bonds remain intact. This state is referred to as the **Leathery State**. The transition of the specimen from the glassy to the leathery state is known as the glass transition temperature.

When the temperature increases beyond the glass transition temperature the molecules of the polymeric chain becomes entangled due to the flexibility and the length of the chains. This state is referred as the **Rubbery State**. When the temperature increases further the primary bonds are affected by temperature and are consequently broken

resulting in the decomposition of the material. This state is referred as the **Decomposition State**.

#### 4.2.1 Skin

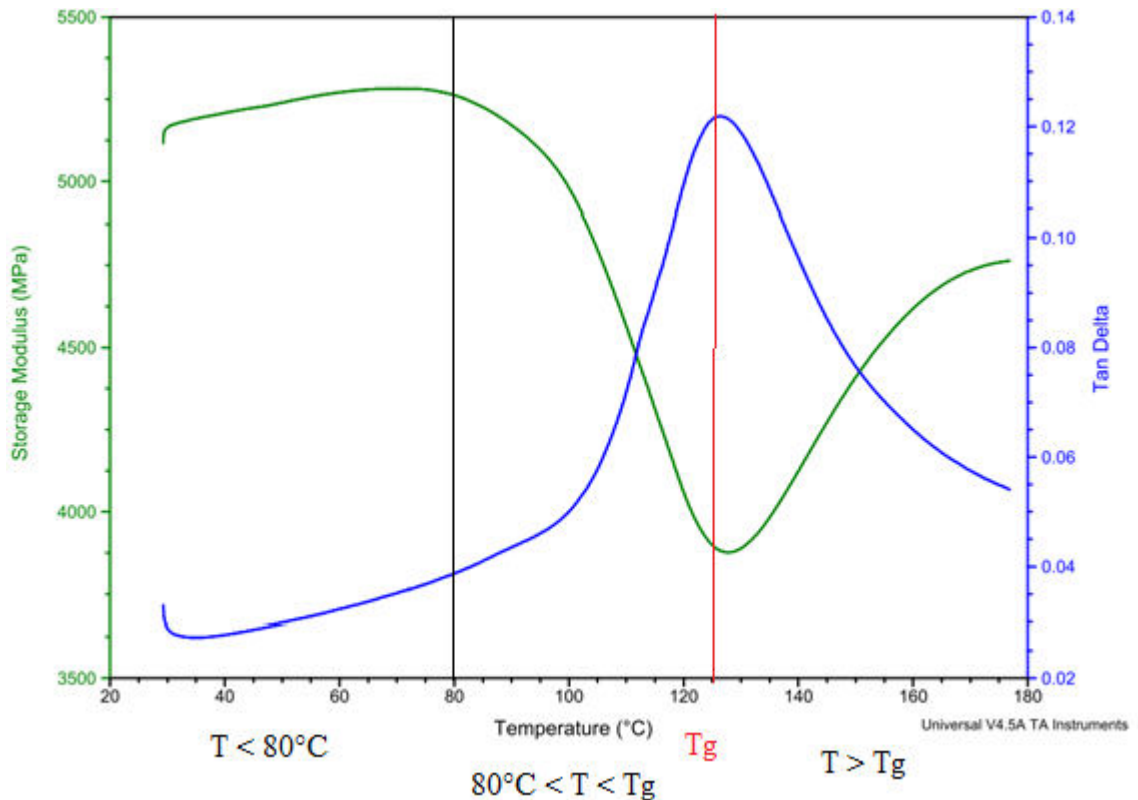


Figure 4.1 DMA result of the skin

The figure 4.1 shows the results of the DMA test on the skin. The figure shows two curves representing the storage and the Tan delta. The green curve represents the storage modulus ( $E'$ ) and the blue curve represents the tan delta. As stated in the section 3.5.1 of the chapter 3, the dynamic mechanical analysis is conducted according to the ASTM D 4065-2001 specifications and the maximum of the Tan delta curve represents the glass transition temperature of the specimen. Hence, the glass transition temperature of the skin specimen is found to be around 125.06°C.

From the figure 4.1, it can be observed that the mechanical properties of the composite skin vary with the temperature. The variation of the mechanical properties of the skin specimen can be explained by three phases namely:

**Phase 1:** This is the phase exists below  $80^{\circ}\text{C}$  ( $T < 80^{\circ}\text{C}$ ). In this phase, a slow decrease in the storage modulus ( $E'$ ) and a slow increase in the Tan delta are observed.

**Phase 2:** This phase exists between  $80^{\circ}\text{C}$  and the glass transition temperature,  $T_g$  ( $80^{\circ}\text{C} < T < 125.06^{\circ}\text{C}$ ). There is a rapid decrease in the storage modulus ( $E'$ ) and the curve reaches its minimum at the glass transition temperature. Similarly the Tan delta increases rapidly with the curve reaching its maximum value at the glass transition temperature.

**Phase 3:** The last phase exists beyond the glass transition temperature ( $T > 125.06^{\circ}\text{C}$ ). During this phase the storage modulus ( $E'$ ) begins to increase rapidly and the Tan delta begins to drop rapidly. The trend of the curve during this increase and the decrease is found to be similar to that during the steep decrease and increase of the storage modulus and Tan delta as explained in the previous phase.

## 4.2.2 Core

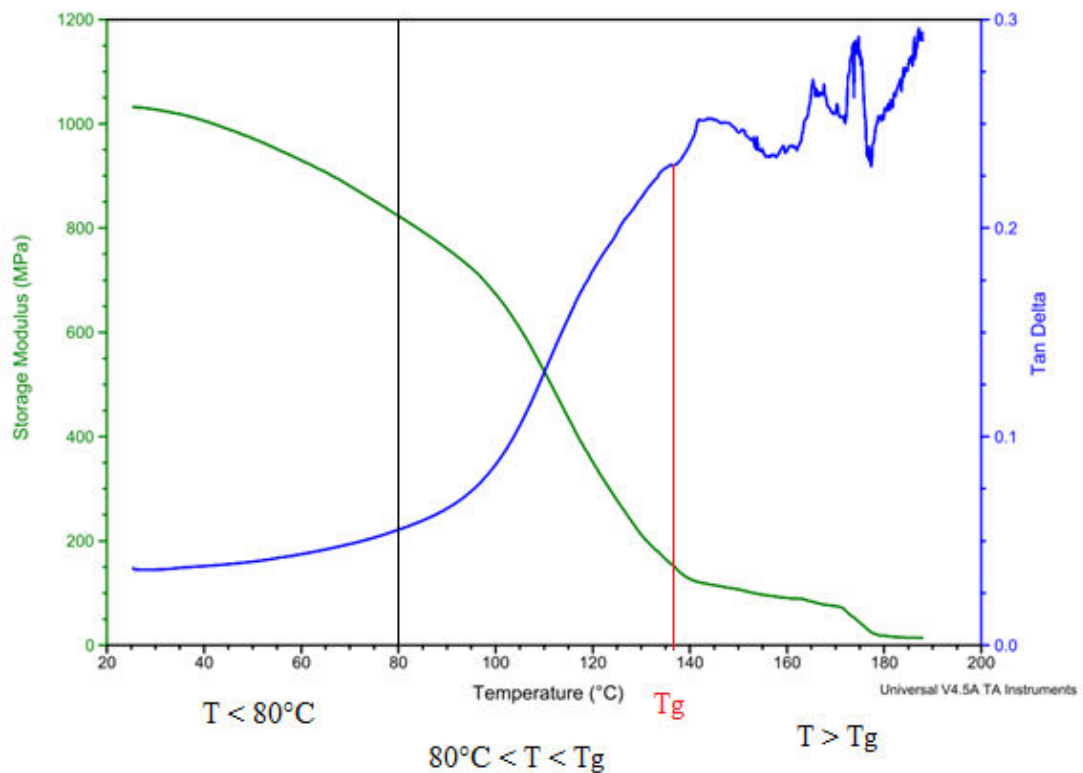


Figure 4.2 DMA results of the core

The figure 4.2 shows the results of the dynamic mechanical analysis of the core specimens. As stated in the previous section the maximum of the tan delta curve represents the glass transition temperature of the specimen, hence the glass transition temperature is found to be 136.11°C from the above graph. The changes in the mechanical properties of the resin core with the temperature are also seen from the graph. The changes in the mechanical properties of the resin core can be explained in detail by three phases namely:

**Phase 1:** This phase explains the behaviour of the resin core below 80°C ( $T < 80^{\circ}\text{C}$ ). It is found that the resin core behaves in a manner similar to the composite in this phase. The storage modulus ( $E'$ ) of the resin core exhibits a slow decrease in its values with temperature while Tan delta exhibits a slow increase in its values.

**Phase 2:** This phase explains the behaviour of the resin core beyond 80°C and below the glass transition temperature of the resin core which is 136.11°C ( $80^{\circ}\text{C} < T$

<136.11°C). During this phase too the resin core behaves in a manner similar to the composite skin where the Storage modulus of the core ( $E'$ ) decreases rapidly with temperature and the Tan delta shows a rapid increase in its values. At the glass transition temperature, the storage modulus reaches its minimum while the Tan delta reaches its maximum value.

**Phase 3:** This phase explains the variation of the mechanical properties of the resin core beyond the glass transition temperature ( $T > 136.11^\circ\text{C}$ ). Unlike the composite skin the behaviour of the resin core beyond the glass transition temperature follows a different pattern. From the tan delta curve of the graph, it can be observed that the resin core exhibits an irregular pattern which may be attributed to the decomposition of the resin core beyond the glass transition temperature.

### 4.3. Behaviour of the Skin

#### 4.3.1 Load Deflection Relation

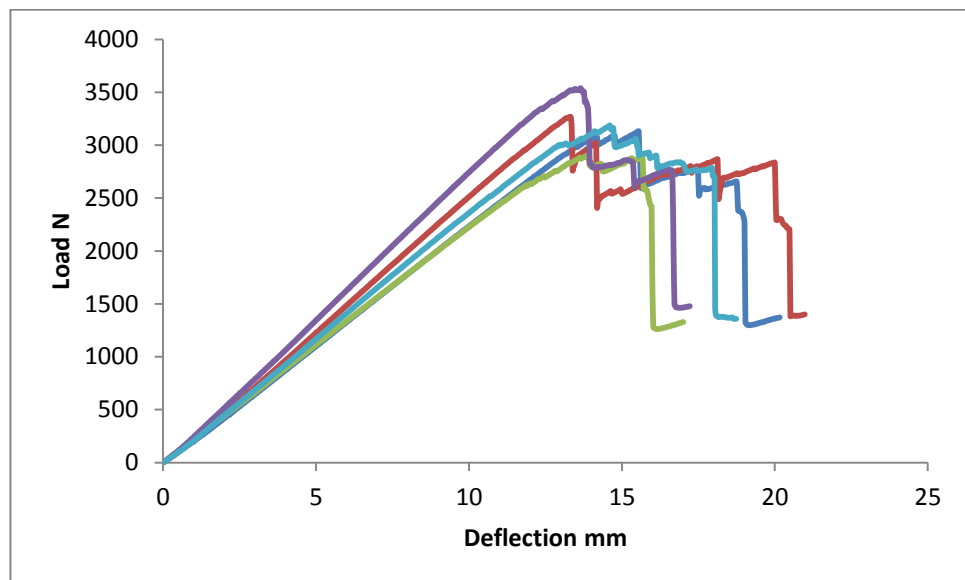


Figure 4.3 Load – Deflection diagram for the skin at 21°C

Results from the load-deflection relation for the specimens tested at 21° reveal that the skin exhibits a linear fashion with the peak load ranging between 3000-3500 N,

thereafter a rapid reduction in the load carrying capacity of the specimen before failing completely at a load between 2500-2500 N. The decrease in the load carrying capacity may be attributed to the appearance of cracks on the tension side (top side) of the specimen. Ultimately the skin tested at 21°C failed due to compressive failure and debonding between the individual plies was observed which may be due to the interlaminar shear.

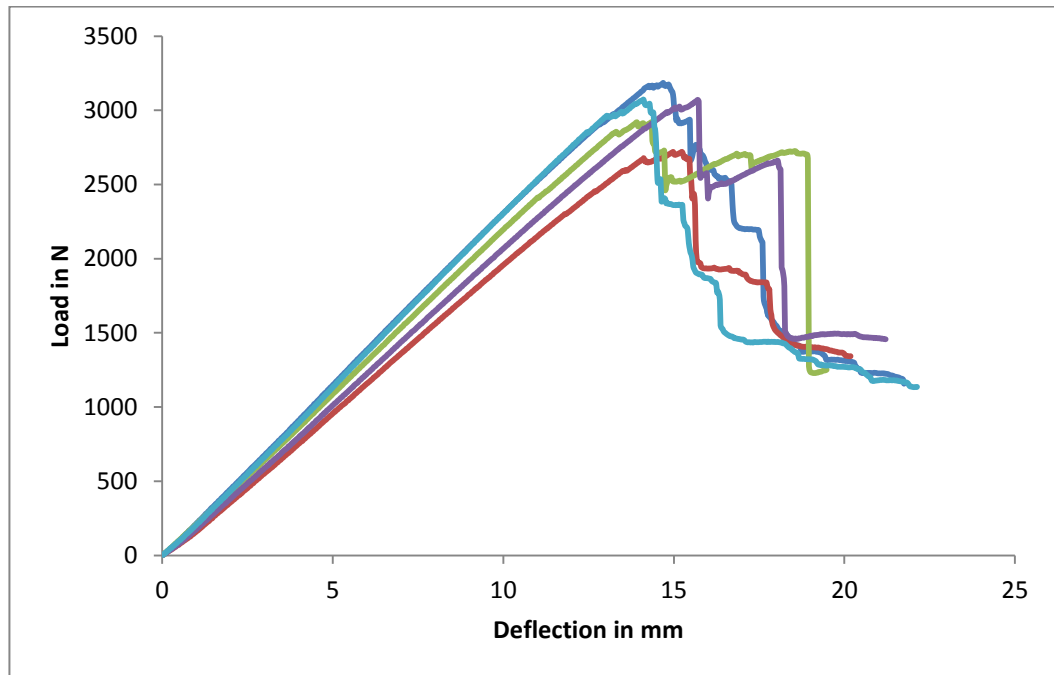


Figure 4.4 Load – Deflection diagram for the skin at 35°C

The figure 4.4 shows the load deflection diagram for the skin specimens tested at 35°C. The load and displacement of the skins at 35°C vary linearly with each other until 2500-3000 N similar to the specimens at 21°C before starting to fail in a brittle manner. The specimens start exhibiting a slight ductile behaviour which may be attributed to the cracks developed on the compression sides. The ultimate failure is initiated by interlaminar shear in this case too.



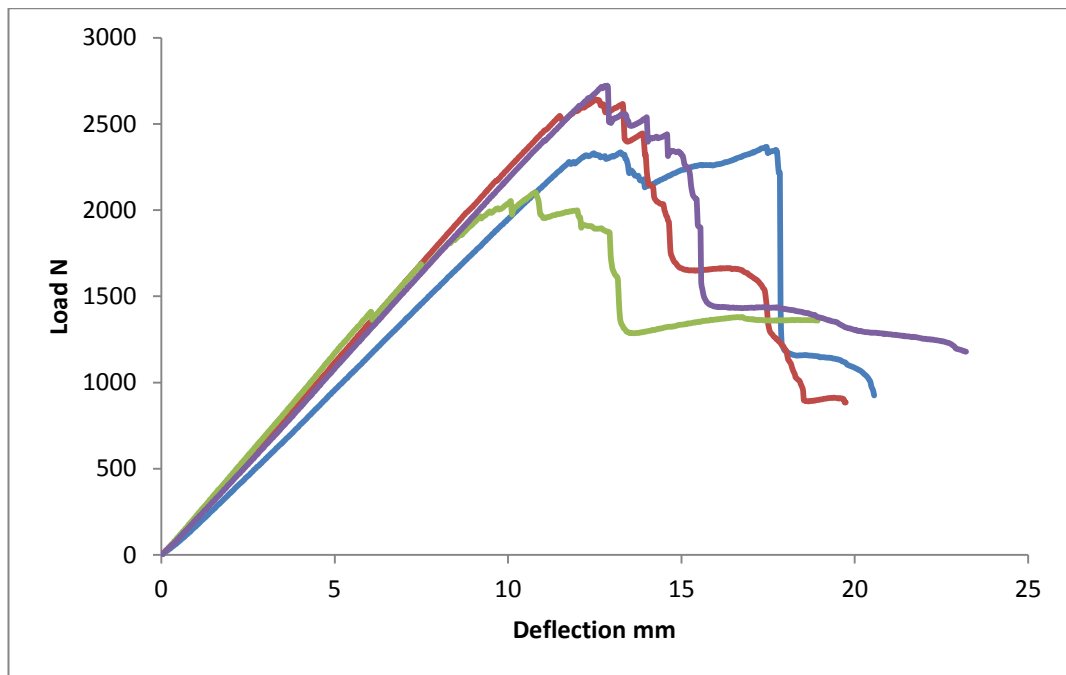


Figure 4.5 Load – Deflection diagram for the skin at 50°C

The figure 4.5 shows the load deflection relation for the skin specimens tested at 50°C. The load and deflection curve for the specimens tested at 50°C varies linealy with each other and the peak load varies between 2000-2500 N. It may be observed that the failure tends to follow a plastic mode just before the brittle failure. This phenomenon may be attributed to the softening of the resin matrix. The resin softening is characterized by the indentations found at the point of loading. The decrease in the peak load capacities may be attributed to the cracks developed on the tension and compression side of the specimen. However, interlaminar shear dominates the ultimate failure.

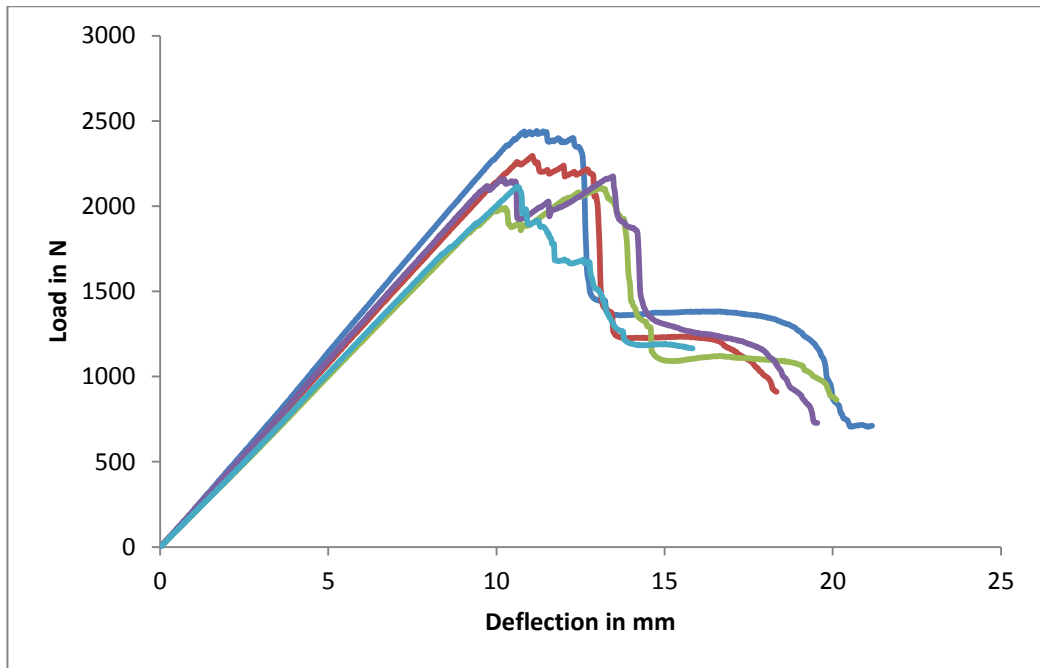


Figure 4.6 Load – Deflection diagram for the skin at 65°C

The figure 4.6 shows the load deflection diagram for the skin specimens tested at 65°C. The load and deflection varies linearly with peak load from 2000-2500°C. The behaviour of the skin panel is similar to the behaviour exhibited at 50°C. The plastic phase is more clearly observed at this temperature. The ultimate failure is due to the interlaminar shear.

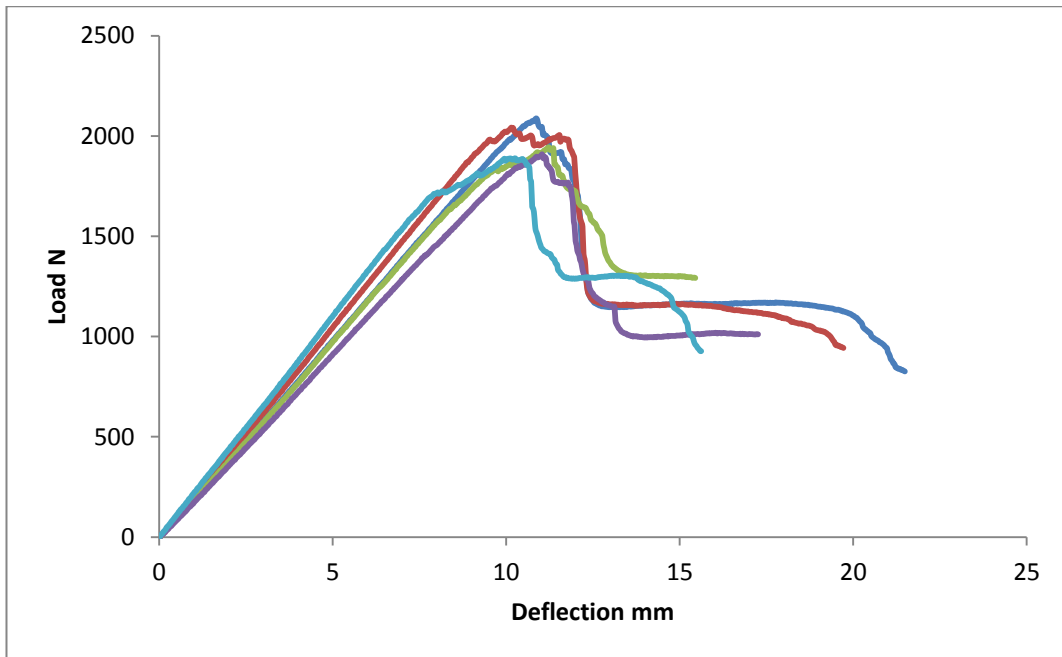


Figure 4.7 Load – Deflection diagram for the skin at 80°C

The figure 4.7 shows the load displacement diagram for the skin specimens tested at 80°C. The load displacement relation varies linearly until the peak load capacities ranging between 1500-2000°C. There is clear indication of the resin softening characterized by indentations. The peak deflections are between 5-10 mm. Interlaminar shear dominates the failure.

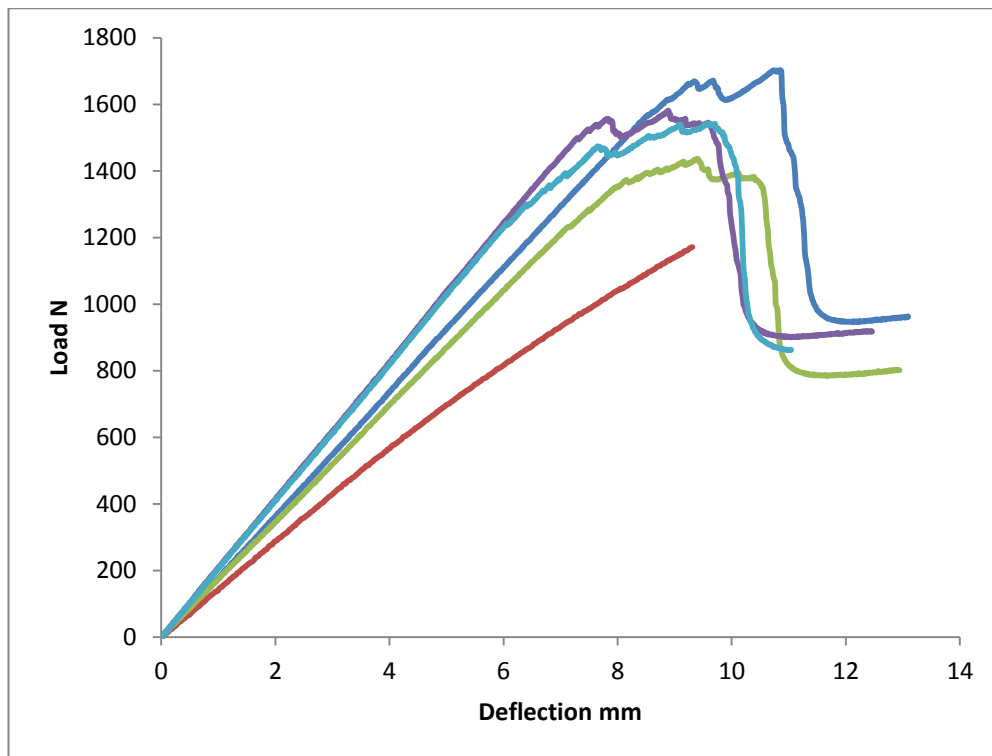


Figure 4.8 Load – Deflection diagram for the skin at 100°C

The figure 4.8 shows the load-deflection relation for the skin specimens tested at 100°C. The load deflection relation varies linearly and the failure tends to follow a more plastic trend after the peak load range of 1400-1600 N. The specimens tested at 100°C reveal a phenomenon of resin embrittlement.. However, interlaminar shear dominates the ultimate failure.

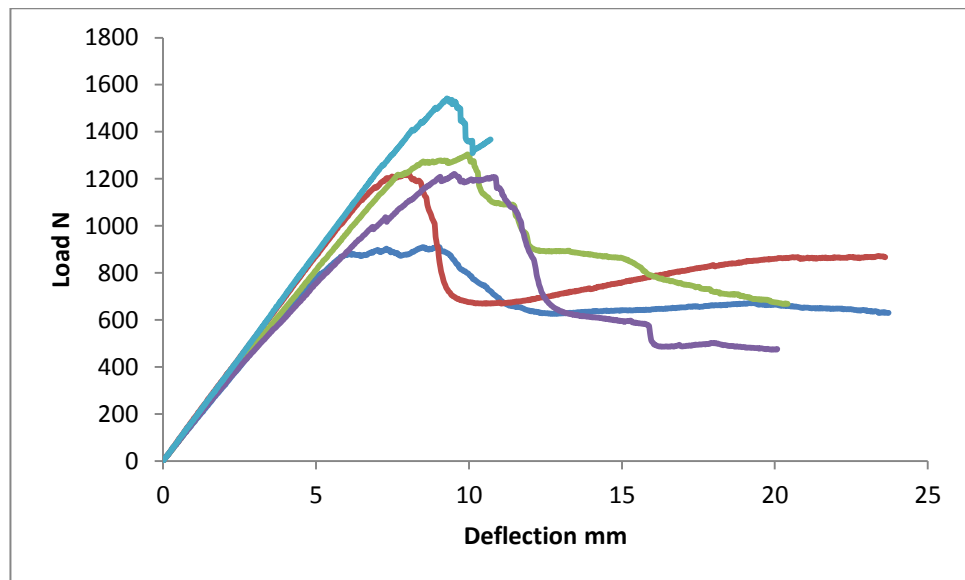


Figure 4.9 Load – Deflection diagram for the skin at 120°C

The figure 4.9 shows the load deflection relation for the skin specimens tested at 120°C. The load deflection path is linear until the failure of the specimen and the failure is no longer brittle as the failure takes place completely by a plastic mode. The peak load carrying capacity also decreases to between 800-1400°C. Due to the effect of the temperature the resin tends to soften initially characterized by strong indentations at the loading point and leads to the decrease in the load carrying capacity of the specimen. However as the test progresses the resin tends to turn brittle. The ultimate failure takes place by cracks on the compression side due to interlaminar shear.

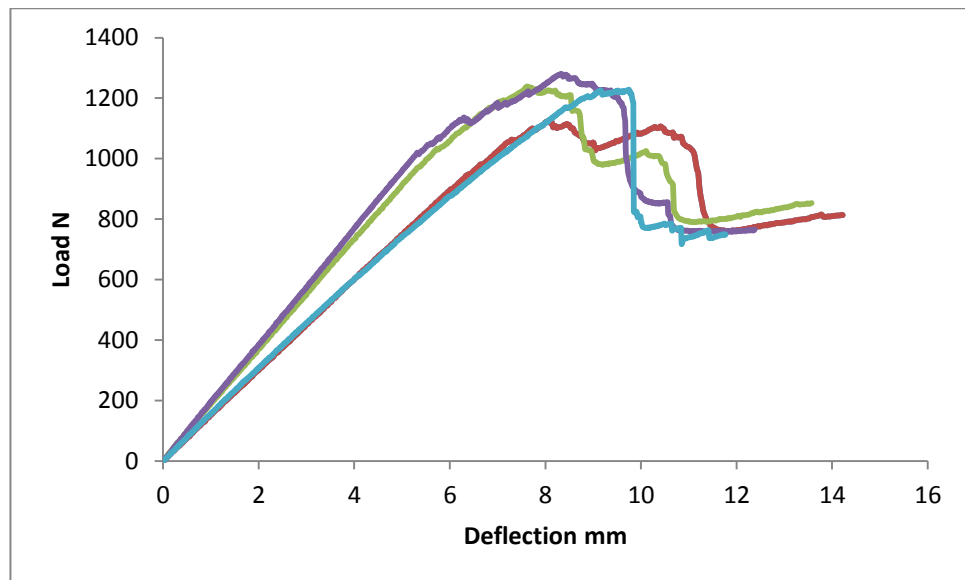


Figure 4.10 Load – Deflection diagram for the skin at 150°C

The figure 4.10 shows the load-displacement diagram for the skin specimens tested at 150°C. The load and displacement varies linearly before the plastic failure of the specimen. There is a slight increase in the peak load carrying capacities of the specimens 1000 N to just above 1200 N, which is due to the phenomenon of resin turning brittle characterized by the surface cracking at the loading point. Although the failure is initiated due to the cracks on the compression side of the specimen the brittle resin takes little higher load before failing completely due to interlaminar shear. It can be observed that the phenomenon of resin softening attributes to the plastic failure in this case also.

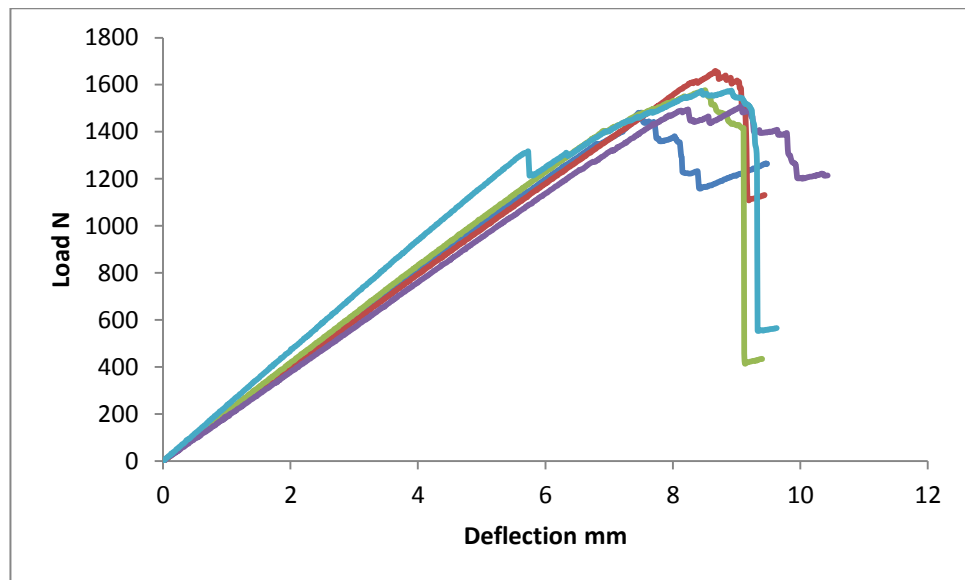


Figure 4.11 Load – Deflection diagram for the skin at 180°C

The figure 4.11 shows the load displacement diagram for the skin specimens tested at 180°C. The load displacement diagram reveals that the specimens exhibit a completely plastic behaviour. It can be observed that there is an increase in the load bearing capacities on comparison with the previous graphs with the peak load ranging between 1400-1600°C. The resin embrittlement is clearly characterized by the cracks on the compression side of the specimen.

#### 4.4. Failure Modes of the Skin

The composite skins tested under three point static bending were studied for their characteristic failure modes under each temperature range. On observing the specimens after the tests it was found that the specimens failed by exhibiting different failure modes under each temperature.

##### 4.4.1. Failure Mode at 21°C

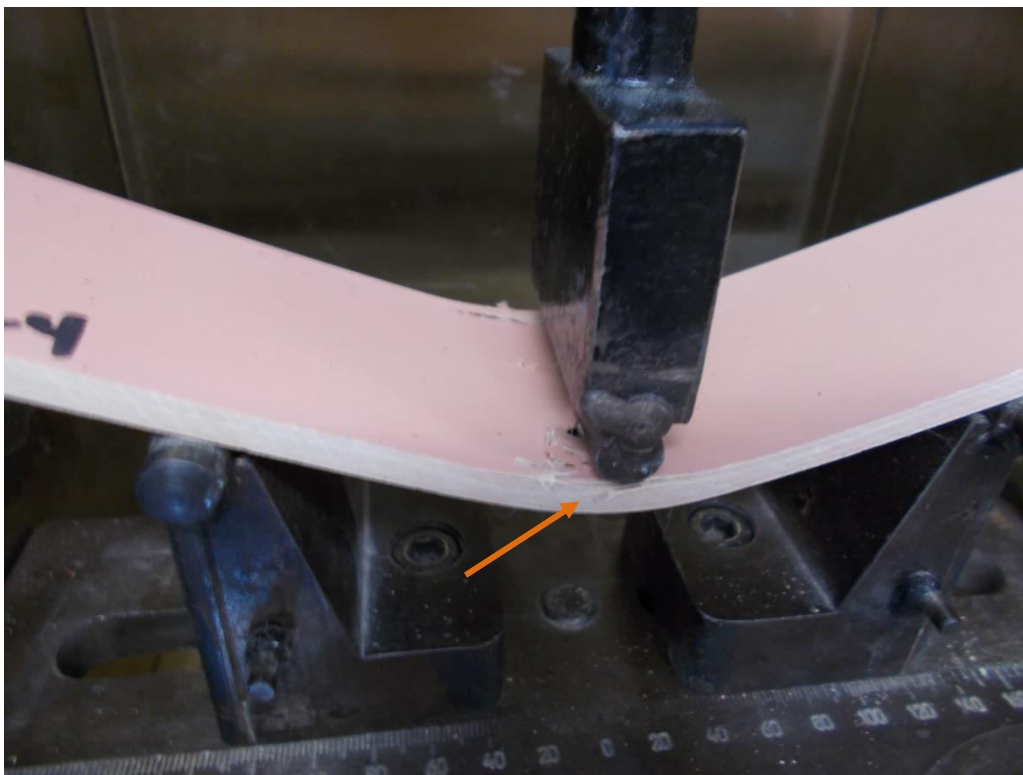


Figure 4.12 Failure of the specimen at 21°C



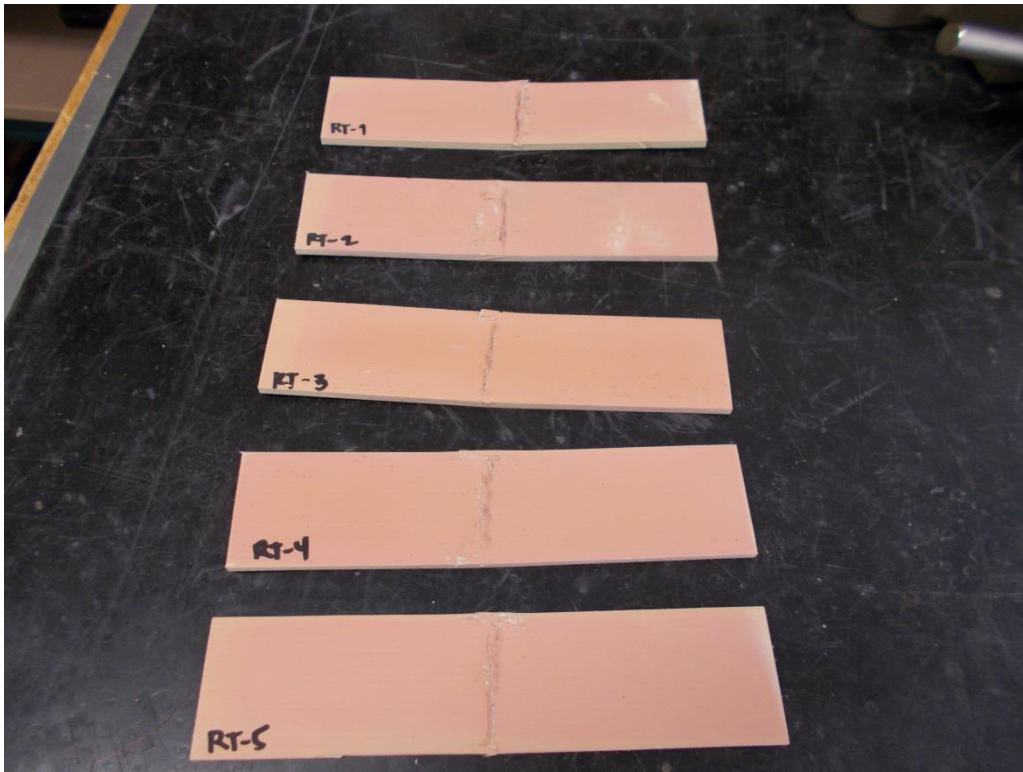


Figure 4.13 Cracks on the compression side of the specimen at 21°C

The figure 4.12 and 4.13 shows the failure mode at room temperature (21°C). From the figure it can be found that the specimen at room temperature fails in a brittle manner as discussed in the chapter 4. The failure of the specimen is dominated by interlaminar shear. The skin specimen brittle failure of the skin specimen is initiated by the cracks on the compression side (Top side) of the specimen as indicated in the above figure.

#### 4.4.2 Failure Mode at 35°C

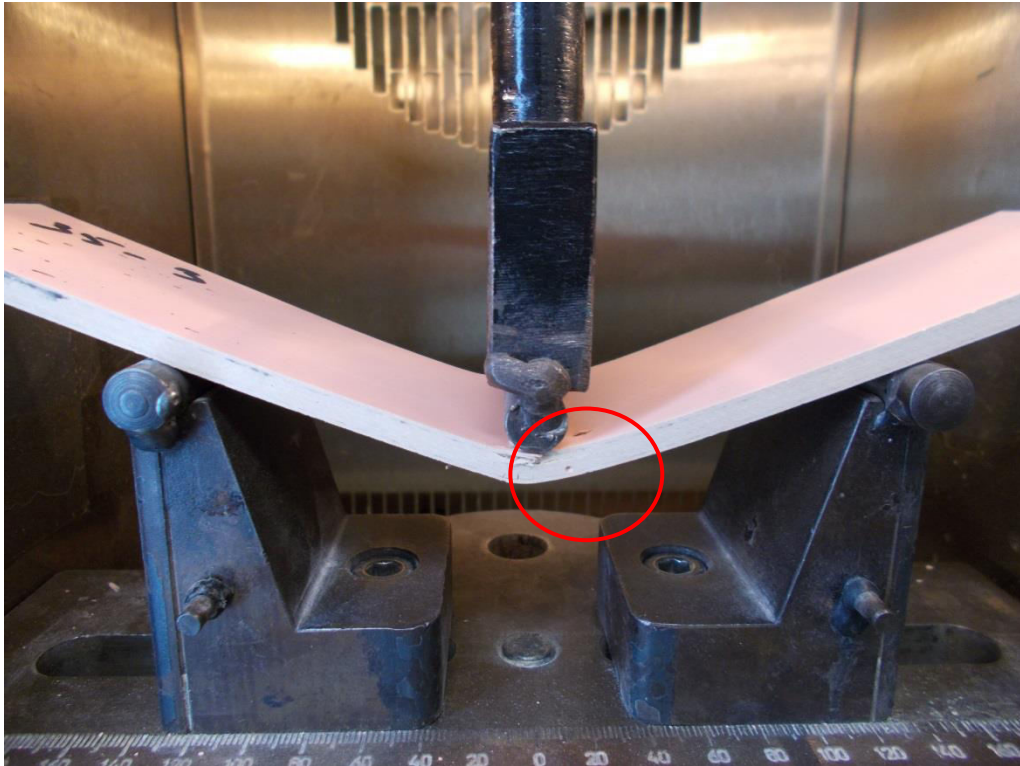


Figure 4.14 Failure of the specimen at 35°C



Figure 4.15 Cracks on the tension side of the skin at 35°C

The skin specimens tested at 35°C failed in a brittle manner by developing cracks on both the compression and the tension sides of the specimen. The figures 4.14 and 4.15 shows the failure modes of the specimen tested at 35°C. The ultimate failure of the specimen was governed by the interlaminar shear.

#### 4.4.3 Failure Modes at 50°C, 65°C and 80°C.

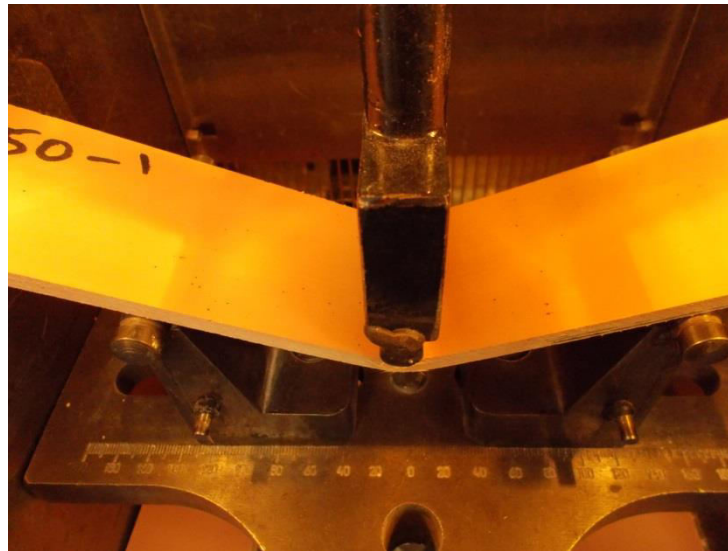


Figure 4.16 Failure of the Specimen at 50°C

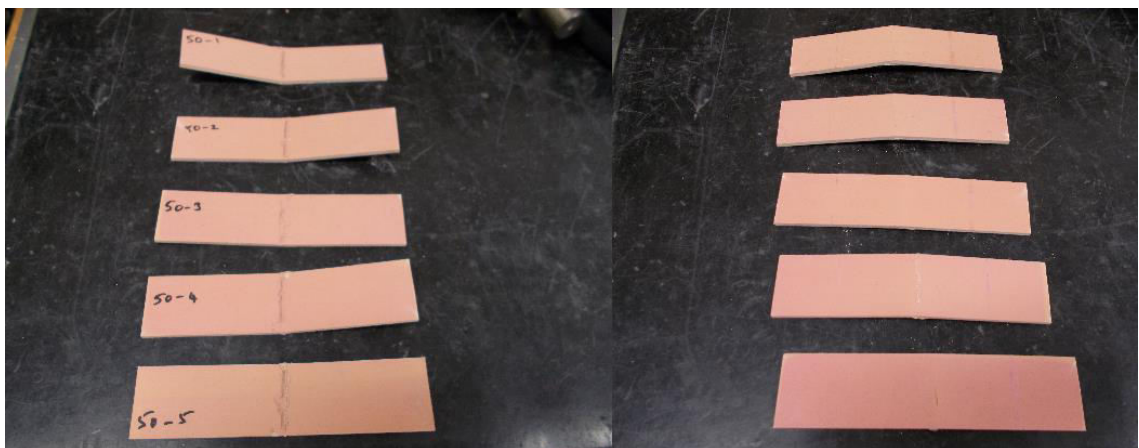


Figure 4.17 Compression and tension cracks on the specimen at 50°C

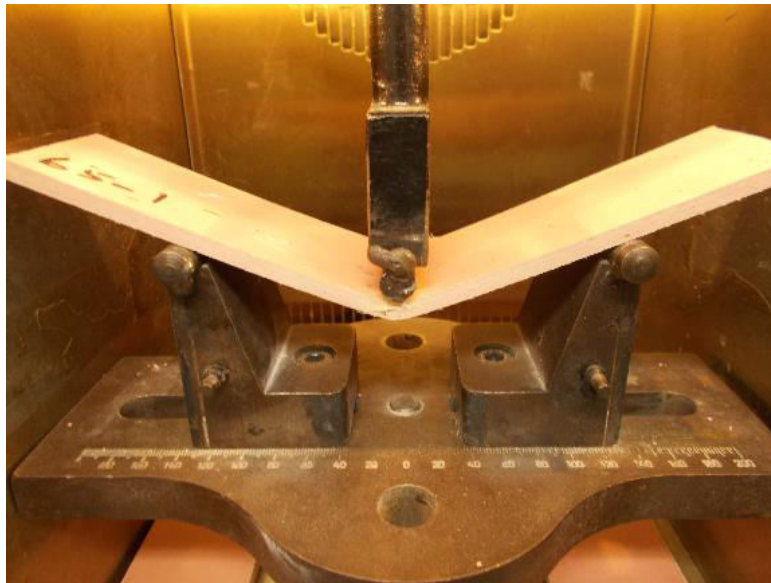


Figure 4.18 Failure of the specimen at 65°C

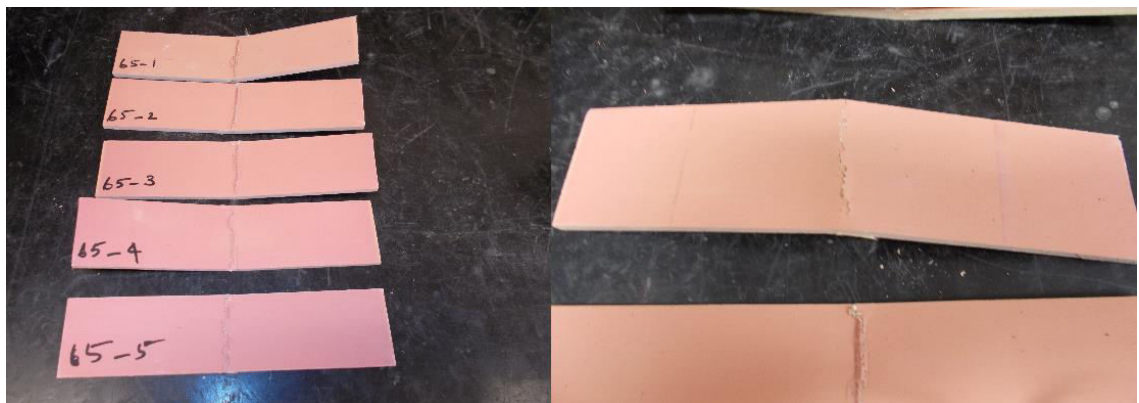


Figure 4.19 Compression and Tension cracks on the specimen at 65°C

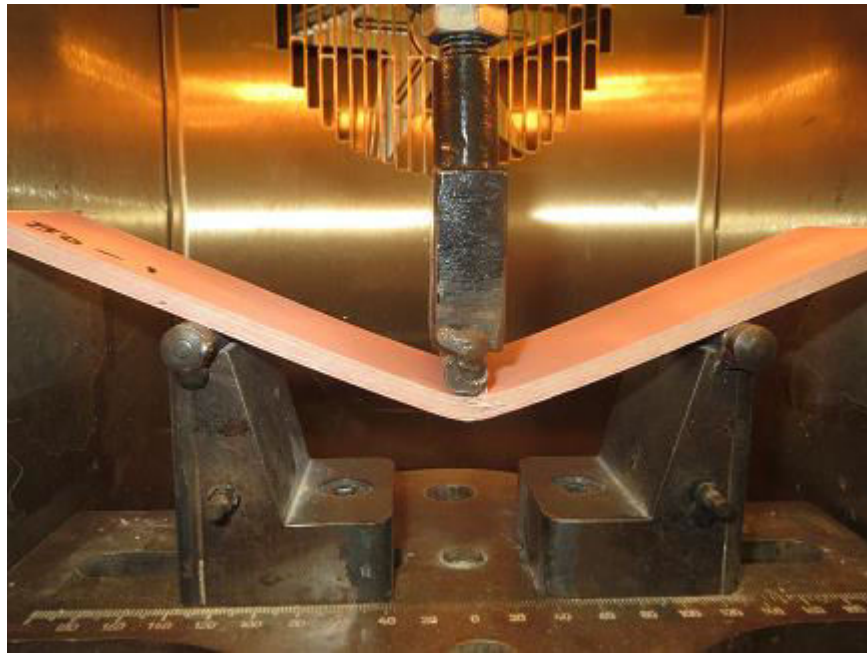


Figure 4.20 Failure of the specimen at 80°C



Figure 4.21 Compression and Tension cracks on the specimen at 80°C

The specimens tested under 50°C, 65°C and 80°C fails in similar manner with variations in their peak strength and Young's modulus values. The specimens tested under this temperature range fail in a brittle manner with the ultimate failure dominated by interlaminar shear. However, all the specimens tested at this temperature range fail by exhibiting a plastic phase just before the brittle failure which was observed in the load-displacement diagrams of the specimens. The plastic phase observed during the failure of the specimens is attributed to the phenomenon of the softening of resin as a result of exposure to temperature which was observed during the DMA test conducted

on the composite skin and the resin core. The phenomenon of the softening of the resin is observed in the form of indentations observed on the top surface of the skin specimens at the point of loading as shown in the above figures.

#### 4.4.4 Failure modes at 100°C and 120°C

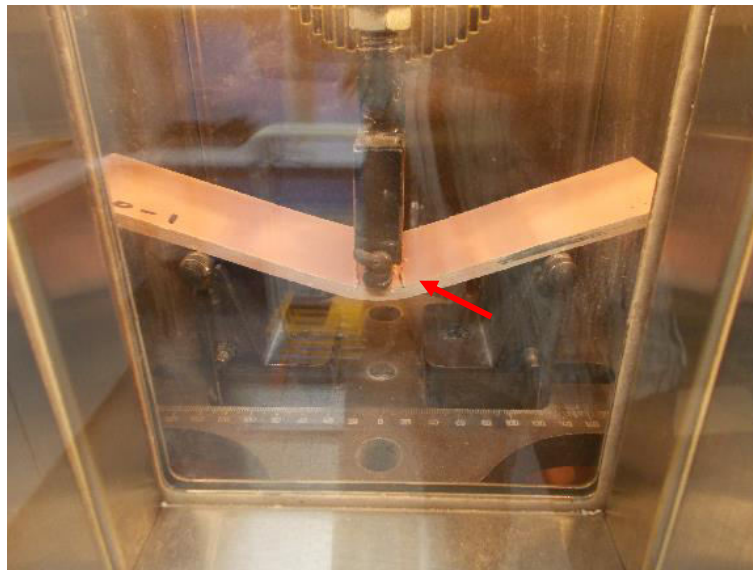


Figure 4.22 Failure of the specimen at 100°C

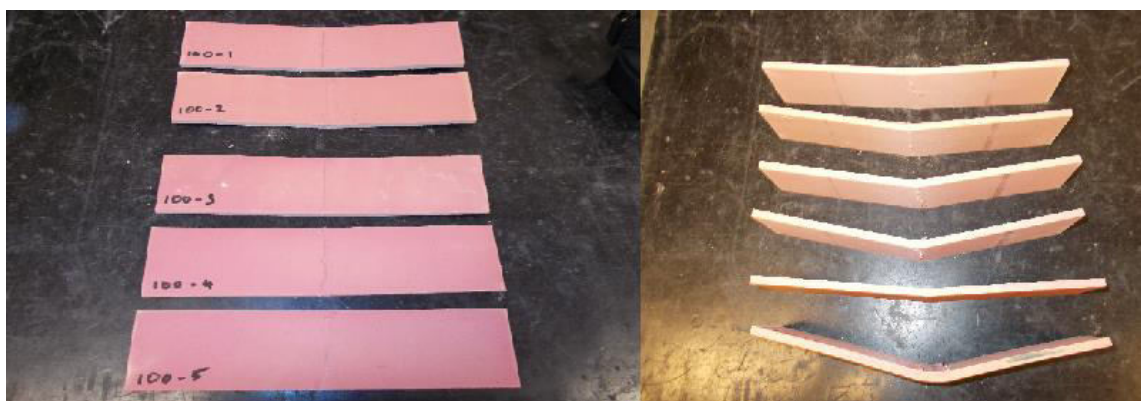


Figure 4.23 Compression and tension cracks on the specimen at 100°C

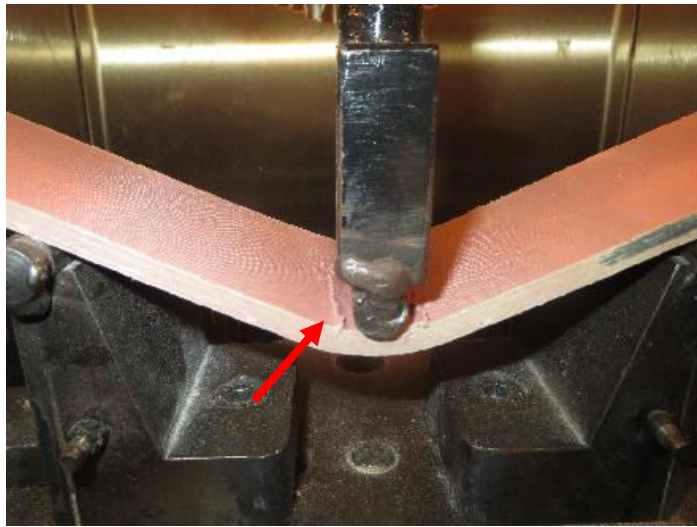


Figure 4.24 Failure of the specimen at 120°C



Figure 4.25 Compression and Tension cracks on the specimen at 120°C

The failure mode of the specimens tested at 100°C and 120°C ceases to be brittle and follows a plastic mode of failure which is observed from the load-displacement diagrams of the specimens. The change in the failure mode is due to the effect of the elevated temperature on the resin of the composite. Cracking was observed on both the tension and the compression sides of the specimens. At temperatures beyond 100°C the resin starts to turn brittle as observed in the DMA tests. This phenomenon is attributed to the expulsion of the moisture content from the specimen, which was discussed in the previous sections. The ultimate failure of the specimen is due to the interlaminar shear between the plies.

#### 4.4.5 Failure modes at 150°C and 180°C

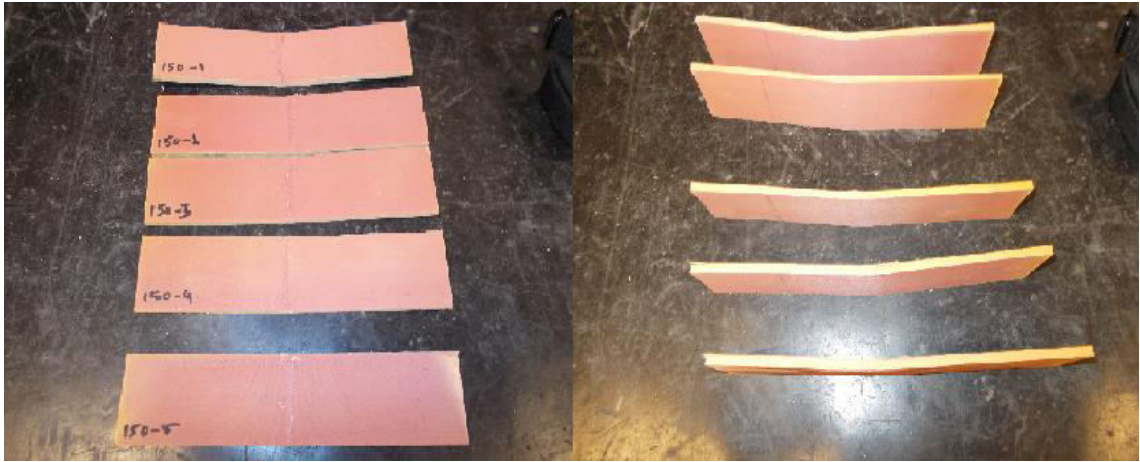


Figure 4.26 Compression cracks on the specimen at 150°C

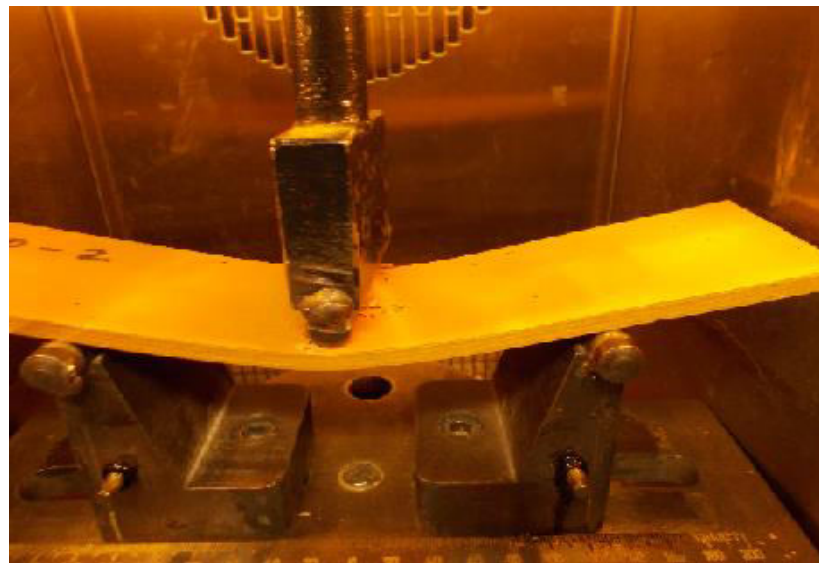


Figure 4.27 Failure of the specimen at 180°C





Figure 4.28 Failure on the compression side of the specimen at 180°C

The specimens tested at 150°C and 180°C failed in plastic manner as observed from the load-deflection diagrams of the specimens. The plastic failure is due to the phenomenon of softening of the resin as observed in the previous cases. As discussed earlier, the resin turns brittle beyond the glass transition due to the removal of the moisture content from the resin. The phenomenon of resin softening was observed in the form of indentations at the point of loading and the phenomenon of the resin turning brittle was observed in the form of wrinkling of the top layer of the skin as shown in the figure 4.28. It was also observed that the cracking occurs only on the compression side of the specimen unlike the previous cases and the ultimate failure occurs due to interlaminar shear as observed in the previous failures.

## 4.5 Behaviour of the Sandwich Panel

### 4.5.1 Load-Deflection Relation

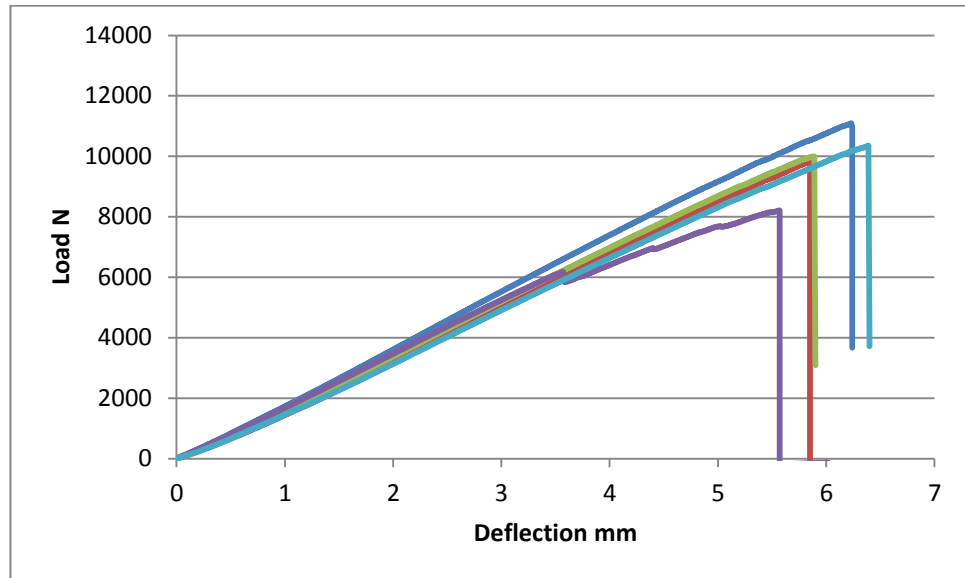


Figure 4.29 Load-Deflection diagram for the Sandwich Panels at 21°C

The figure 4.29 shows the load-deflection relationship of the sandwich panels tested for their flexure at 21°C. The graph showing the load-displacement behaviour of the sandwich panel can be divided into two phases namely a linear and a non-linear phase. The linear phase is that phase which describes the stiff behaviour of the panel as a cohesive unit offering the resistance to the applied load. At the end of this phase a non-linear behaviour is observed which is due to the formation of the cracks on the compression side (top skin). The non-linear phase is that phase where the failure of the panel is initiated in the form the compression cracks before the ultimate failure due to core shear. From the graph it may be observed that the failure takes place in a brittle manner at a peak load range between 8000-11100 N with a mid-span deflection range of 5-7 mm.

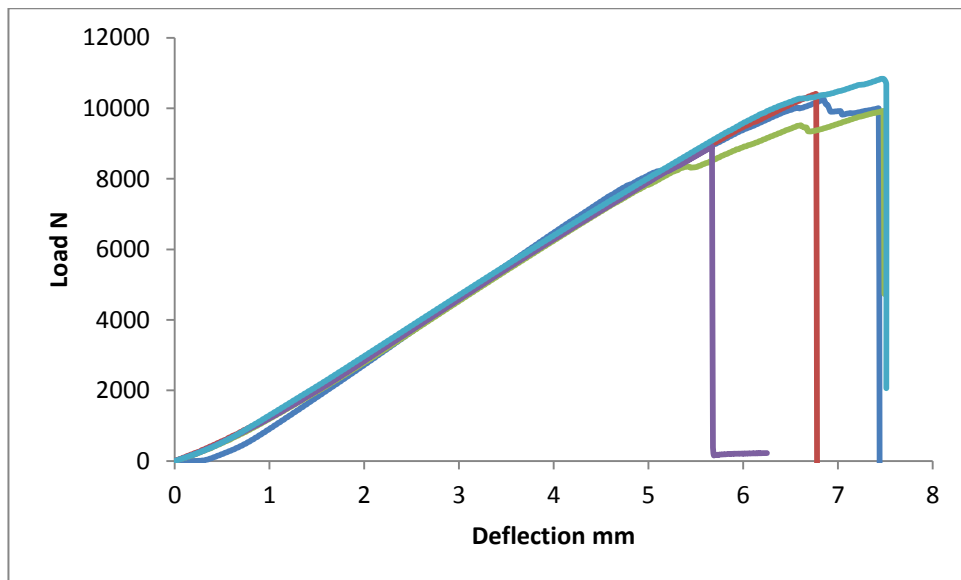


Figure 4.30 Load-Deflection diagram for the Sandwich Panels at 35°C

The figure 4.30 shows the load-deflection relationship for the sandwich panel specimens tested at 35°C. The load-deflection relation for the sandwich panels tested at 35°C is presents a very close similarity to the sandwich panels tested at 21°C. The curve exhibits a linear and a non-linear phase. The failure of the sandwich panels are initiated due to the cracks on the compression side followed by the brittle failure at a peak load range of 9000-10100 N and the peak deflection range of 5-7 mm.

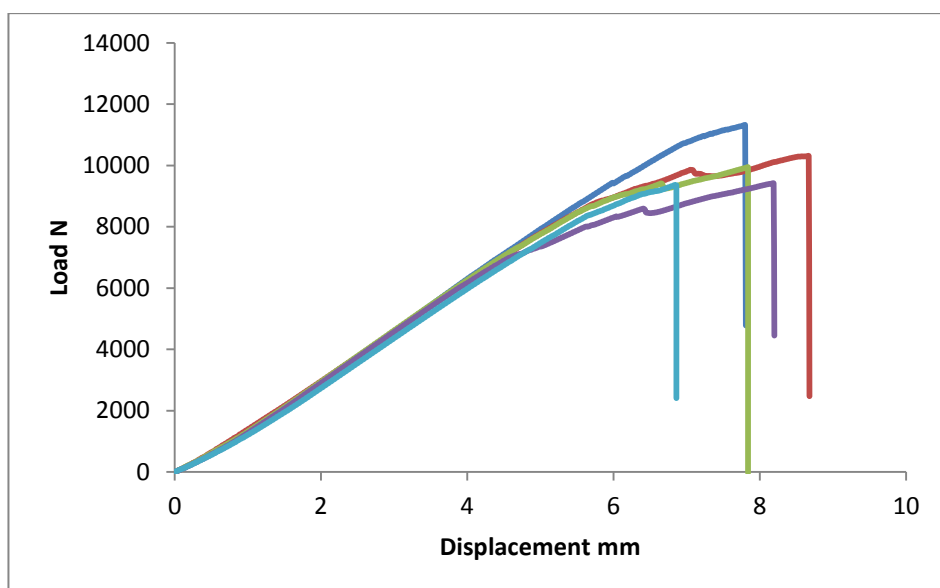


Figure 4.31 Load-Deflection diagram for the Sandwich Panels at 50°C

The figure 4.31 shows the load-deflection relationship for the sandwich panel specimens tested at 50°C. The graph representing the load- deflection relationship of the sandwich panels may be divided into three phases namely a linear phase, plastic phase and failure phase. The linear phase represents the stiffness of the sandwich panel against the applied load. In contrast to the previous case where the linear phase is followed by a non-linear phase leading to failure of the specimen, the linear phase in this case is followed by a small plastic phase due to the effect of the temperature. This plastic phase is characterized by very minor indentations formed in the core region of the specimen. The plastic phase is followed immediately by the brittle failure of the specimen at a peak load range of 9400-11300 N and peak mid-span deflection range of 6-9mm. The ultimate failure is caused due to the interlaminar shear forces developed in the core.

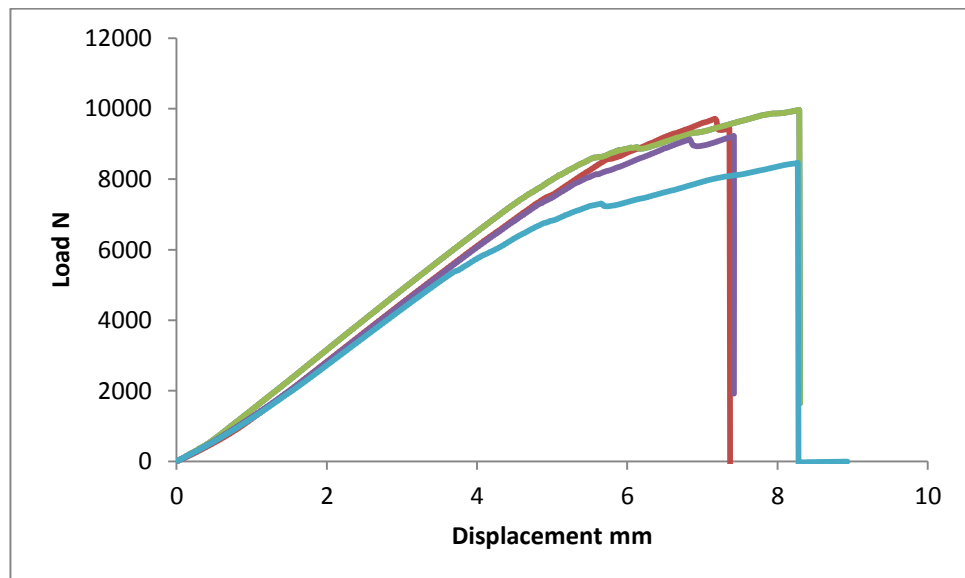


Figure 4.32 Load-Deflection diagram for the Sandwich Panels at 65°C

The figure 4.32 shows the load-deflection relationship for the sandwich panel specimens tested at 65°C. The load - deflection relationship curve is similar to the previous curve with three major phases. It may be observed that the curve possess the initial linear phase followed by the plastic phase which is more clearly identified in the graph followed by another linear phase before the final brittle failure of the specimen. The peak load range is 8500-10000 N with mid-span deflection range of 7-8.5 mm. The plastic phase exhibited is characterized by the indentations on the core before the brittle

failure. The ultimate failure of the specimen is brought about by the interlaminar shear forces developed in the core.

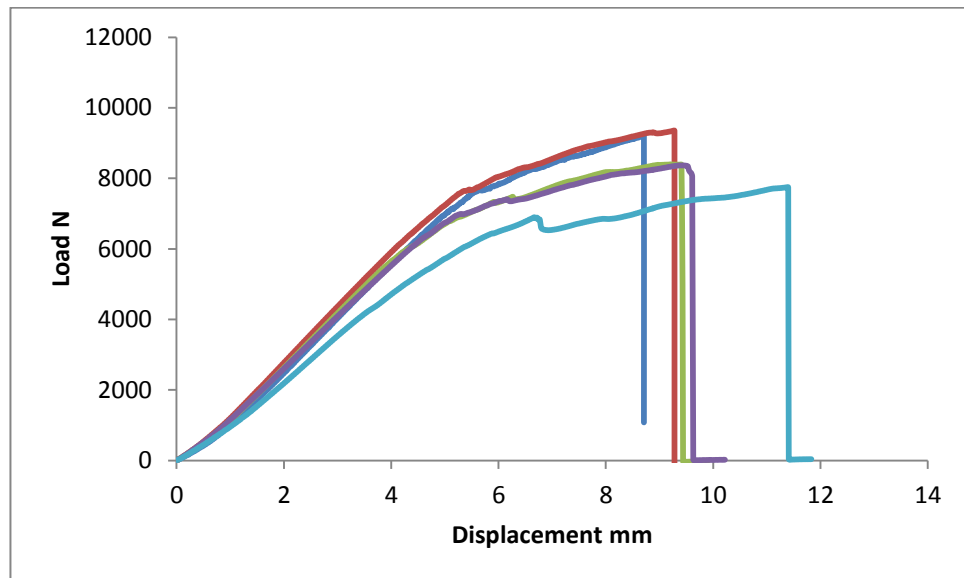


Figure 4.33 Load-Displacement diagram for the Sandwich Panels at 80°C

The figure 4.33 shows the load – displacement relationship for the sandwich panel specimens tested at 80°C. The load – displacement curve can be divided into three phases namely the linear, plastic and failure phase. The curve begins with initial linear phase followed by the plastic phase. Unlike the previous case, the plastic phase is followed immediately by the brittle failure of the specimen with a peak load range of 7750 – 9200 N and mid-span deflection range of 8.7 – 11.50 mm. The effect of temperature is characterised by the indentations formed in the core before the failure and in the skin at the point of loading. However the ultimate failure is characterised by the interlaminar shear developed in the core of the specimen.

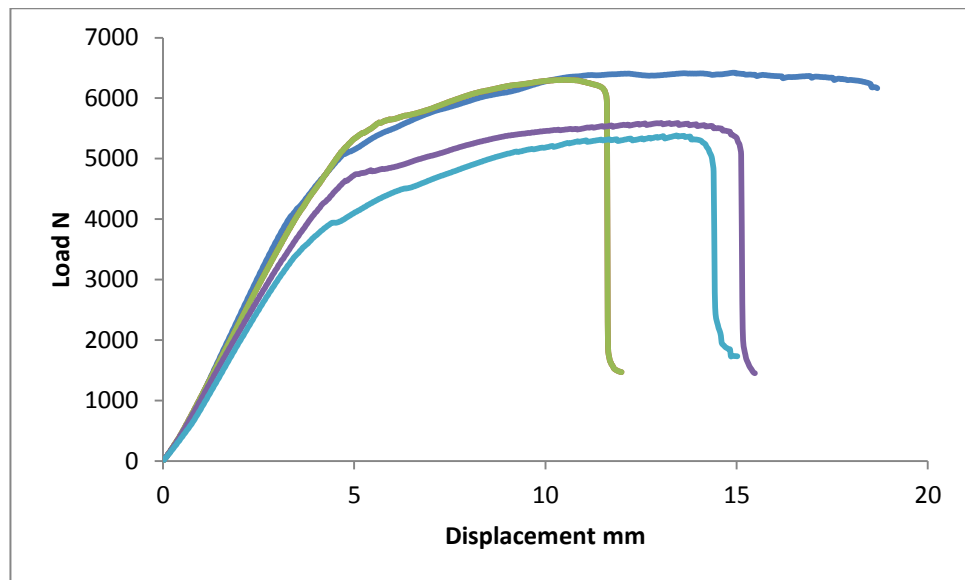


Figure 4.34 Load-Deflection diagram for the Sandwich Panels at 100°C

The figure 4.34 shows the load – displacement relationship for the sandwich panel specimens tested at 100°C. The curve representing the load – displacement may be divided into two phases namely the linear phase followed by the plastic phase. It may be observed that the failure of the specimen ceases to be brittle in nature and tends to follow a plastic mode of failure. This change in the failure mode followed may be attributed to the phenomenon of core softening which is characterized by the appearance of major indentations on the core and the indentations formed on the skin directly below the point of loading. The failure takes place at a peak load range of 5300 – 6500 N and the mid-span deflection range of 10 – 14 mm. The ultimate failure of the specimen takes place due to the interlaminar shear forces developed in the core.

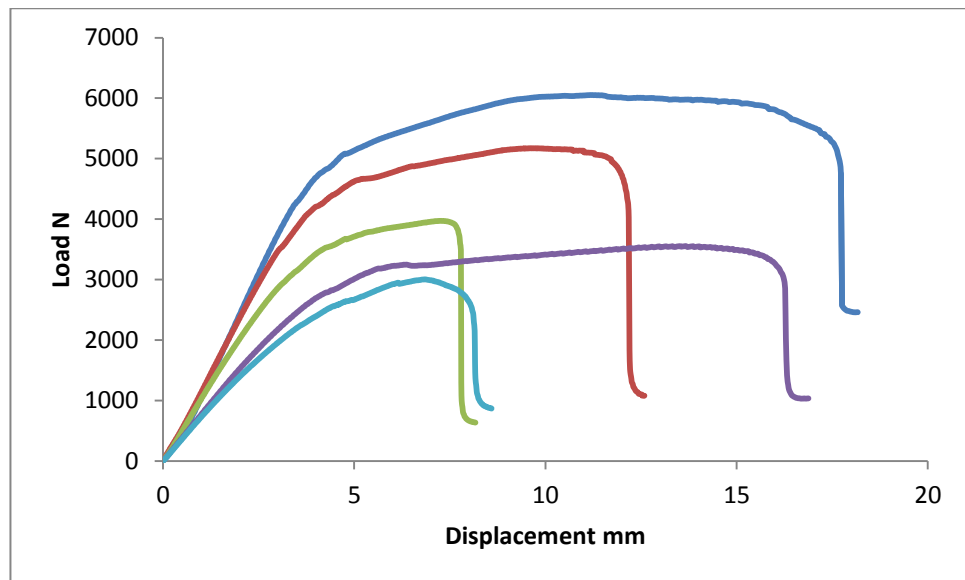


Figure 4.35 Load – Displacement diagram of the Sandwich Panels at 120°C

The figure 4.35 shows the load – displacement relationship for the sandwich panel specimens tested at 120°C. The curve showing the load – displacement relationship for the specimens tested at 120°C is divided into two phases similar to the previous curve. It can be observed from the graph that the curve follows a more plastic failure mode than that exhibited in the previous modes. The effect of temperature is attributed by the indentations found on the core as a result of the core softening phenomenon. The indentations are visible clearly even after the failure of the specimen due to interlaminar core shear. The failure occurs at a peak load range of 3000 – 6050 N and the mid-span deflection range of 6.5 – 13.5 mm.

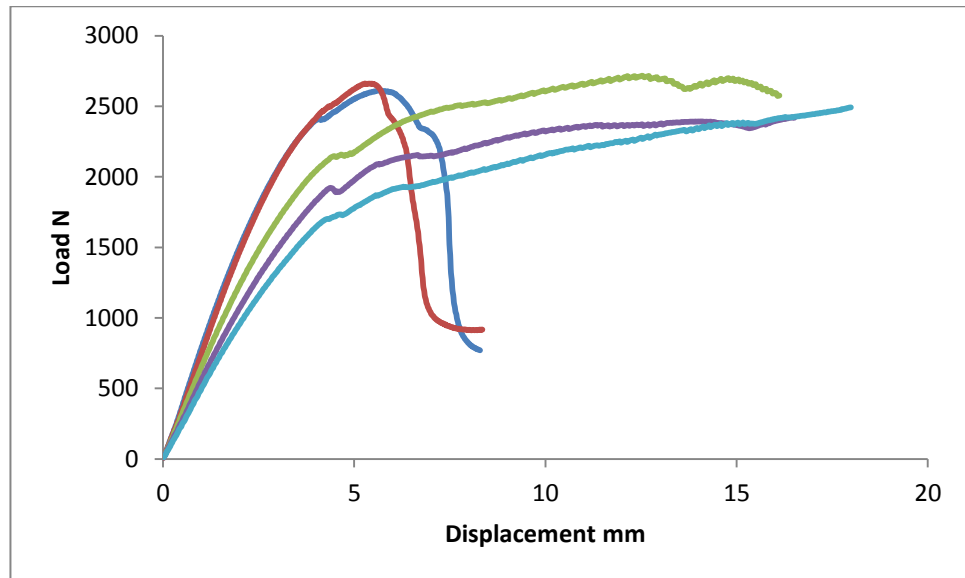


Figure 4.36 Load-Deflection diagram for the Sandwich Panels at 150°C

The figure 4.36 shows the load – displacement relationship of the sandwich panels tested at 150°C. From the graph it may be observed that the curve follows a completely plastic mode of failure. This may be attributed to phenomenon of the resin core being affected more by the temperature than the composite skins. As the core is exposed to the temperature beyond the glass transition temperature ( $T_g$ ), the resin core starts to decompose leading to the plastic failure. The phenomenon of the resin embrittlement observed in the skin when exposed to higher temperatures in the earlier tests is also clearly observed in case of the specimens tested at 150°C. A distinct odour of burning of the epoxy was observed during the heating of the specimen. The peak load range reduces to 2400 – 2800 N and the mid-span deflection range is between 5 - 18 mm.



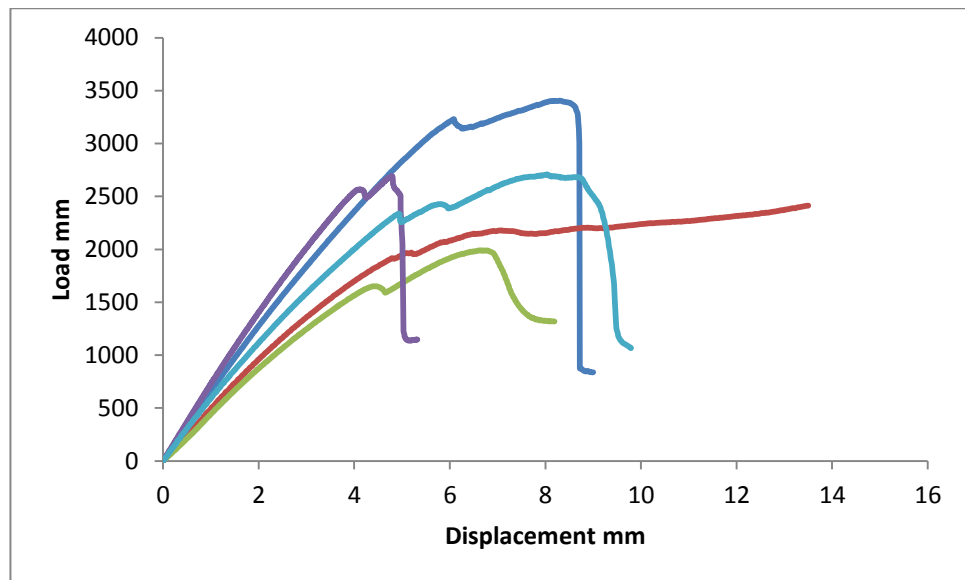


Figure 4.37 Load-Deflection diagram for the Sandwich Panels at 180°C

The figure 4.37 shows the load – deflection relation of the sandwich panels tested at 180°C. The phenomenon of the resin decomposition beyond the glass transition temperature is clearly visible beyond the linear phase of the curve exhibited in the graph before the plastic failure of the specimen. A strong odour marking the burning of the epoxy was observed as the specimen was exposed to the elevated temperature of 180°C. There is a slight increase in the peak load carrying capacity which lies in the range of 1900 – 3400 N and the mid span deflection lies in the range of 8 – 13.5 mm.

## 4.6 Failure Modes of the Sandwich Panels

### 4.6.1 Failure modes at 21°C and 35°C



Figure 4.38 Failure modes at 21°C and 35°C

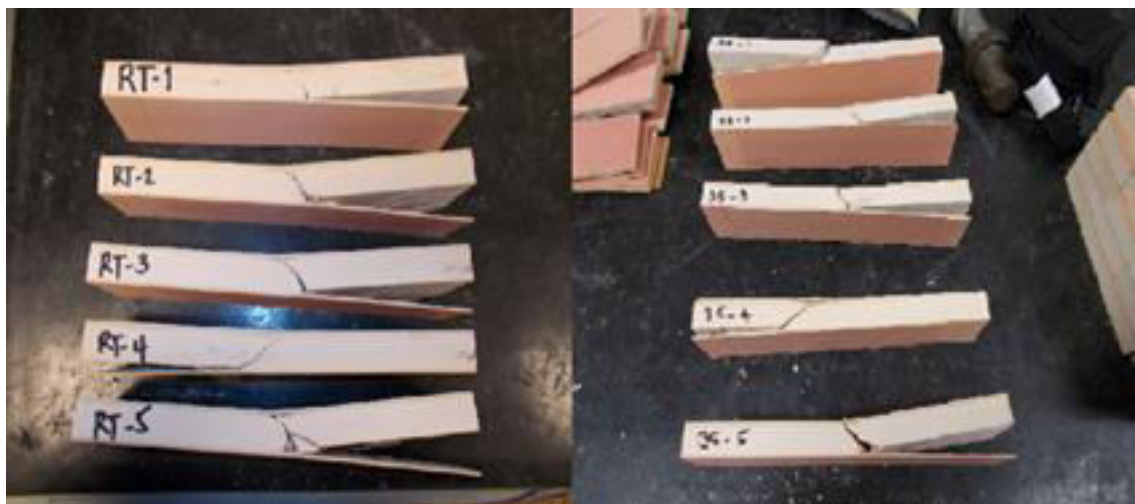


Figure 4.39 Delamination failures at 21°C and 35°C

The figure 4.38 shows the failure modes of the specimens tested at the temperature range of 21°C and 35°C. From the figure it is observed that the specimens follow the same mode of failure from room temperature and 35°C. The failure is initiated due to the cracks developed on the compression side of the specimen followed by the ultimate failure due to interlaminar shear developed in the core which results in the breaking of the structure. From the figure 4.39, it can also be observed that the failure is characterised by the de-bonding between the skin and the core due to the delamination of the individual plies of the skin laminate from the core.

#### 4.6.2 Failure modes at 50°C, 65°C and 80°C

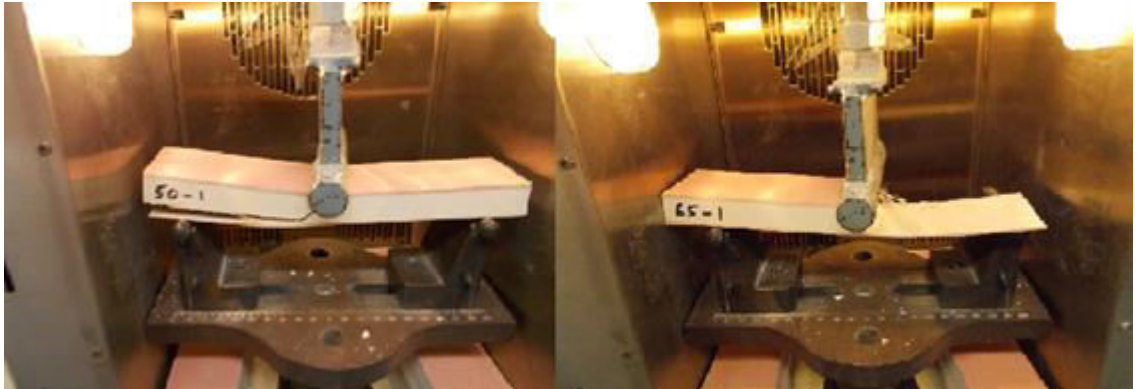


Figure 4.40 Failure modes at 50°C and 65°C

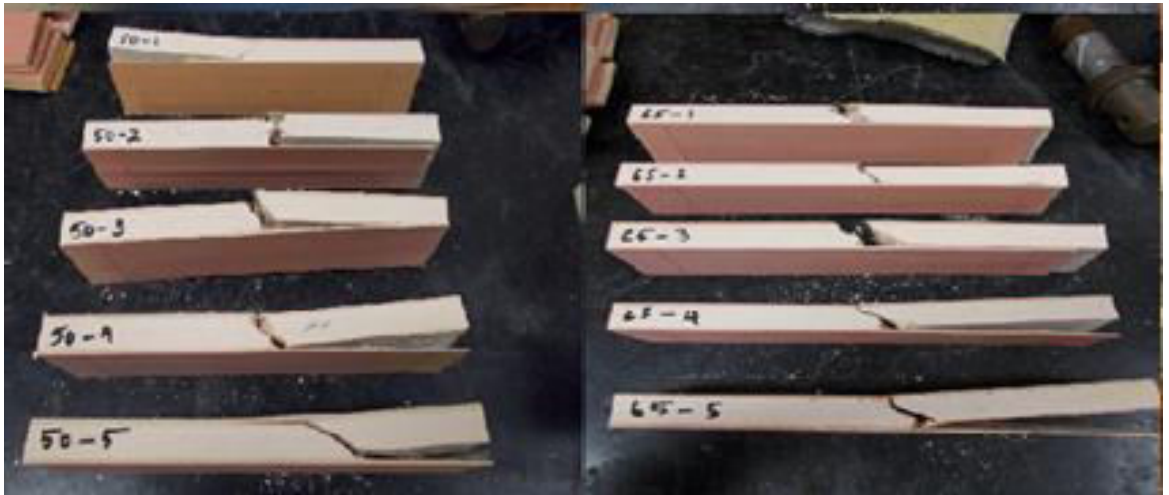


Figure 4.41 Delamination failures at 50°C and 65°C

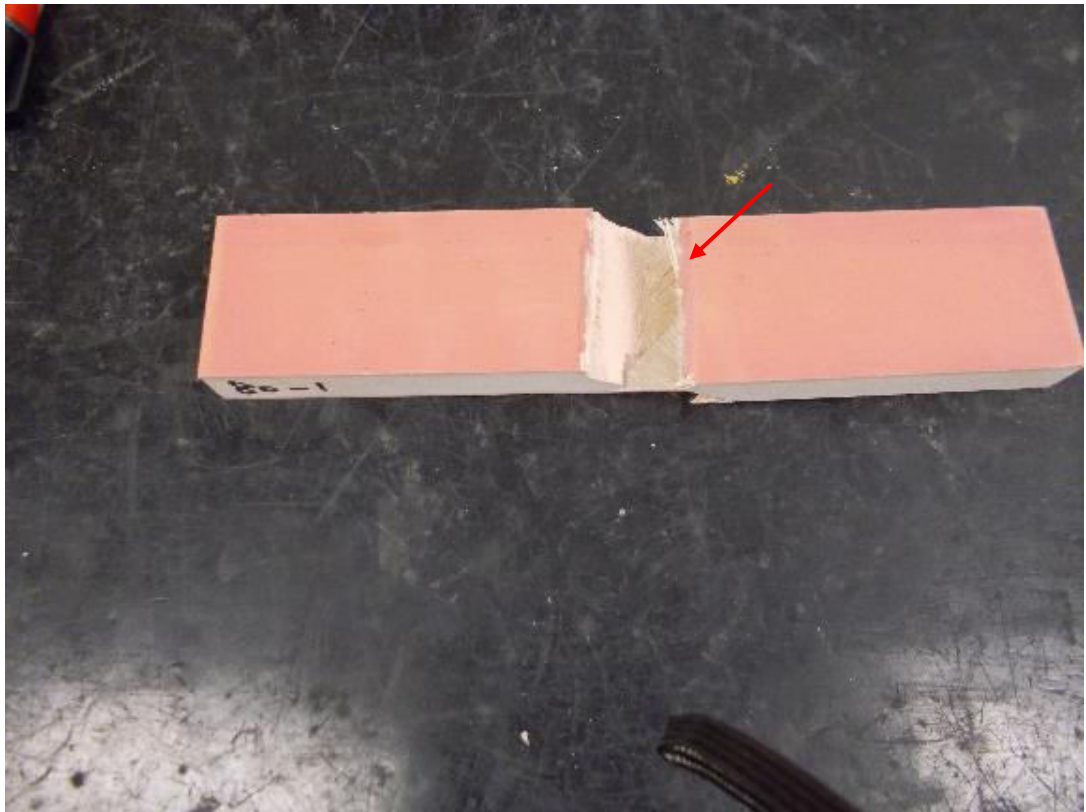


Figure 4.42 Failure mode of the specimen at 80°C

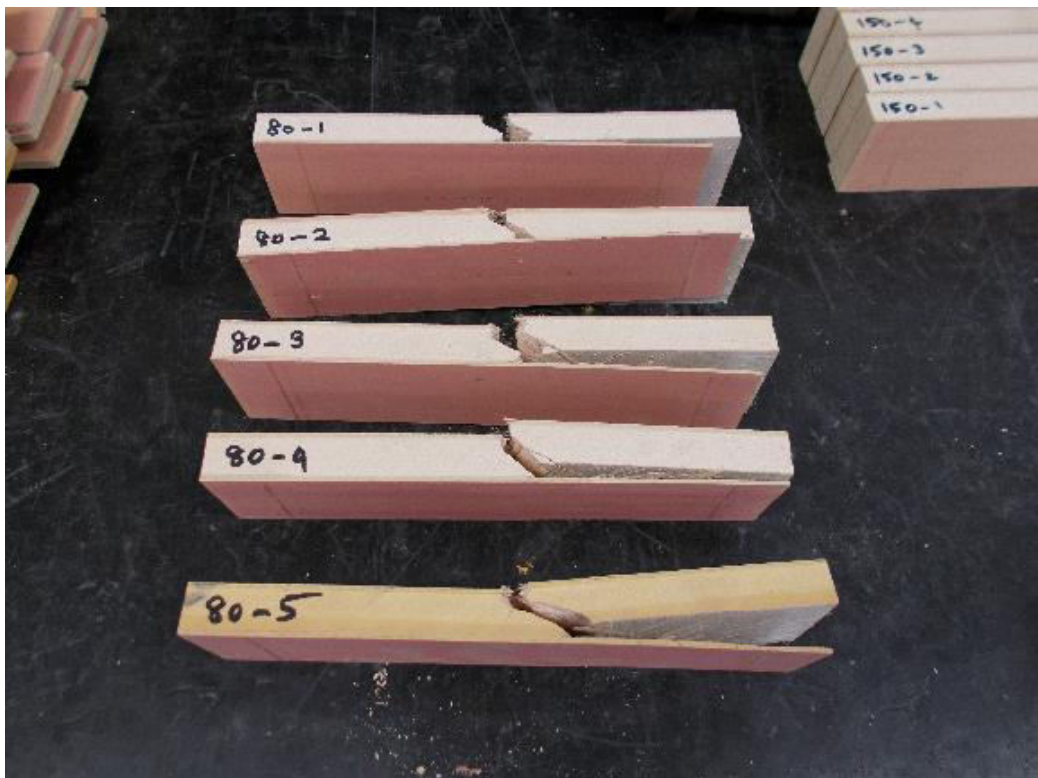


Figure 4.43 Delamination of the plies at 80°C

The figure 5.25 to 5.28 shows the failure modes followed by the sandwich panel from the temperature range of 50°C to 80°C. From the load-displacement diagram of the sandwich panels tested from 50°C to 80°C, it was observed that the panels exhibit a plastic phase before failing in a brittle manner due to the inter-laminar shear in the core of the panel. This plastic phase may be due to the effect of temperature on the resin which is observed in the form of indentations in the top skin of the panel at the point of loading which is indicated in the figure 4.42. It is also observed that the de-bonding between the skin and the core occurs due to the delamination of the individual plies of the skin which is similar to the failure modes observed in the previous temperature range.

#### 4.6.3. Failure Modes at 100°C and 120°C



Figure 4.44 Failure mode of the specimen at 100°C

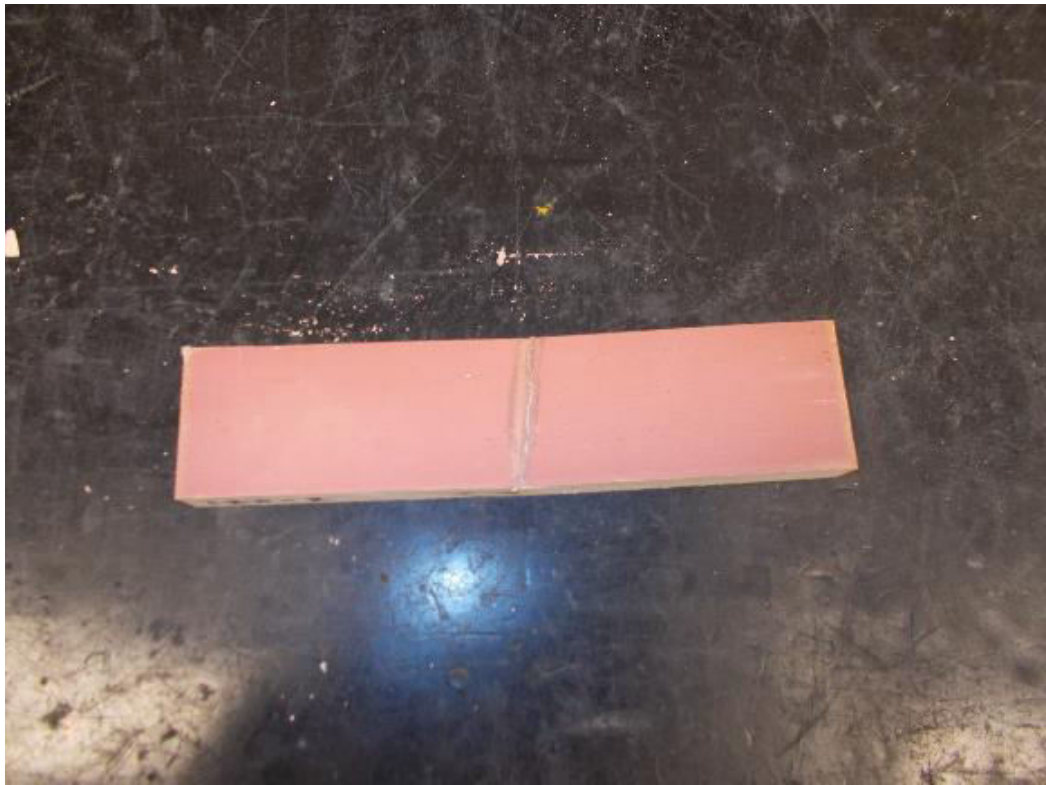


Figure 4.45 Failure mode of the specimen at 120°C

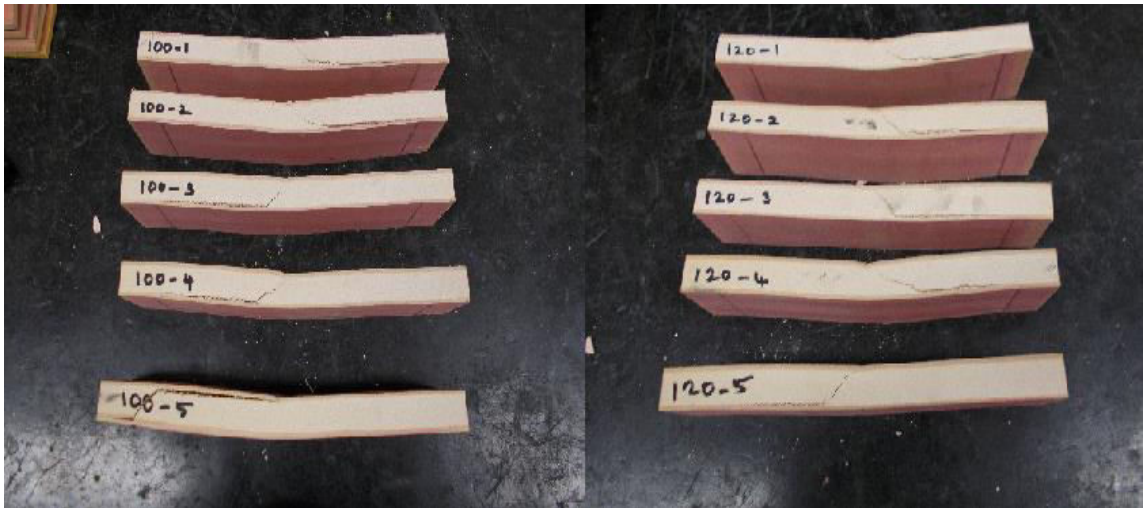


Figure 4.46 Delamination of the core at 100°C and 120°C

The figures 4.44, 4.45 and 4.46 show the failure modes of the sandwich panel specimens at 100°C and 120°C. From the load-displacement diagrams of the specimens tested at 10°C and 120°C, it was found that the failure beyond 100°C ceases to be brittle and follows a plastic mode of failure. This plastic mode of failure may be attributed to the

phenomenon of core softening which is observed in the top skin as well as the resin core of the sandwich panels in the form of indentations as shown in the figures 4.44 and 4.45. From the figure 4.46 it can be observed that the de-bonding of the skin and the core takes place due to delamination of the core with the skin remaining intact which is also due to the phenomenon of core softening at higher temperature. The ultimate failure takes place by the interlaminar shear failure of the core.

#### **4.6.4 Failure modes of the sandwich panel at 150°C and 180°C**

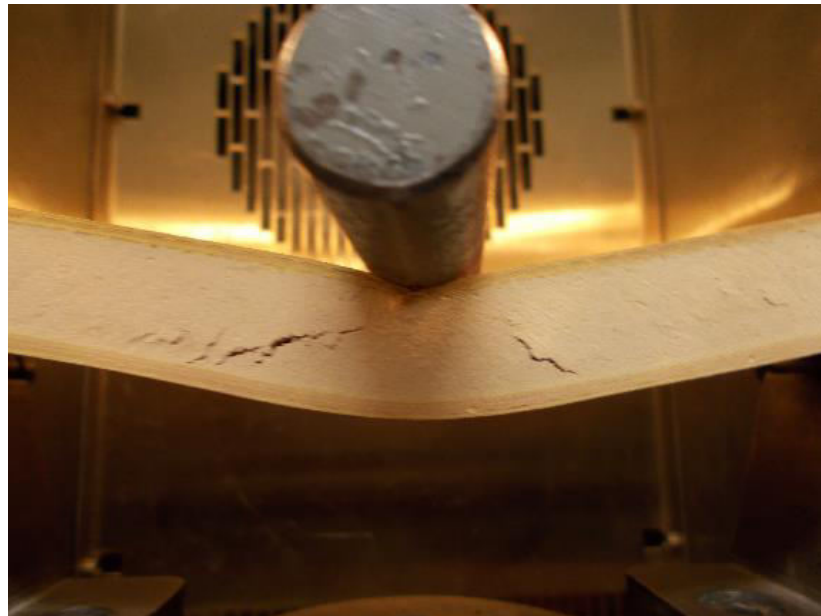


Figure 4.47 Failure of the specimen at 150°C



Figure 4.48 Failure of the specimen at 180°C

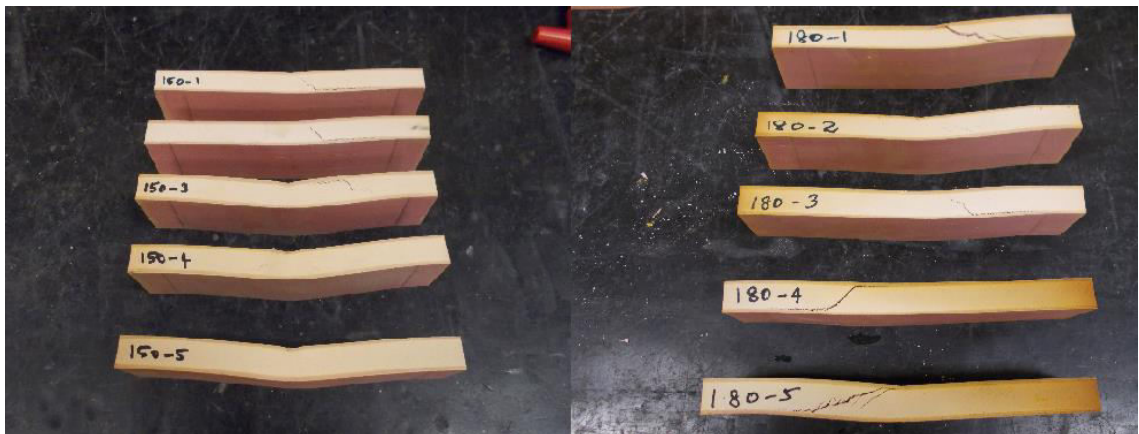


Figure 4.49 Delamination of the core at 150°C and 180°C

The figures 4.47 and 4.48 show the failure modes of the sandwich panel specimens at 150°C and 180°C. From the load displacement diagram of the sandwich panels it was observed that the specimens exhibit plastic mode of failure which attributed to the phenomenon of core softening as an effect of temperature. The phenomenon of the core softening is characterized by indentations as shown in the figures 4.47 and 4.48. At temperatures beyond the glass transition temperature the resin turns brittle which is characterized by the wrinkling of the top skin at the point of loading. The de-bonding of



the skin and the core takes place due to the delamination of the core from the skin as a result of core softening which is observed beyond 100°C. Similar to the other failure modes, the ultimate failure of the specimen takes place due to the interlaminar shear at the resin core of the sandwich panel.

#### **4.7. Summary**

In this section the various results and the observations made during the testing of the skin and the sandwich panel specimens was discussed in detail. The results observed from the Dynamic Mechanical Analysis of the skin and core reveal the behaviour of the composite skin and the resin core under elevated temperatures and the glass transition temperature of the skin and the core were identified as 125.06°C and 136.11°C respectively. The load-deflection diagrams obtained from the testing of the skin and the sandwich panels were explained in detail in order to identify the behaviour of the sandwich panels under elevated temperature. Finally the various failure modes observed under each temperature range was discussed in detail in order to understand the ultimate failure behaviour exhibited by the skin and the sandwich panel specimens.

## Chapter 5 – Discussion

### 5.1. Mechanical Properties of the skin and core under Dynamic Mechanical Analysis (DMA)

The composite skin and the resin core exhibit the glassy, leathery and the transition from glassy to leathery state which explains the similar behaviour observed in the phases 1 and 2 from the results of the DMA test on the skin and the core. A similar observation in the behaviour of the composite and the resin was observed by Lauobi et al (2014) from the DMA results of E-glass fibre reinforced with unsaturated polyester. The results from the study made on E-glass fibre indicates that for the composites at temperatures lower than 60°C, a slow decrease in storage modulus ( $E'$ ) is observed in the phase 1 followed by the steep decrease in the storage modulus from temperature range of 60°C to  $T_g$  of around 81°C for the composite and temperatures less than  $T_g$  of 64°C for the resin which is observed in phase 2. The phase 1 which is specific to the composite as observed by Lauobi et al is absent for the composite skin tested in this study. Bai and Keller (2009) also observed a similar trend in the DMA curve of GRPF laminates with polyester resin, where the storage modulus continuously decreased until the glass transition temperature of 155°C for the composite. However, beyond the glass transition temperature ( $T_g$ ), the composite skin under studied in this research exhibits the transition from the leathery to rubbery state where the polymeric chains tends to towards an entangled molecular structure with broken secondary bonds and intact primary bonds. This behaviour is characterized by the decrease in the Tan delta or the loss factor curve observed in the graph. On the other hand, the resin core exhibits a decomposition phase which is characterized by broken primary and secondary bonds. This behaviour is observed as the irregularity in the graph beyond the glass transition temperature ( $T_g$ ) in the tan delta curve. This behaviour of the composite skin and the resin core beyond the glass transition temperature is in contrast to the results observed from the DMA results of the previous studies conducted on composites and resins. It was also observed that the composites used in the previous studies are made of polyester resin unlike the phenol-formaldehyde resin which was used in this research.

From the DMA analysis of the skin it was observed that the resin oozes out from the skin composite as shown in the figure 5.1. This phenomenon of the resin oozing out from the composite is caused as a result of the melting of the resin at higher temperature. It was also observed that the resin turns brittle the specimen is subjected to

the effect of elevated temperatures beyond 100°C. According to Lauobi et al (2014), the moisture content of the specimen is removed in the form of evaporation at 200°C. This phenomenon of resin turning brittle beyond 100°C may be attributed to this effect where the moisture content is removed from the specimen as the temperature raises.



Figure 5.1 Skin Specimens before and after DMA



Figure 5.2 DMA result of the skin

## 5.2. Load – Displacement Diagram of the Skin under Three Point Bending Test

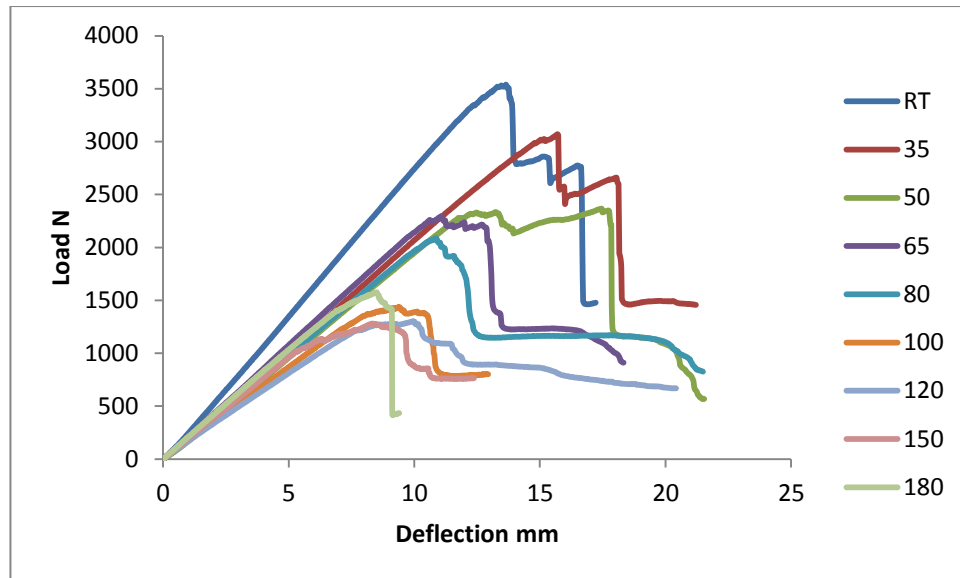


Figure 5.3 Load – Displacement diagram of the skin specimen at different Temperatures

The figure shows the load - displacement diagram of the composite skin specimens tested for their flexure under the influence of elevated temperature. From the figure 5.3 it can be observed that the behaviour of the composite skin is influenced by the effect of temperature under the three point bending test. The figure reveals three different phases that can be observed in the above graph namely the linear phase, non-linear phase and the failure phase which is either brittle or plastic. A similar observation was made by Laoubi et al (2014), when E-glass fibres with unsaturated polyesters were studied for the thermal behaviour where the specimens exhibited a linear and non-linear phase at different temperatures. The linear phase indicates the stiffness of the laminate which fails ultimately by brittle failure dominated by the interlaminar shear between the individual plies of the laminate. The linear phase is observed in the initial stages in all the specimens at all temperature ranges for the specimens studied in this research. The specimens tested under room temperature and 35°C exhibit a linear phase followed by the brittle failure of the specimen. The non-linear phase or the plastic phase indicates the phenomenon of the resin becoming soft as a result of the effect of elevated temperature. This non-linear phase is observed just after the linear phase in the

specimens tested from 50°C to 80°C. Until the temperature of 80°C the specimen fails in a brittle manner. Beyond 80°C the specimen failure of the specimen ceases to be brittle and follows a plastic mode which is a clear indication of the phenomenon of the resin softening. Similar observation of the failure modes of composites at elevated temperature was made by Wong and Wang (2004), where the composite specimens failed by crushing with a loud bang at temperatures below 90°C and beyond 90°C the specimens failed as a result of softening of the resin and by Li et al (2012), for the three point bending test of E-glass/epoxy braided composites tested for the effect of temperature on the bending properties and failure mechanisms where the composites failed in a brittle manner until 75°C and from 100°C the specimens failed in a plastic manner due to resin softening. A characteristic dis-coloration of the specimen is observed from 80°C. The specimens exhibit a pale pink colour at 80°C and 100°C and at 120°C to 150°C the specimens exhibit a yellow shade at the edges. At 180°C the specimens exhibit a brown shade indicating the effect of temperature on the physical properties of the specimen. According to Alsayed et al (2012), the change in the colour of the specimens is attributed to the decomposition of the polymer matrix and is proportional to the exposure temperature and exposure periods. According to Wong and Wang (2009), the brown colour is believed to be carbon, which indicates the beginning of the decomposition of the resin.

### 5.3. Load – Displacement Diagram of the Sandwich Panel under Three Point Bending Test

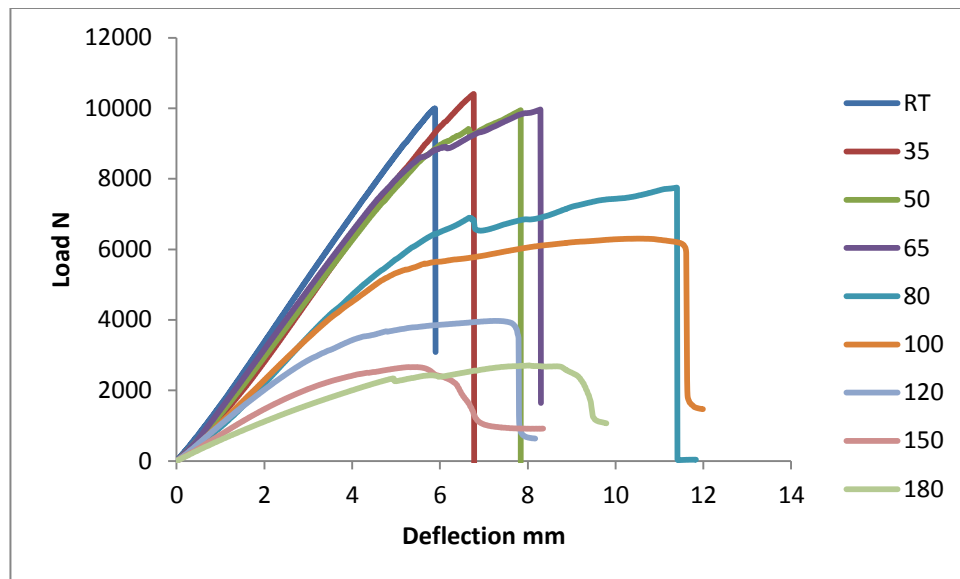


Figure 5.4 Load – Deflection diagram of Sandwich Panel specimen at different temperatures

The figure 5.4 shows the load – deflection diagram of the sandwich panel specimens tested for their flexure at elevated temperature. The specimens tested for their behaviour under three point bending test exhibited three different phases namely the linear phase, non-linear phase and the failure phase similar to the skin specimens discussed in the previous section. The sandwich panel specimens tested under room temperature and 35°C exhibit a linear phase followed by a very small non-linear phase which indicates the failure of the specimen being initiated by the formation of cracks on the compression side of the specimen. The non-linear phase is followed by the brittle failure of the specimen. The specimens tested under the temperature range of 50°C to 80°C exhibit a linear phase which is followed by a non-linear phase or the plastic phase which indicates the phenomenon of the resin core softening as a result of the effect of temperature on the sandwich panel. At temperatures beyond 80°C the linear phase is followed by a plastic phase and the failure of the sandwich panel ceases to brittle in nature by failing in a plastic manner attributed to the softening of the resin core. At the temperature of 150°C and 180°C the linear phase is immediately followed by the plastic failure indicating the failure of the core beyond the glass transition temperature of the resin which was found as 136.11°C from the DMA. The behaviour of the sandwich

panel is governed by the composite skin at lower temperature range of 21°C to 80°C and from 100°C to 180°C the behaviour of the sandwich panel is governed by the resin core than the skin. The ultimate failure of all specimens is dominated by the interlaminar shear of the core. The specimens exhibit a characteristic discoloration and a distinct odour at 150°C and 180°C. According to Liu et al (2013), the discoloration is attributed to the thermal-oxidation occurring at the surface of the epoxy resin and the exposure to high temperature had an important effect on the failure modes of the sandwich panel as observed in this study also. A similar odour of the burning of the resin was observed beyond 150°C by Liu et al (2013), which is attributed to some decomposition of the polymer matrix when exposed to elevated temperature.

#### 5.4. Effect of Elevated Temperature on the Strength of the Skin

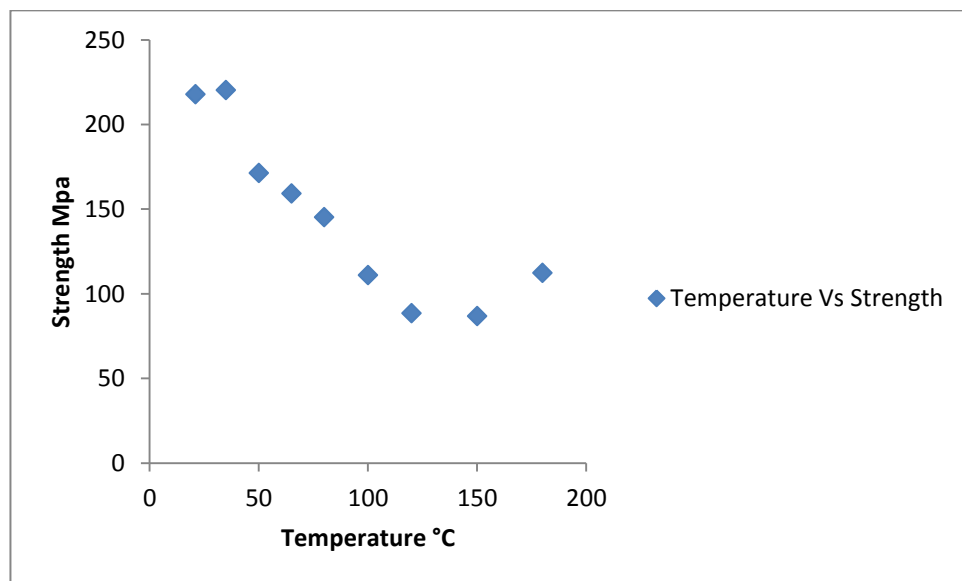


Figure 5.5 Strength Vs Temperature of the skin

The figure 5.5 shows the variation of the strength properties of the skin with temperature. From 21°C to 120°C the strength of the skin specimen shows a steady decrease with the increase in the temperature. According to Wong and Wang (2009), this steady decrease in the strength is attributed to the effect of temperature on the resin of the composite. As the temperature increases the resin softens leading to the decrease in the strength of the specimen. As the temperature progresses beyond the glass

transition temperature the effect temperature leads to the expulsion of the moisture from the resin, thereby rendering it brittle. As the resin turns brittle it results in the significant increase in the strength of the panel before the failure of the specimen.

### 5.5. Effect of Elevated Temperature on the Modulus of the Skin

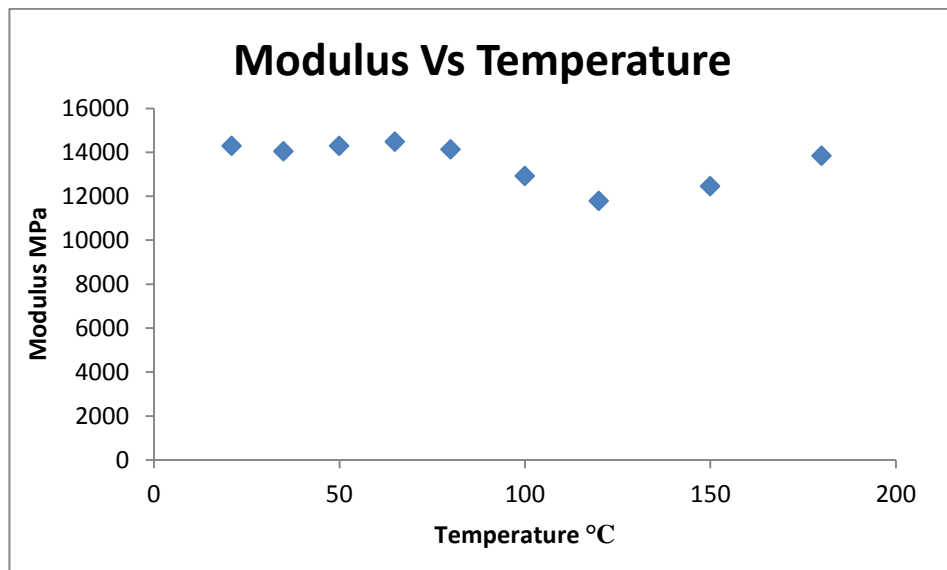


Figure 5.6 Modulus Vs Temperature of the skin

The figure 5.6 shows the variation of the Young’s modulus of the composite skin with the temperature. From the figure it is observed that the modulus of the skin is not greatly influenced by the effect of temperature until 80°C as the modulus varies steadily with the temperature. A drop in the modulus of the skin is observed at 100°C and 120°C followed by the consequent increase in the values of the modulus beyond 180°C. As the temperature progresses towards the glass transition temperature the viscosity of the specimen increases leading to the sudden change in the modulus known as the leathery state. However, beyond the glass transition temperature, the specimen enters the transition from the leathery to the rubbery state during which the viscosity of the specimen decreases leading to the increase in the modulus of the specimen as discussed in the section 5.1. A similar change of states of the composite was observed by Bai and Kellar (2009), from the DMA results of FRP composites. However, the trend of the



Young's modulus composites obtained from the results of this study contrast the observations made by Gudlur et al (2012), where the Young's Modulus of the Al/Al<sub>2</sub>O<sub>3</sub> composite decreases steadily with increase in temperature.

## 5.6. Effect of Elevated Temperature on the Strength of the Sandwich Panel

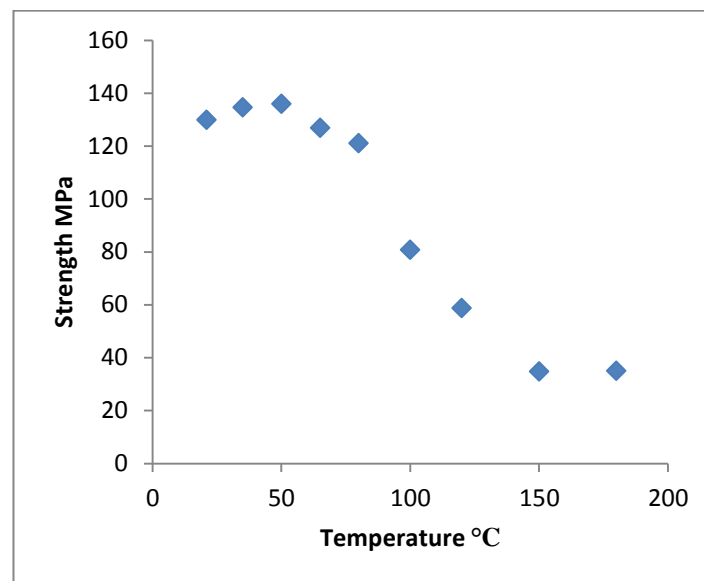


Figure 5.7 Strength Vs Temperature of the Sandwich Panel

The figure 5.7 shows the variation of the strength of the sandwich panels with temperature. From the graph it may be observed that strength of the sandwich panel shows a slight increase in the strength until 50°C before showing a steady decrease in the peak strength until 150°C and finally shows a slight increase in strength at 180°C. Although the strength of the composite skin tested under three point bending test shows a steady decrease in strength on exposure to the increasing temperature which was discussed in the previous sections, the strength of the sandwich panel shows a slight increase in its strength until 50°C which may be attributed to the increased stiffness of the sandwich panel. When the temperature is increased a fall in the strength of the sandwich panel is observed which is attributed to the effect of the temperature on the resin core. The effect of temperature on the core is observed in form of minor indentations on the top skin and the core of the sandwich panel before the brittle failure

of the specimen. When the temperature of the sandwich panels reaches 100°C and progresses towards the glass transition temperature, a rapid fall in strength is observed before the plastic failure of the specimen. The phenomenon of core softening due to the effect of temperature was observed which was characterised by strong indentations in the top skin at the point of loading and in the core. As the temperature increases beyond the glass transition temperature and reaches 150°C, a further decrease in the strength of the sandwich panel is observed which is attributed to the effect of core softening followed by the phenomenon of resin turning brittle which results in the wrinkling of the surface of the top skin of the sandwich panel. As the temperature reaches 180°C, the core softens initially which is characterised by indentations, followed by the phenomenon of the resin turning brittle as observed during the DMA tests which leads to the slight increase in the strength of the sandwich panel. The trend of the variation of the strength properties with temperature observed in this study is in contrast to the observations made by Liu et al (2013), as the strength of the carbon sandwich panels steadily decreases with the increase in the temperature.

### 5.7. Effect of Elevated Temperature on the Modulus of the Sandwich Panel

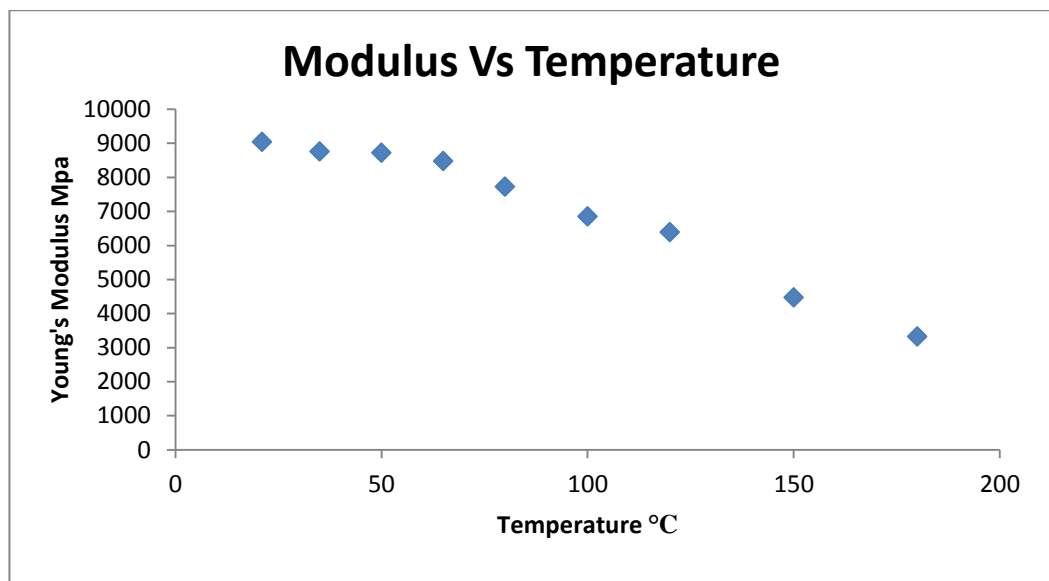


Figure 5.8 Modulus Vs Temperature of the Sandwich Panels

The figure 5.8 shows the variation of the Young's modulus of the specimen with temperature. It is found that the Young's modulus of the specimen decreases steadily with the increase in temperature until 120°C followed by a rapid decrease in the modulus of the specimen beyond the glass transition temperatures of the skin and the core. The steady decrease in the modulus of the sandwich panel may be attributed to the effect of temperature on the resin core as the trend followed by the Young's modulus curve is similar to that of the Storage modulus curve observed during the DMA test of the core. The rapid drop in the modulus beyond the glass transition temperature may be attributed to the decomposition of the core which was characterised by the irregularity observed in the results of the DMA analysis of the core. Hence, based on the results and the observations made it is found that the Young's Modulus of the sandwich panel is influenced by the behaviour of the resin core under elevated temperature. According to Liu et al the viscosity of the polymer matrix increases with exposure to temperature resulting in the decrease in the young's modulus of the specimens which indicates that the resin is susceptible to the elevated temperature.

## **5.8. Summary**

The flexural behaviour of the skin and the sandwich panel has been examined through the experimental analysis. The primary cause of the failure of the skin material at room temperature is found to be due to the compressive cracks developed at the point of loading. When the skin is subjected to a raise in temperature range of 35°C to 80°C, it is observed that the failure is initiated by the cracks developed on both the compression and the tension side of the specimen before failing due to inter-laminar shear between the individual plies of the skin. At the temperature of 100°C and 120°C the resin starts to soften before failing due to the formation of cracks and inter laminar shear between the plies. Finally at 150°C and 180°C the resin starts to decompose as it is exposed to temperatures beyond the glass transition temperature (T<sub>g</sub>). This leads to the phenomenon of the resin turning brittle due to the removal of the moisture content from the specimen.

The results from the sandwich panel reveal that the panels fail under room temperature due to the compressive failure of the skin which is closely followed by the inter-laminar

shear in the core and finally the de-bonding of the skin and the core materials. This mode of failure is observed at almost all temperatures. At 80°C a plastic phase is observed before the specimen fails in a brittle manner. The skin bends and cracks before the break failure of the specimen. It is observed that the failure takes place by the de-bonding of the skin which is characterized by the de-lamination between the individual plies of the skin. At 100°C the failure ceases to be brittle and the specimen tends to follow a plastic mode of failure. The change in the failure mode may be due to the phenomenon of core softening where the core yields characterized by indentations. The specimen bends and the failure is initiated at the tension side (bottom skin). A steep decrease in the strength is observed while the flexural modulus remains relatively the same. It is observed that the de-bonding of the skin and core takes place due to core delamination. At 120°C the failure is more plastic which is attributed to the softening of the core. The effect of core softening is characterised by major indentations on the core during the process of loading. The softening of the resin is also observed at the point of loading in the form of indentations along with cracks on the compression side. At 150°C the specimen fails primarily due to the decomposition of the core as the specimen is exposed to temperatures beyond the glass transition ( $T_g$ ). As a result of this the moisture content in core is removed which leads to the phenomenon of the resin turning brittle which is observed in both the skin and the core. The failure is characterised by major indentations at the loading point. There is a drop in the value of the flexural modulus and the peak strength. At 180°C the phenomenon of the resin decomposition is clearly characterized by the formation of cracking of the top surface of the skin just below the loading point which is similar to the result observed during the testing of the skin material under ambient temperature conditions

# Chapter 6 – Theoretical prediction of composite sandwich behaviour at elevated temperature

## 6.1. Introduction

This chapter will explain the assumptions made during the numerical analysis of the sandwich panels. The process adopted to develop the empirical equation describing the flexural behaviour of the sandwich panels under elevated temperature are also explained in this section. Finally a comparison of the experimental and the theoretical results is presented in this section.

## 6.2. Assumptions made for the Theoretical Prediction Equation

The numerical analysis of the sandwich panel is done based on the Simple Bending Theory or the Theory of flexure. The following assumptions are made for the purpose of numerical analysis of the sandwich panels under elevated temperature:

- Beam is initially **straight**, and has a **constant cross-section**.
- Beam is made of **homogeneous material** and the beam has a **longitudinal plane of symmetry**.
- Resultant of the applied loads lies in the plane of symmetry.
- The geometry of the overall member is such that bending not buckling is the primary cause of failure.
- Elastic limit is nowhere exceeded and 'E' is same in tension and compression.
- Plane cross - sections remains plane before and after bending.

## 6.3. Prediction of the Strength and the Modulus of the Skin and the Core of the Sandwich Panel

The prediction equations were calculated from the normalised curves using Microsoft Excel using the Trend line option which calculates the equation using the process of arithmetic regression. Normalisation of data was carried out by dividing the values of the strength and modulus at each temperature by the values obtained at ambient temperature. A comparison was made between the different equations types such as the exponential, linear, logarithmic and polynomial equations of various degrees. The best

fit curve was selected based on the  $R^2$  value of the equation. The  $R^2$  value denotes the how closely the developed equation fits the experimental data. In other words it denotes the accuracy of the predicted equation.

### 6.3.1. Prediction Equation for the Flexural Modulus of the skin

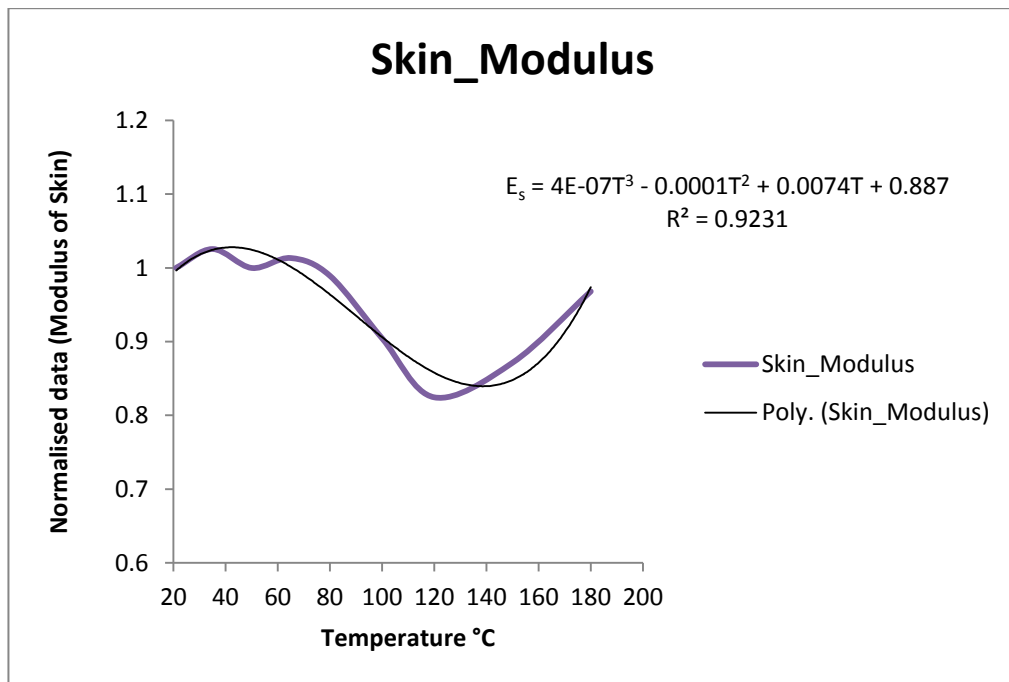


Figure 6.1 Prediction Equation for the Modulus of the skin

The equations predicting the flexural modulus of the skin was obtained from the normalised values of the average flexural modulus obtained from the three point bending test under each temperature range. The prediction equation for the modulus of the skin of the sandwich panel is developed as a 3 degree polynomial equation as it was found as the best fit to the experimental values. Further the other forms of equations were found to have an  $R^2$  value of less than 0.5. The equation predicting the flexural modulus of the skin of the sandwich panel is obtained from the above graph as

$$E_s = 4E-07T^3 - 0.0001T^2 + 0.0074T + 0.887$$

Where,

$E_s$  = Young's Modulus of the Skin

T = Temperature in °C

### 6.3.2. Prediction Equation for the Flexural Strength of the Skin

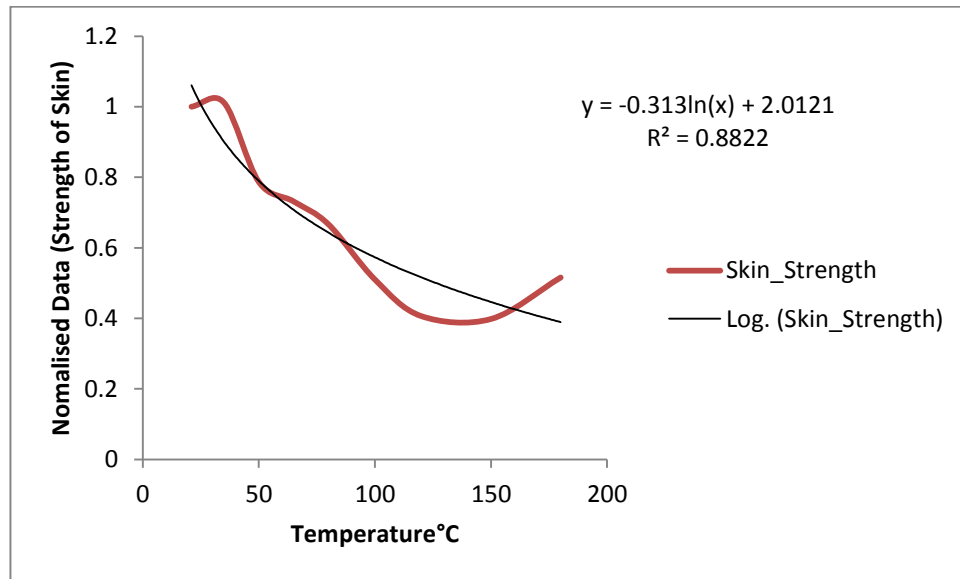


Figure 6.2 Prediction Equation for the Strength of the Skin

The strength of the skin was obtained from the normalised values of the average flexural strength obtained from the results of the three point bending test under elevated temperature. The prediction equation for the strength of the skin of the sandwich panel is computed as logarithmic equation with an  $R^2$  value of 0.88. On comparing with the other equation types it was found that the logarithmic equation and a polynomial equation of 2 degree provided the best fit. Hence for the purpose of simplicity a logarithmic equation predicting the flexural strength of the skin of the sandwich panel is obtained from the above graph as

$$\sigma_s = 4E-07T^3 - 7E-05T^2 - 0.0029T + 1.1116$$

Where,

$\sigma_s$  = Flexural Strength of the Skin

T = Temperature in °C

### 6.3.3. Prediction Equation for the Flexural Strength and Flexural Modulus of the Core

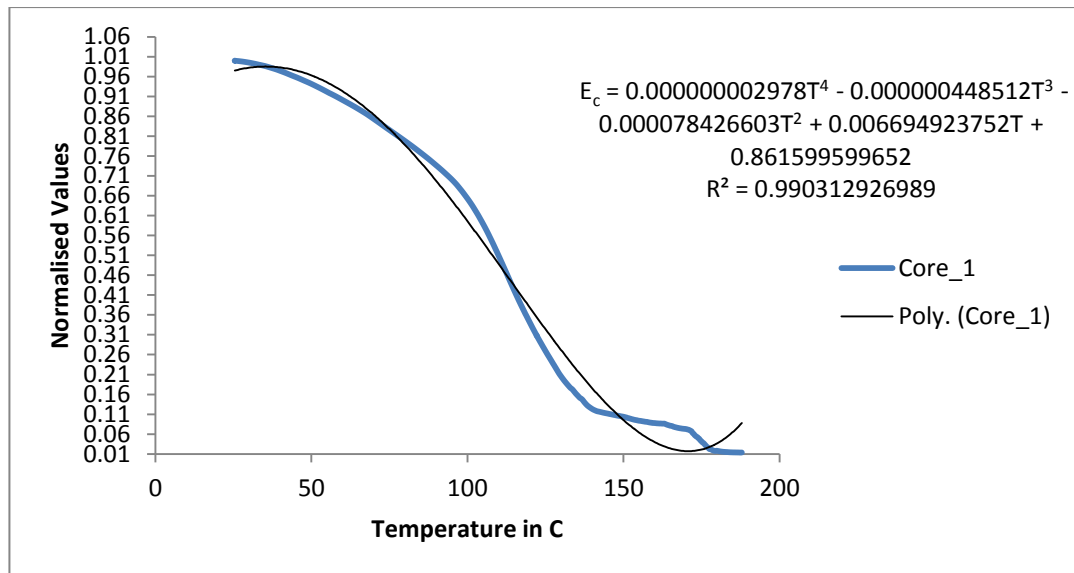


Figure 6.3 Prediction Equation for the Modulus of the Core

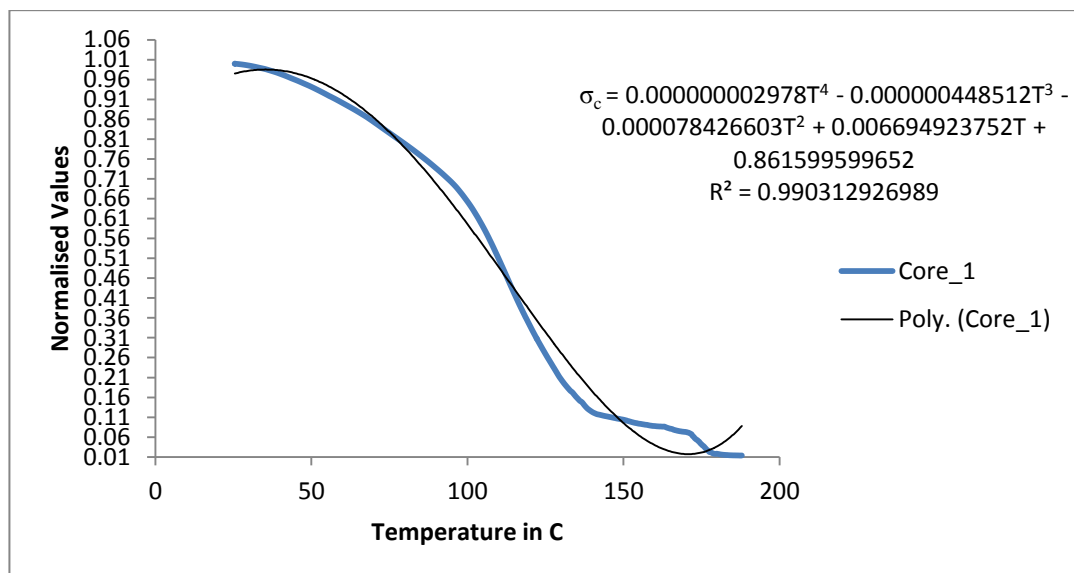


Figure 6.4 Prediction Equation for the Strength of the Core



The equations predicting the flexural strength and the modulus of the core were obtained from the normalised values of the Storage modulus obtained from the DMA of the core. This procedure was adopted to ensure that the strength and the modulus of the core followed the same trend under elevated temperature. On comparing with the other types of equations the polynomial equation was selected as the best fit for the curve with an  $R^2$  value of 0.99. A fourth degree polynomial with very high precision was selected in order to account for the values under 0.1.

Hence, the equation predicting the flexural modulus and the flexural strength of the core of the sandwich panel under elevated temperature is obtained from the above graph as

$$E_c = 0.000000002978T^4 - 0.000000448512T^3 - 0.000078426603T^2 + 0.006694923752T + 0.861599599652$$

$$\sigma_c = 0.000000002978T^4 - 0.000000448512T^3 - 0.000078426603T^2 + 0.006694923752T + 0.861599599652$$

Where,

$E_c$  = Young's Modulus of the Core

$\sigma_c$  = Flexural Strength of the Core

T = Temperature in °C

## 6.4. Empirical Equations

The empirical equation predicting the behaviour of the sandwich panels is obtained from the following procedure:

### 6.4.1. Prediction of the Theoretical Young's Modulus ( $E_{sw}$ )

The results obtained from the Dynamic Mechanical Analysis and the flexure test of the skin is normalised to capture the trends of the curves depicting its behaviour at elevated temperatures. The normalisation was carried out by dividing each value of the flexural modulus of the skin specimens obtained by the three point bending test at each

temperature by the flexural modulus of the skin specimen obtained by three point bending test at room temperature. Similarly the DMA results of the skin were normalised by dividing the values of the storage modulus ( $E'$ ) at each temperature by the storage modulus obtained by DMA at the first temperature. On comparing the normalised curves with each other it was found that the curves followed the same trend as shown in the figure 6.5

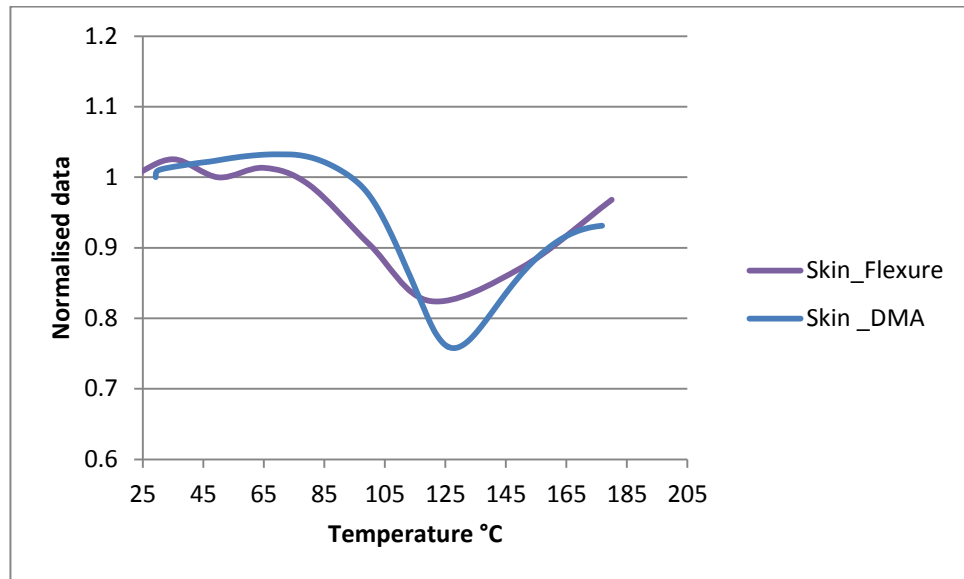


Figure 6.5 Normalised data of the skin

In order to obtain the trend of the DMA results of the core the values are normalised. The normalisation was carried out using the same procedure adopted for the skin specimens. The values of the storage modulus ( $E'$ ) obtained by DMA at each temperature was divided by the first value of the storage modulus in order to capture the trend of the normalised curve. The values of the flexural modulus of the sandwich panel obtained through the three point bending test are also normalised to capture the behaviour of the sandwich panel.

The stiffness of the sandwich panel is given by the relation:

$$E_{sw} \times I_{sw} = 2 \times E_s \times I_s + E_c \times I_c$$

Where,

$E_{sw}$  – Young’s Modulus of the sandwich panel at each temperature

$E_s$  – Young’s modulus of the composite skin at each temperature

$E_c$  – Young’s modulus of the resin core at each temperature

$I_{sw}$  – Moment of Inertia of the sandwich panel

$I_s$  – Moment of Inertia of the composite skin

$I_c$  – Moment of Inertia of the resin core

Hence the Theoretical Flexural Modulus is calculated as:

$$E_{sw} = (2E_s I_s + E_c \times I_c) / I_{sw}$$

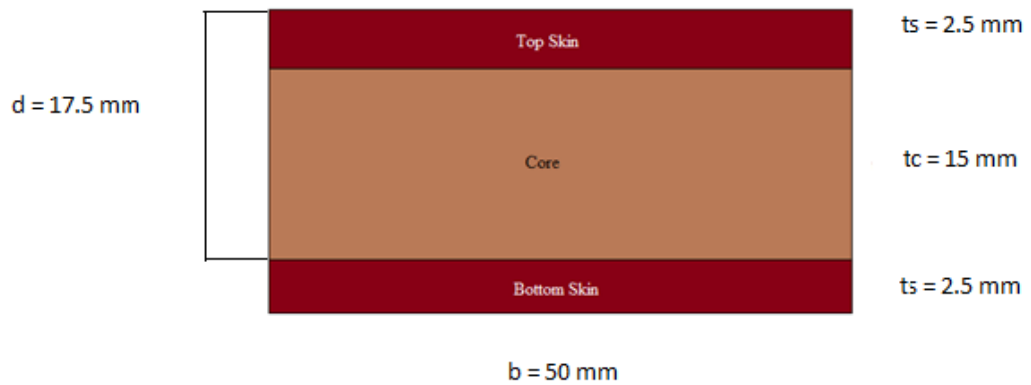


Figure 6.6 Dimensions of the Sandwich Panel

The flexural modulus of the skin obtained for each temperature from the three point bending test and the flexural modulus of the core calculated from the normalised curve using the modulus of the core at ambient temperature is incorporated in the above equation to obtain the flexural modulus of the sandwich panel at each temperature range.

#### 6.4.2. Prediction of the Strength of the Skin and the Core

The flexural strength of the sandwich panel is given by the relation:

$$\sigma = M y / I$$

Hence the theoretical strength of the skin and the core is calculated using the relation:

$$\sigma_s = (M y E_s) / (EI)_{sw}$$

$$\sigma_c = (M y E_c) / (EI)_{sw}$$

$$(EI)_{sw} = 2 * [E_s * (b * (t_s^3)) / 12 + (b * t_s * (d^2)) / 4] + E_c * b * (d^3) / 12$$

Where,

$\sigma_s$  – Strength of the skin of the sandwich panel

$\sigma_c$  – Strength of the resin core of the sandwich panel

M – Maximum bending moment of the sandwich panel

y – Distance from the neutral axis

$E_s$  – Young's modulus of the composite skin at each temperature

$E_c$  – Young's modulus of the resin core at each temperature

$(EI)_{sw}$  – Effective equivalent stiffness of the sandwich panel

b – Width of the sandwich panel

$t_s$  – Thickness of the skin

d –  $t_s + t_c$

## 6.5. Comparison of the Results

The results obtained from the theoretical prediction equation are compared with the experimental results in order to validate the prediction equation.

### 6.5.1. Comparison of the Theoretical Modulus with the Experimental Modulus

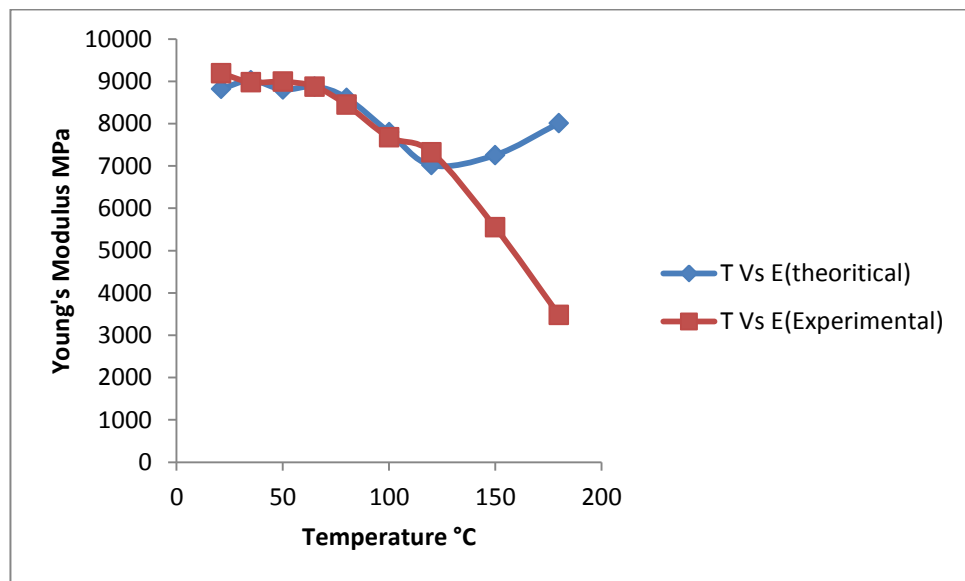


Figure 6.7 Comparison of the theoretical and experimental modulus of the skin

The figure 6.7 shows the comparison of the flexural modulus of the sandwich panel obtained by the empirical prediction equation and the experimental results obtained from the three point bending test. From the figure it is observed that the theoretical results obtained from the empirical equation correlate with the experimental results until the 120°C and beyond the glass transition temperature it is observed that the results do not correlate with the experimental results. This difference in the results may be attributed to the hypothesis of the partial loss in the composite action of the sandwich panel where the top and the bottom skins and the core behave as if they are not bonded with each other. Based on this hypothesis the partial interaction factors at 150°C and 180°C is calculated as 1.30 and 2.31 respectively.

### 6.5.2. Comparison of the Theoretical Strength of the Skin and the Core of the Sandwich Panel with the Experimental Strength

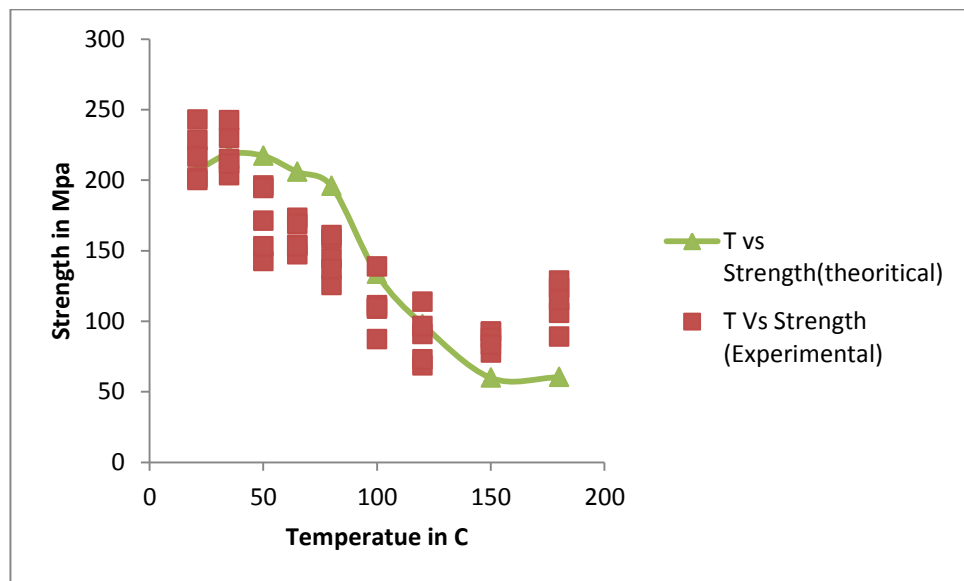


Figure 6.8 Comparison of the theoretical strength and experimental strengths of the skin

The figure 6.8 shows the comparison of the flexural strength of the skin of the sandwich panel that was obtained from the prediction equation and the three point static bending test. From the figure it can be observed that the flexural strength of the skin obtained by the experimental tests and the flexural strength obtained from the theoretical prediction equation follow the same trend with variations in their values. From this it was found that the theoretical prediction equation is able to predict the behaviour of the skin of the sandwich panel under elevated temperature.

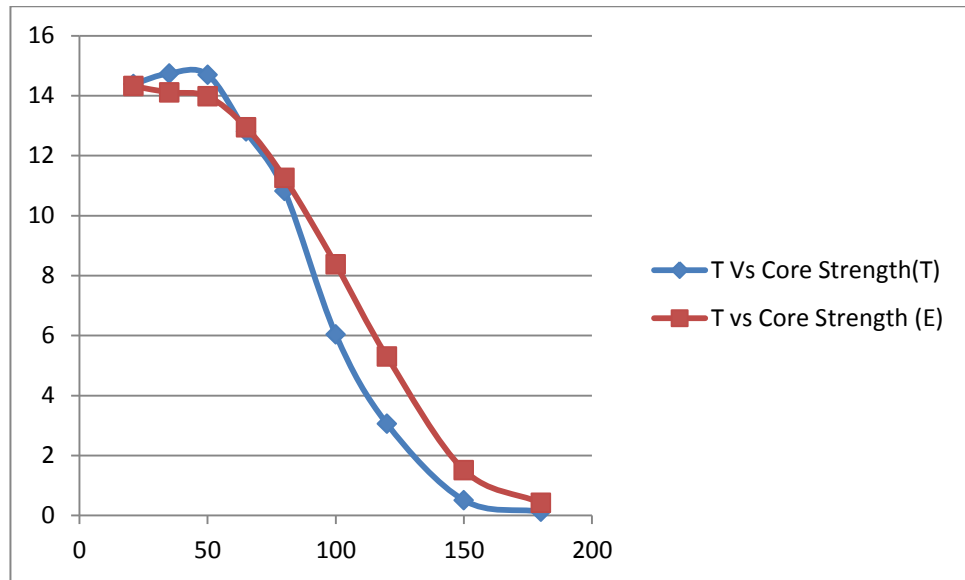


Figure 6.9 Comparison of the theoretical and Experimental Strengths of the Core

The figure 6.9 shows the comparison of the flexural strength of the core of the sandwich panel obtained from the prediction equation and the flexural strength obtained from the normalisation of the values. From the figures it can be observed that the flexural strength obtained from the prediction equation and the values obtained from the normalisation of the graph follow the same trend as observed in the of the skin of the sandwich panel in the previous case.

The variation in the theoretical and the experimental strength at temperatures may be attributed to the value of the Young’s Modulus value that is applied to calculation of the strength from the prediction equation. The theoretical strength of the skin and the core of the sandwich panel are calculated from the relations,

$$\sigma_s = (M \times y \times E_s) / (EI)_{sw}$$

$$\sigma_c = (M \times y \times E_c) / (EI)_{sw}$$

respectively as discussed in the section 6.3.2 of the chapter 6. The Young’s modulus of the skin is obtained from the linear portion of the load – displacement graph rather and not from the peak, while the moment (M) of the sandwich panel is obtained from the peak load. Further, the values of the Young’s modulus used in the above prediction equation to incorporate the effects of temperature are the average values of the flexural modulus obtained for the each temperature of the skin and the core with might significantly contribute to the variation of the result obtained.

## **6.6. Summary**

The development of the empirical equation predicting the behaviour of the sandwich panels under elevated temperature was discussed in this chapter. The various assumptions made for the purpose of developing the prediction equations was also briefly discussed in this chapter. The methods adopted to develop the prediction equations for the skin and the core were under elevated temperature was also outlined clearly. Finally a comparison of the results obtained from the experimental study and the empirical equations were compared.



# Chapter 7 – Conclusion and Recommendation

## 7.1. Conclusion

This project has studied the effect of elevated temperature on the flexural strength and the modulus of the sandwich panel under elevated temperature. The CarbonLOC<sup>®</sup> sandwich panels incorporate the use of novel phenolic core which is manufactured primarily for structural applications. The test specimens were manufactured by CarbonLOC Pvt Ltd in the manufacturing facility located at the University of Southern Queensland. The flexural behaviour of the sandwich panels under elevated temperature was determined by three point static bending tests. The mechanical properties of the constituent materials under elevated temperature were determined by Dynamic Mechanical Analysis (DMA) of the skin and the core. The results from the experimental results were used to develop an empirical equation predicting the behaviour of the sandwich panels under elevated temperature. The results of the empirical equation were compared with the obtained experimental results to validate the equations developed.

Based on the results of this investigation, the following conclusions were drawn:

- The DMA revealed that the glass transition temperature of the skin and the core was 125°C and 136°C, respectively. Further the variation of the storage modulus with the temperature was also obtained for the skin and the core which indicates the behaviour of the constituent materials of the sandwich panel under elevated temperature. Beyond the glass transition temperature the resin oozed out from the skin specimen as a result of resin softening and the resin turned brittle which is due to the expulsion of the moisture from the specimen.
- From the results of the bending test it was observed that the strength of the skin laminate decreased steadily with the increase in temperature until 120°C. The steady decrease in the strength of the skin was attributed to the effect of temperature on the resin of the composite. Beyond 120°C, the strength of the skin showed a significant increase which is attributed to the phenomenon of the resin turning brittle due to the expulsion of the moisture from the specimen as observed in the DMA.
- The strength of the sandwich panel showed a slight increase in the strength of the sandwich panel until 50°C which is attributed to the stiffness of the sandwich

panel, followed by a steady decrease in the strength until 100°C. The steady decrease in the strength of the sandwich panel is attributed to the phenomenon of resin softening which is a result of the effect of elevated temperature on the resin core of the sandwich panel. From 120°C there is a steep decrease in the strength of the sandwich panel which is attributed to the failure of the resin beyond the glass transition temperature. At 180°C, a slight increase in the strength of the sandwich panel is observed which is attributed to the phenomenon of the resin in the composite skin becoming brittle.

- The effect of temperature on the Young's Modulus of the sandwich panel was observed from the three point bending test conducted on the composite skin specimens. It was found that the modulus of the skin was not greatly influenced by the temperature until 80°C. From 100°C a steep decrease in the modulus of the skin is observed which is attributed to the increase in the viscosity of the specimen as the temperature progresses towards the glass transition temperature and the specimen enters the leathery state from the glassy state. From 120°C, the modulus tends to increase which is attributed to the decrease in the viscosity as it enters the rubbery state from the leathery state.
- The Young's modulus of the sandwich panel was observed from the three point bending test conducted under elevated temperature. The test revealed that the modulus of the sandwich panels steadily decreased until 120°C attributed to the effect of the temperature on the resin core. A sudden decrease in the modulus is observed at 150°C and 180°C, which is attributed to the phenomenon of the decomposition of the resin core which is indicated in the form of irregularities in the DMA curve of the core.
- The composite skin specimens exhibited failure modes which vary with temperature. The skin specimens tested under room temperature failed in a brittle manner by developing cracks on the compression side (top surface) of the specimen. The specimen tested at 35°C too failed in a brittle manner but the specimens developed cracks on both the compression and the tension side. The specimens tested at 50°C, 65°C and 80°C failed in a brittle manner but the specimens exhibited a plastic phase just before failing in a brittle manner which is attributed to the effect of temperature on the resin. This is characterised by minor indentation but the point of loading. At 100°C and 120°C, the failure of the skin specimens ceases to be brittle and fails in a more plastic manner. This behaviour is attributed to the phenomenon of resin softening under elevated

temperature. At 150°C and 180°C, the skin specimens fail in a completely plastic manner which is attributed to the phenomenon of the resin softening which was observed in the previous cases. At 150°C and 180°C the cracks were observed only on the compression side of the specimen. The ultimate failure occurred due to the interlaminar shear between the plies of the skin laminate.

- The sandwich panel specimens tested at room temperature and 35°C failed in a brittle manner with the failure dominated by the interlaminar shear of the core. The specimens tested at 50°C, 65°C and 80°C exhibited a plastic phase before failing in a brittle manner. The plastic phase exhibited by the sandwich panels is attributed to the effect of temperature on the resin core of the panel which is characterised by minor indentations on the core and on the top skin below the point of loading. Until 80°C, the skin de-bonds from the core due to the delamination of the individual plies of the skin. The specimens tested at 100°C and 120°C fail in a completely plastic manner which is attributed to the phenomenon of resin softening which is characterised by strong indentations on the top skin and the core at the point of loading. At 150°C and 180°C, the specimens fail in a completely plastic manner similar to the previous case. The phenomenon of resin softening is characterised by strong indentation on the core and the phenomenon of the resin turning brittle is observed in the top skin of the specimen. From 100°C the de-bonding of the skin and the core takes place due to the delamination of the core from the skin while the skin laminate stays intact.
- The theoretical equation predicting the flexural behaviour of the sandwich panel under elevated temperature was developed based on the principles of pure bending theory. The modulus of the sandwich panel was calculated from the empirical equation incorporating the effects of elevated temperature. The results from the prediction equation were compared with the experimental results. On comparison it was found that there is a partial loss in the composite behaviour of the sandwich panel at temperatures beyond the glass transition temperature 136.11°C. The strength of the skin and the core of the sandwich panel were calculated from the empirical equation and the results were compared to the experimental results. On comparison it was found that strength of the skin and the core of the sandwich panels correlated well with experimental results.

## **7.2. Recommendations for Future Work**

The results of the experimental and numerical analysis of the sandwich panels under elevated temperature reveal that the strength and the stiffness of the sandwich panels vary with the increase in the temperature. On comparing the theoretical results with the experimental results of the flexural modulus it was found that there is a partial loss in the composite action of the sandwich panel. This hypothesis could be subjected to further investigation in order to analyse the behaviour of the sandwich panels. Finally the finite element analysis of the sandwich panels is to be done in order to analyse the behaviour of the sandwich panels under elevated temperature by comparing them against the experimental results observed.

In some situation, only one side of the sandwich panel is subjected to the effect of elevated temperature. Although this scenario can be predicted through the empirical equation developed in this research, further investigation may be made in order to account for the exact temperature to which the resin core and the top and the bottom skins are subjected to.

## References

Abbasi, A & Hogg, PJ 2005, 'Temperature and environmental effects on glass fibre rebar: modulus, strength and interfacial bond strength with concrete', *Composites Part B: Engineering*, vol. 36, no. 5, pp. 394-404.

Alsayed, S, Al-Salloum, Y, Almusallam, T, El-Gamal, S & Aqel, M 2012, 'Performance of glass fiber reinforced polymer bars under elevated temperatures', *Composites Part B: Engineering*, vol. 43, no. 5, pp. 2265-71.

Asaro, RJ, Lattimer, B & Ramroth, W 2009, 'Structural response of FRP composites during fire', *Composite Structures*, vol. 87, no. 4, pp. 382-93.

Ateş, E & Barnes, S 2012, 'The effect of elevated temperature curing treatment on the compression strength of composites with polyester resin matrix and quartz filler', *Materials & Design*, vol. 34, pp. 435-43.

Awad, ZK, Aravinthan, T & Manalo, A 2012, 'Geometry effect on the behaviour of single and glue-laminated glass fibre reinforced polymer composite sandwich beams loaded in four-point bending', *Materials & Design*, vol. 39, pp. 93-103.

Awad, ZK, Aravinthan, T, Zhuge, Y & Manalo, A 2013, 'Geometry and restraint effects on the bending behaviour of the glass fibre reinforced polymer sandwich slabs under point load', *Materials & Design*, vol. 45, pp. 125-34.

Bai, Y & Keller, T 2009, 'Modeling of mechanical response of FRP composites in fire', *Composites Part A: Applied Science and Manufacturing*, vol. 40, no. 6-7, pp. 731-8.

Bai, Y & Keller, T 2011, 'Delamination and kink-band failure of pultruded GFRP laminates under elevated temperatures and compression', *Composite Structures*, vol. 93, no. 2, pp. 843-9.

Bai, Y, Keller, T & Vallée, T 2008, 'Modeling of stiffness of FRP composites under elevated and high temperatures', *Composites Science and Technology*, vol. 68, no. 15-16, pp. 3099-106.

Bosze, EJ, Alawar, A, Bertschger, O, Tsai, Y-I & Nutt, SR 2006, 'High-temperature strength and storage modulus in unidirectional hybrid composites', *Composites Science and Technology*, vol. 66, no. 13, pp. 1963-9.

Carvelli, V, Pisani, MA & Poggi, C 2013, 'High temperature effects on concrete members reinforced with GFRP rebars', *Composites Part B: Engineering*, vol. 54, pp. 125-32.

Çavdar, A 2012, 'A study on the effects of high temperature on mechanical properties of fiber reinforced cementitious composites', *Composites Part B: Engineering*, vol. 43, no. 5, pp. 2452-63.

Correia, JR, Gomes, MM, Pires, JM & Branco, FA 2013, 'Mechanical behaviour of pultruded glass fibre reinforced polymer composites at elevated temperature: Experiments and model assessment', *Composite Structures*, vol. 98, pp. 303-13.

da Costa Mattos, HS, Reis, JML, Paim, LM, da Silva, ML, Amorim, FC & Perrut, VA 2014, 'Analysis of a glass fibre reinforced polyurethane composite repair system for corroded pipelines at elevated temperatures', *Composite Structures*, vol. 114, pp. 117-23.

Davies, JM 2013, 'Thermal elongation of sandwich panels', *Proceedings of the ICE - Structures and Buildings*, vol. 166, no. 3, pp. 125-38.

De Monte, M, Moosbrugger, E & Quaresimin, M 2010, 'Influence of temperature and thickness on the off-axis behaviour of short glass fibre reinforced polyamide 6.6 – cyclic loading', *Composites Part A: Applied Science and Manufacturing*, vol. 41, no. 10, pp. 1368-79.

Fam, A & Sharaf, T 2010, 'Flexural performance of sandwich panels comprising polyurethane core and GFRP skins and ribs of various configurations', *Composite Structures*, vol. 92, no. 12, pp. 2927-35.

Feih, S & Mouritz, AP 2012, 'Tensile properties of carbon fibres and carbon fibre–polymer composites in fire', *Composites Part A: Applied Science and Manufacturing*, vol. 43, no. 5, pp. 765-72.

Feih, S, Boiocchi, E, Mathys, G, Mathys, Z, Gibson, AG & Mouritz, AP 2011, 'Mechanical properties of thermally-treated and recycled glass fibres', *Composites Part B: Engineering*, vol. 42, no. 3, pp. 350-8.

Galgano, A, Di Blasi, C, Branca, C & Milella, E 2009, 'Thermal response to fire of a fibre-reinforced sandwich panel: Model formulation, selection of intrinsic properties and experimental validation', *Polymer Degradation and Stability*, vol. 94, no. 8, pp. 1267-80.

Gibson, AG, Torres, MEO, Browne, TNA, Feih, S & Mouritz, AP 2010, 'High temperature and fire behaviour of continuous glass fibre/polypropylene laminates', *Composites Part A: Applied Science and Manufacturing*, vol. 41, no. 9, pp. 1219-31.

Gu, P & Asaro, RJ 2012, 'Skin wrinkling of sandwich polymer matrix composite panels subjected to fire exposure', *Thin-Walled Structures*, vol. 51, pp. 139-46.

Hollaway, LC 2010, 'A review of the present and future utilisation of FRP composites in the civil infrastructure with reference to their important in-service properties', *Construction and Building Materials*, vol. 24, no. 12, pp. 2419-45.

Islam, MM & Aravinthan, T 2010, 'Behaviour of structural fibre composite sandwich panels under point load and uniformly distributed load', *Composite Structures*, vol. 93, no. 1, pp. 206-15.

Laoubi, K, Hamadi, Z, Ahmed Benyahia, A, Serier, A & Azari, Z 2014, 'Thermal behavior of E-glass fiber-reinforced unsaturated polyester composites', *Composites Part B: Engineering*, vol. 56, pp. 520-6.

Li, D, Fanga, D, Zhanga, G & Hub, H 2012, 'Effect of temperature on bending properties and failure mechanism of three-dimensional braided composite', *Materials and Design*, vol. 41, pp. 167 - 70.

Liu, J, Zhou, Z, Wu, L & Ma, L 2013, 'Mechanical Behavior and Failure Mechanisms of Carbon Fiber Composite Pyramidal Core Sandwich Panel after Thermal Exposure', *Journal of Materials Science & Technology*, vol. 29, no. 9, pp. 846-54.

Liu, J, Zhou, Z, Ma, L, Xiong, J & Wu, L 2011, 'Temperature effects on the strength and crushing behavior of carbon fiber composite truss sandwich cores', *Composites Part B: Engineering*, vol. 42, no. 7, pp. 1860-6.

Manalo, A, Aravinthan, T & Karunasena, W 2012, 'Mechanical properties characterization of the skin and core of a novel composite sandwich structure', *Journal of Composite Materials*, pp. 1-16.

Manalo, A, Aravinthan, T, Karunasena, W & Islam, M 'Flexural Behaviour in Flatwise and Edge-wise Positions', *Composite Structures*.

Manalo, AC 2013, 'Behaviour of fibre composite sandwich structures under short and asymmetrical beam shear tests', *Composite Structures*, vol. 99, pp. 339-49.

Manalo, AC, Aravinthan, T & Karunasena, K 2012, 'Prediction of the Flexural Behavior of Fibre Composite Sandwich Beams', in *APIFS, 2012: proceedings of the APIFS, 2012* Hokkaido University, Japan.

Nardone, F, Di Ludovico, M, De Caso y Basalo, FJ, Prota, A & Nanni, A 2012, 'Tensile behavior of epoxy based FRP composites under extreme service conditions', *Composites Part B: Engineering*, vol. 43, no. 3, pp. 1468-74.

Nigro, E, Cefarelli, G, Bilotta, A, Manfredi, G & Cosenza, E 2014, 'Guidelines for flexural resistance of FRP reinforced concrete slabs and beams in fire', *Composites Part B: Engineering*, vol. 58, pp. 103-12.

Petras, A & Sutcliffe, MPF 1999, 'Failure mode maps for honeycomb sandwich panels ', *Composite Structures*, vol. 44, pp. 237-52.

Pihtili, H 2009, 'An experimental investigation of wear of glass fibre–epoxy resin and glass fibre–polyester resin composite materials', *European Polymer Journal*, vol. 45, no. 1, pp. 149-54.

Pradeep Gudlura, Adam Fornessa, Jonathan Lentz, Miladin Radovic & Muliana, A 2012, 'Thermal and mechanical properties of Al/Al<sub>2</sub>O<sub>3</sub> composites at elevated temperatures', *Materials Science and Engineering*, vol. 531, no. A, pp. 18 - 27.

Rudzinski, S, Häussler, L, Harnisch, C, Mäder, E & Heinrich, G 2011, 'Glass fibre reinforced polyamide composites: Thermal behaviour of sizings', *Composites Part A: Applied Science and Manufacturing*, vol. 42, no. 2, pp. 157-64.

Sun, Y & Gao, L 2013, 'Mechanical behavior of all-composite pyramidal truss cores sandwich panels', *Mechanics of Materials*, vol. 65, pp. 56-65.

Trey, SM, Kristofer Gamstedt, E, Mäder, E, Jönsson, S & Johansson, M 2011, 'Glass fiber reinforced high glass transition temperature thiol–ene networks', *Composites Part A: Applied Science and Manufacturing*, vol. 42, no. 11, pp. 1800-8.

Wang, K, Young, B & Smith, ST 2011, 'Mechanical properties of pultruded carbon fibre-reinforced polymer (CFRP) plates at elevated temperatures', *Engineering Structures*, vol. 33, no. 7, pp. 2154-61.

Wang, YC, Wong, PMH & Kodur, V 2007, 'An experimental study of the mechanical properties of fibre reinforced polymer (FRP) and steel reinforcing bars at elevated temperatures', *Composite Structures*, vol. 80, no. 1, pp. 131-40.

Wong, PMH & Wang, YC 2007, 'An experimental study of pultruded glass fibre reinforced plastics channel columns at elevated temperatures', *Composite Structures*, vol. 81, no. 1, pp. 84-95.

Wong, PMH, Davies, JM & Wang, YC 2004, 'An experimental and numerical study of the behaviour of glass fibre reinforced plastics (GRP) short columns at elevated temperatures', *Composite Structures*, vol. 63, no. 1, pp. 33-43.

Yu, B, Till, V & Thomas, K 2007, 'Modeling of thermo-physical properties for FRP composites under elevated and high temperature', *Composites Science and Technology*, vol. 67, no. 15-16, pp. 3098-109.

Zhang, Z, Chen, X & Wang, Y 2010, 'Uniaxial ratcheting behavior of polytetrafluoroethylene at elevated temperature', *Polymer Testing*, vol. 29, no. 3, pp. 352-7.



# Appendix A

## Project Specification

University of Southern Queensland

Faculty of Engineering and Surveying

### ENG8411/8412 RESEARCH PROJECT

#### PROJECT SPECIFICATION

FOR: **SWETHA SURENDAR**

TOPIC: Flexural Behaviour of Sandwich Panels Under Elevated Temperature

SUPERVISOR: Dr. Allan Manalo

ENROLMENT: ENG 8411 – S1, 2014  
ENG 8412 – S2, 2014

PROJECT AIM: The aim of this research is to understand and analyse the effect of elevated temperature on the flexural behaviour of the fibre reinforced sandwich panels through experimental investigation and analytical studies.

SPONSORSHIP: LOC Composites Pty Ltd

PROGRAMME: Issue B, 28<sup>th</sup> October 2014

1. Conduct literature review on the FRP sandwich panel and its behaviour
2. To understand and analyse the behavioural characteristics of the core and the skin materials under elevated temperature.
3. To determine the flexural behaviour of the FRP panels under elevated temperature
4. To establish an empirical equation describing the behaviour of the sandwich panels.
5. Compare the results from the experimental study and the empirical equation
6. Analysis and interpretation of results
7. Writing and submission of the thesis

AGREED

S. Seth (Student), Allan Manalo (Supervisor)  
28/10/2014 (Date) 28/10/2014 (Date)

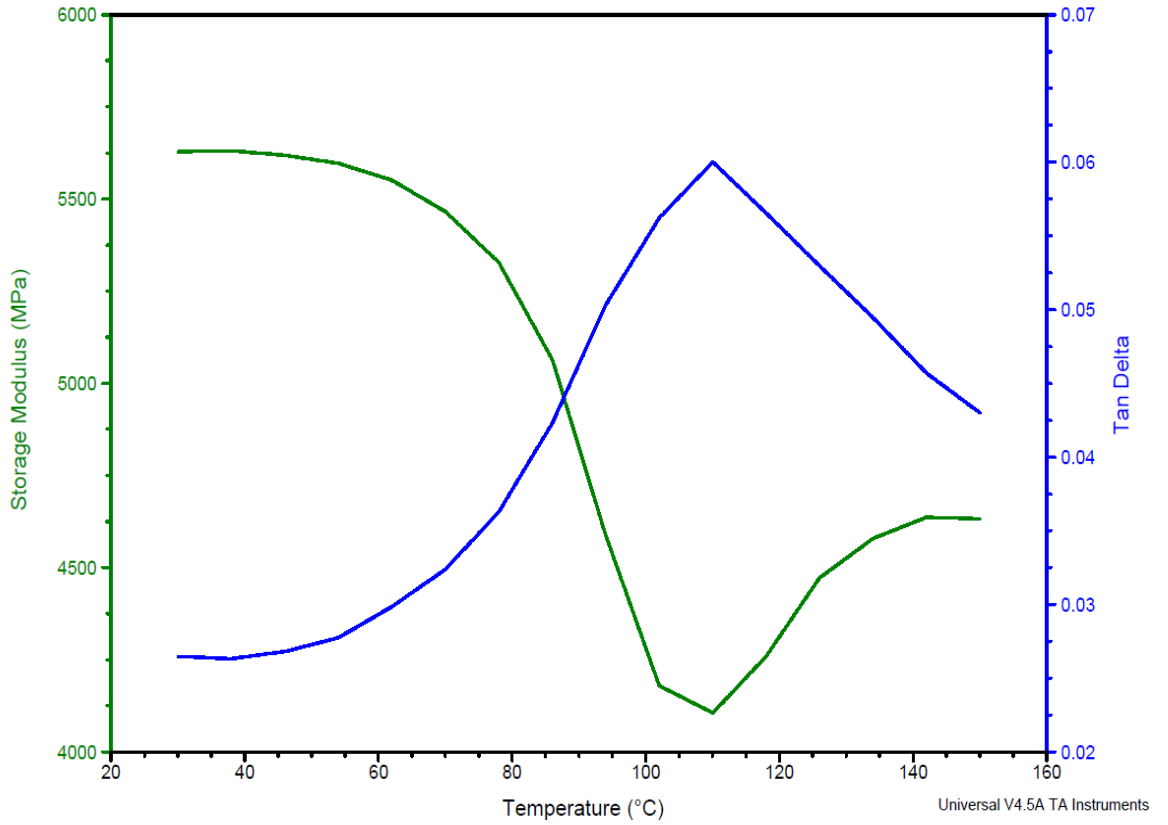
# Appendix B

## Appendix B1 Dynamic Mechanical Analysis of the Skin

Sample: CarbonLOC\_skin\_2  
Size: 35.0000 x 10.0000 x 4.9600 mm  
Method: Temp Step / Freq Sweep

DMA

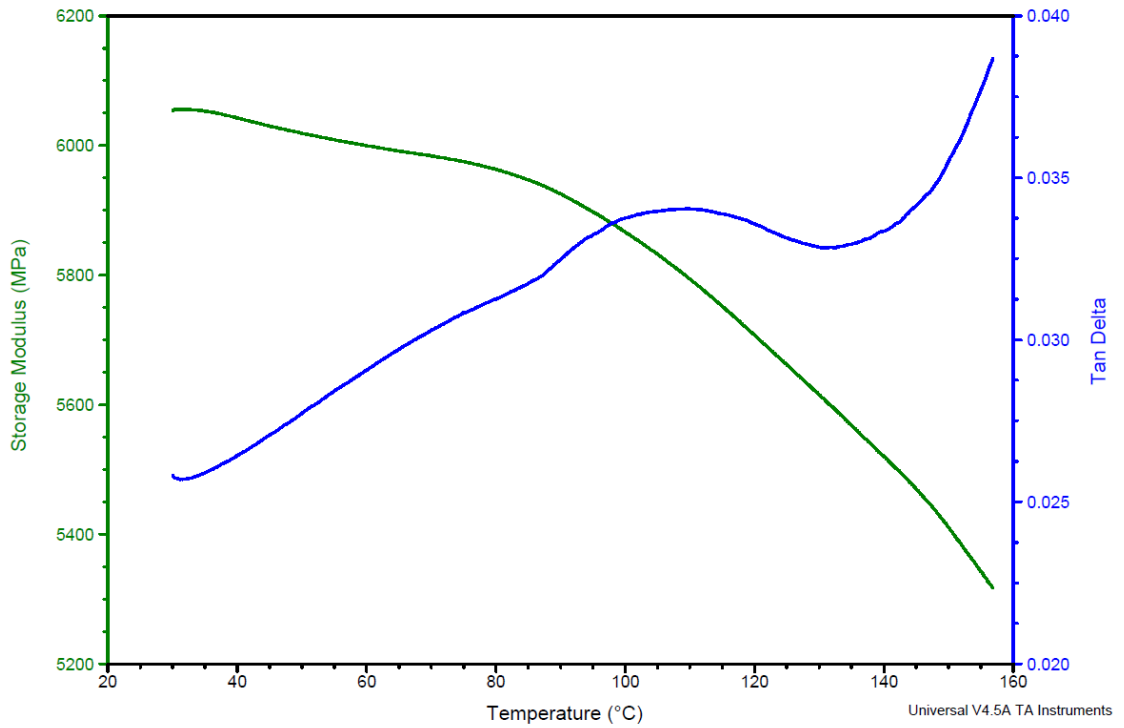
File: C:\...DMA\Allan\CarbonLOC\_Skin\_2.001  
Operator: ACM  
Run Date: 16-Jul-2014 09:18  
Instrument: DMA Q800 V5.1 Build 92



Sample: CarbonLOC\_skin\_4  
Size: 35.0000 x 9.7900 x 4.7500 mm  
Method: Temperature Ramp

DMA

File: C:\...DMA\Allan\CarbonLOC\_Skin\_4.001  
Operator: ACM  
Run Date: 16-Jul-2014 09:18  
Instrument: DMA Q800 V5.1 Build 92

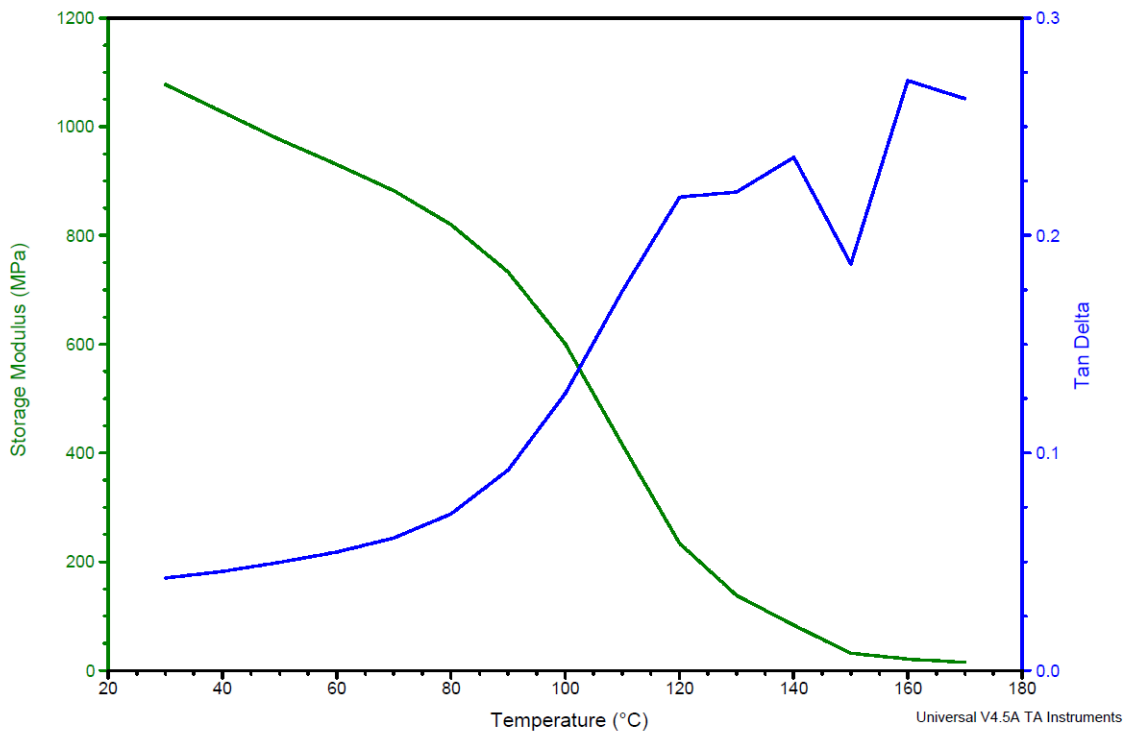


## Appendix B2 Dynamic Mechanical Analysis of the Core

Sample: Core\_2  
Size: 35.0000 x 10.1600 x 4.5300 mm  
Method: Temp Step / Freq Sweep

DMA

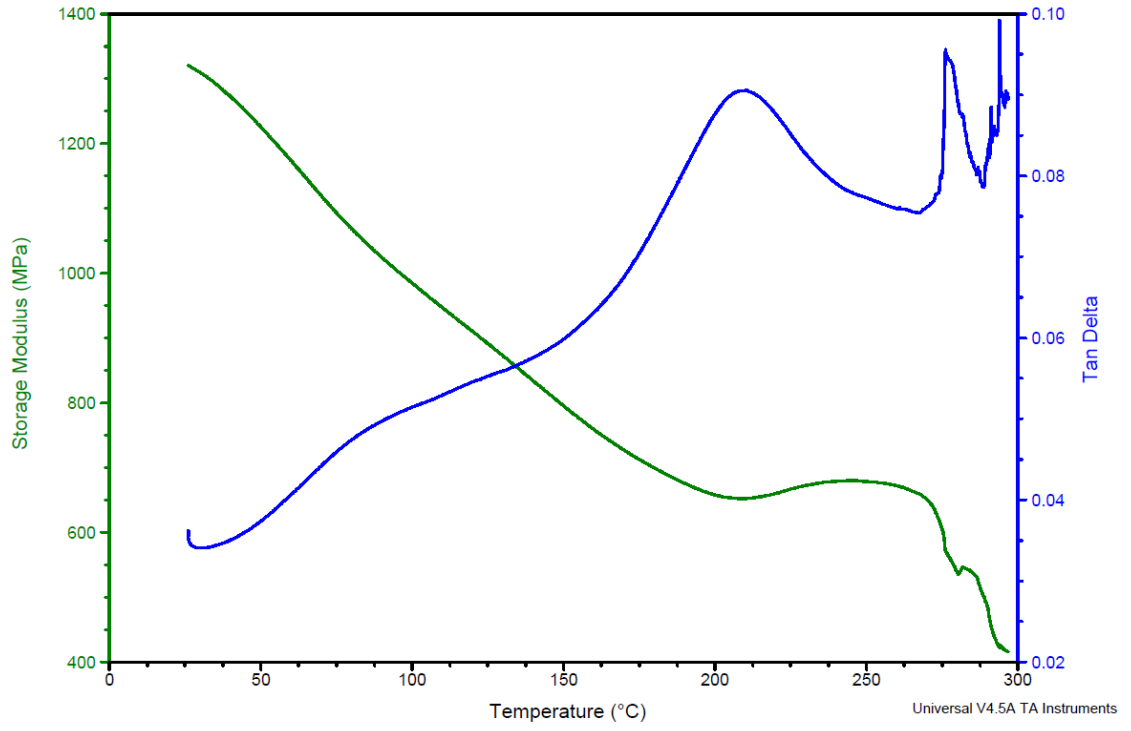
File: C:\...DMA\Allan\CarbonLOC\_Core\_2.003  
Operator: ACM  
Run Date: 24-Jun-2014 15:49  
Instrument: DMA Q800 V5.1 Build 92



Sample: Core\_5  
Size: 35.0000 x 9.7900 x 4.7500 mm  
Method: Temperature Ramp

DMA

File: C:\...DMA\Allan\CarbonLOC\_Core\_5.001  
Operator: ACM  
Run Date: 16-Jul-2014 09:18  
Instrument: DMA Q800 V5.1 Build 92



## Appendix B3 Dimensions of the Skin Specimens

### Specimen Results:

| Specimen # | Thickness 1<br>mm | Thickness 2<br>mm | Thickness 3<br>mm | Width 1<br>mm | Width 2<br>mm | Width 3<br>mm | Average Width<br>mm | Average Thickness<br>mm |
|------------|-------------------|-------------------|-------------------|---------------|---------------|---------------|---------------------|-------------------------|
| 1          | 5.22              | 5.22              | 5.22              | 51.54         | 51.54         | 51.54         | 51.54               | 5.22                    |
| 2          | 4.85              | 4.85              | 4.85              | 51.78         | 51.78         | 51.78         | 51.78               | 4.85                    |
| 3          | 5.06              | 5.06              | 5.06              | 51.19         | 51.19         | 51.19         | 51.19               | 5.06                    |
| 4          | 5.21              | 5.21              | 5.21              | 51.67         | 51.67         | 51.67         | 51.67               | 5.21                    |
| 5          | 5.09              | 5.09              | 5.09              | 51.38         | 51.38         | 51.38         | 51.38               | 5.09                    |
| 6          | 5.24              | 5.24              | 5.24              | 51.63         | 51.63         | 51.63         | 51.63               | 5.24                    |
| 7          | 4.72              | 4.72              | 4.72              | 51.41         | 51.41         | 51.41         | 51.41               | 4.72                    |
| 8          | 4.71              | 4.71              | 4.71              | 51.78         | 51.78         | 51.78         | 51.78               | 4.71                    |
| 9          | 4.72              | 4.72              | 4.72              | 51.47         | 51.47         | 51.47         | 51.47               | 4.72                    |
| 10         | 5.04              | 5.04              | 5.04              | 51.77         | 51.77         | 51.77         | 51.77               | 5.04                    |
| 11         | 4.67              | 4.67              | 4.67              | 50.10         | 50.10         | 50.10         | 50.10               | 4.67                    |
| 12         | 5.20              | 5.20              | 5.20              | 51.68         | 51.68         | 51.68         | 51.68               | 5.20                    |
| 13         | 5.09              | 5.09              | 5.09              | 51.55         | 51.55         | 51.55         | 51.55               | 5.09                    |
| 14         | 5.34              | 5.34              | 5.34              | 51.62         | 51.62         | 51.62         | 51.62               | 5.34                    |
| 15         | 4.95              | 4.95              | 4.95              | 51.75         | 51.75         | 51.75         | 51.75               | 4.95                    |
| 16         | 4.98              | 4.98              | 4.98              | 51.42         | 51.42         | 51.42         | 51.42               | 4.98                    |
| 17         | 4.90              | 4.90              | 4.90              | 51.20         | 51.20         | 51.20         | 51.20               | 4.90                    |
| 18         | 4.92              | 4.92              | 4.92              | 51.11         | 51.11         | 51.11         | 51.11               | 4.92                    |
| 19         | 5.09              | 5.09              | 5.09              | 51.58         | 51.58         | 51.58         | 51.58               | 5.09                    |
| 20         | 4.92              | 4.92              | 4.92              | 51.60         | 51.60         | 51.60         | 51.60               | 4.92                    |
| 21         | 4.84              | 4.84              | 4.84              | 50.90         | 50.90         | 50.90         | 50.90               | 4.84                    |
| 22         | 4.98              | 4.98              | 4.98              | 51.63         | 51.63         | 51.63         | 51.63               | 4.98                    |
| 23         | 5.21              | 5.21              | 5.21              | 51.65         | 51.65         | 51.65         | 51.65               | 5.21                    |
| 24         | 4.60              | 4.60              | 4.60              | 50.70         | 50.70         | 50.70         | 50.70               | 4.60                    |
| 25         | 4.92              | 4.92              | 4.92              | 51.56         | 51.56         | 51.56         | 51.56               | 4.92                    |

|                |             |             |             |              |              |              |              |             |
|----------------|-------------|-------------|-------------|--------------|--------------|--------------|--------------|-------------|
| 26             | 4.67        | 4.67        | 4.67        | 50.94        | 50.94        | 50.94        | 50.94        | 4.67        |
| 27             | 5.34        | 5.34        | 5.34        | 51.41        | 51.41        | 51.41        | 51.41        | 5.34        |
| 28             | 4.78        | 4.78        | 4.78        | 51.13        | 51.13        | 51.13        | 51.13        | 4.78        |
| 29             | 5.05        | 5.05        | 5.05        | 51.57        | 51.57        | 51.57        | 51.57        | 5.05        |
| 30             | 4.96        | 4.96        | 4.96        | 51.75        | 51.75        | 51.75        | 51.75        | 4.96        |
| 31             | 4.84        | 4.84        | 4.84        | 51.18        | 51.18        | 51.18        | 51.18        | 4.84        |
| 32             | 4.88        | 4.88        | 4.88        | 51.16        | 51.16        | 51.16        | 51.16        | 4.88        |
| 33             | 4.88        | 4.88        | 4.88        | 51.31        | 51.31        | 51.31        | 51.31        | 4.88        |
| 34             | 5.43        | 5.43        | 5.43        | 51.40        | 51.40        | 51.40        | 51.40        | 5.43        |
| 35             | 4.88        | 4.88        | 4.88        | 51.52        | 51.52        | 51.52        | 51.52        | 4.88        |
| 36             | 4.70        | 4.70        | 4.70        | 51.19        | 51.19        | 51.19        | 51.19        | 4.70        |
| 37             | 4.64        | 4.64        | 4.64        | 51.09        | 51.09        | 51.09        | 51.09        | 4.64        |
| 38             | 4.86        | 4.86        | 4.86        | 51.53        | 51.53        | 51.53        | 51.53        | 4.86        |
| 39             | 5.05        | 5.05        | 5.05        | 51.63        | 51.63        | 51.63        | 51.63        | 5.05        |
| 40             | 5.08        | 5.08        | 5.08        | 51.73        | 51.73        | 51.73        | 51.73        | 5.08        |
| 41             | 5.12        | 5.12        | 5.12        | 51.57        | 51.57        | 51.57        | 51.57        | 5.12        |
| 42             | 4.68        | 4.68        | 4.68        | 51.24        | 51.24        | 51.24        | 51.24        | 4.68        |
| 43             | 4.92        | 4.92        | 4.92        | 51.26        | 51.26        | 51.26        | 51.26        | 4.92        |
| 44             | 4.55        | 4.55        | 4.55        | 51.24        | 51.24        | 51.24        | 51.24        | 4.55        |
| 45             | 5.57        | 5.57        | 5.57        | 51.57        | 51.57        | 51.57        | 51.57        | 5.57        |
| <b>Mean</b>    | <b>4.96</b> | <b>4.96</b> | <b>4.96</b> | <b>51.40</b> | <b>51.40</b> | <b>51.40</b> | <b>51.40</b> | <b>4.96</b> |
| <b>Std Dev</b> | <b>0.23</b> | <b>0.23</b> | <b>0.23</b> | <b>0.33</b>  | <b>0.33</b>  | <b>0.33</b>  | <b>0.33</b>  | <b>0.23</b> |

**Appendix B4 Dimensions of the Core  
Specimen Results:**

| <b>Specimen #</b> | <b>Thickness 1<br/>mm</b> | <b>Thickness 2<br/>mm</b> | <b>Thickness 3<br/>mm</b> | <b>Width 1<br/>mm</b> | <b>Width 2<br/>mm</b> | <b>Width 3<br/>mm</b> | <b>Average Width<br/>mm</b> | <b>Average Thickness<br/>mm</b> |
|-------------------|---------------------------|---------------------------|---------------------------|-----------------------|-----------------------|-----------------------|-----------------------------|---------------------------------|
| 1                 | 20.59                     | 20.59                     | 20.59                     | 51.45                 | 51.45                 | 51.45                 | 51.45                       | 20.59                           |
| 2                 | 19.92                     | 19.92                     | 19.92                     | 51.33                 | 51.33                 | 51.33                 | 51.33                       | 19.92                           |
| 3                 | 19.87                     | 19.87                     | 19.87                     | 51.13                 | 51.13                 | 51.13                 | 51.13                       | 19.87                           |
| 4                 | 20.11                     | 20.11                     | 20.11                     | 50.99                 | 50.99                 | 50.99                 | 50.99                       | 20.11                           |
| 5                 | 19.65                     | 19.65                     | 19.65                     | 51.12                 | 51.12                 | 51.12                 | 51.12                       | 19.65                           |
| 6                 | 20.48                     | 20.48                     | 20.48                     | 50.97                 | 50.97                 | 50.97                 | 50.97                       | 20.48                           |
| 7                 | 19.72                     | 19.72                     | 19.72                     | 50.97                 | 50.97                 | 50.97                 | 50.97                       | 19.72                           |
| 8                 | 19.63                     | 19.63                     | 19.63                     | 51.28                 | 51.28                 | 51.28                 | 51.28                       | 19.63                           |
| 9                 | 19.81                     | 19.81                     | 19.81                     | 50.95                 | 50.95                 | 50.95                 | 50.95                       | 19.81                           |
| 10                | 19.84                     | 19.84                     | 19.84                     | 50.92                 | 50.92                 | 50.92                 | 50.92                       | 19.84                           |
| 11                | 20.11                     | 20.11                     | 20.11                     | 50.92                 | 50.92                 | 50.92                 | 50.92                       | 20.11                           |
| 12                | 19.71                     | 19.71                     | 19.71                     | 51.29                 | 51.29                 | 51.29                 | 51.29                       | 19.71                           |
| 13                | 19.70                     | 19.70                     | 19.70                     | 51.07                 | 51.07                 | 51.07                 | 51.07                       | 19.70                           |
| 14                | 19.65                     | 19.65                     | 19.65                     | 51.01                 | 51.01                 | 51.01                 | 51.01                       | 19.65                           |
| 15                | 19.55                     | 19.55                     | 19.55                     | 50.97                 | 50.97                 | 50.97                 | 50.97                       | 19.55                           |
| 16                | 19.47                     | 19.47                     | 19.47                     | 51.39                 | 51.39                 | 51.39                 | 51.39                       | 19.47                           |
| 17                | 19.54                     | 19.54                     | 19.54                     | 51.05                 | 51.05                 | 51.05                 | 51.05                       | 19.54                           |
| 18                | 20.35                     | 20.35                     | 20.35                     | 51.12                 | 51.12                 | 51.12                 | 51.12                       | 20.35                           |
| 19                | 19.61                     | 19.61                     | 19.61                     | 51.54                 | 51.54                 | 51.54                 | 51.54                       | 19.61                           |
| 20                | 19.80                     | 19.80                     | 19.80                     | 51.35                 | 51.35                 | 51.35                 | 51.35                       | 19.80                           |
| 21                | 19.52                     | 19.52                     | 19.52                     | 51.17                 | 51.17                 | 51.17                 | 51.17                       | 19.52                           |
| 22                | 20.14                     | 20.14                     | 20.14                     | 50.75                 | 50.75                 | 50.75                 | 50.75                       | 20.14                           |
| 23                | 19.58                     | 19.58                     | 19.58                     | 51.20                 | 51.20                 | 51.20                 | 51.20                       | 19.58                           |
| 24                | 19.52                     | 19.52                     | 19.52                     | 51.17                 | 51.17                 | 51.17                 | 51.17                       | 19.52                           |
| 25                | 18.36                     | 18.36                     | 18.36                     | 50.17                 | 50.17                 | 50.17                 | 50.17                       | 18.36                           |

|                |              |              |              |              |              |              |              |              |
|----------------|--------------|--------------|--------------|--------------|--------------|--------------|--------------|--------------|
| 26             | 19.90        | 19.90        | 19.90        | 50.86        | 50.86        | 50.86        | 50.86        | 19.90        |
| 27             | 19.85        | 19.85        | 19.85        | 51.30        | 51.30        | 51.30        | 51.30        | 19.85        |
| 28             | 19.74        | 19.74        | 19.74        | 51.03        | 51.03        | 51.03        | 51.03        | 19.74        |
| 29             | 19.78        | 19.78        | 19.78        | 51.09        | 51.09        | 51.09        | 51.09        | 19.78        |
| 30             | 20.55        | 20.55        | 20.55        | 51.28        | 51.28        | 51.28        | 51.28        | 20.55        |
| 31             | 19.73        | 19.73        | 19.73        | 51.06        | 51.06        | 51.06        | 51.06        | 19.73        |
| 32             | 19.87        | 19.87        | 19.87        | 51.45        | 51.45        | 51.45        | 51.45        | 19.87        |
| 33             | 19.88        | 19.88        | 19.88        | 50.69        | 50.69        | 50.69        | 50.69        | 19.88        |
| 34             | 19.82        | 19.82        | 19.82        | 51.10        | 51.10        | 51.10        | 51.10        | 19.82        |
| 35             | 19.58        | 19.58        | 19.58        | 51.02        | 51.02        | 51.02        | 51.02        | 19.58        |
| 36             | 19.84        | 19.84        | 19.84        | 50.77        | 50.77        | 50.77        | 50.77        | 19.84        |
| 37             | 19.76        | 19.76        | 19.76        | 50.85        | 50.85        | 50.85        | 50.85        | 19.76        |
| 38             | 20.29        | 20.29        | 20.29        | 50.80        | 50.80        | 50.80        | 50.80        | 20.29        |
| 39             | 19.63        | 19.63        | 19.63        | 51.21        | 51.21        | 51.21        | 51.21        | 19.63        |
| 40             | 19.70        | 19.70        | 19.70        | 51.35        | 51.35        | 51.35        | 51.35        | 19.70        |
| 41             | 20.62        | 20.62        | 20.62        | 50.97        | 50.97        | 50.97        | 50.97        | 20.62        |
| 42             | 19.83        | 19.83        | 19.83        | 50.86        | 50.86        | 50.86        | 50.86        | 19.83        |
| 43             | 19.71        | 19.71        | 19.71        | 51.01        | 51.01        | 51.01        | 51.01        | 19.71        |
| 44             | 19.90        | 19.90        | 19.90        | 50.91        | 50.91        | 50.91        | 50.91        | 19.90        |
| 45             | 19.80        | 19.80        | 19.80        | 51.12        | 51.12        | 51.12        | 51.12        | 19.80        |
| <b>Mean</b>    | <b>19.82</b> | <b>19.82</b> | <b>19.82</b> | <b>51.07</b> | <b>51.07</b> | <b>51.07</b> | <b>51.07</b> | <b>19.82</b> |
| <b>Std Dev</b> | <b>0.37</b>  | <b>0.37</b>  | <b>0.37</b>  | <b>0.24</b>  | <b>0.24</b>  | <b>0.24</b>  | <b>0.24</b>  | <b>0.37</b>  |



## Appendix – C

### Appendix C1 Excel Results for Skin Strength and Modulus Normalisation

| Temperature °C | Flexural Strength MPa | Normalised Data |
|----------------|-----------------------|-----------------|
| 21             | 217.84                | 1               |
| 35             | 220.39                | 1.0114          |
| 50             | 171.35                | 0.787           |
| 65             | 159.29                | 0.731           |
| 80             | 145.17                | 0.666           |
| 100            | 111.08                | 0.51            |
| 120            | 88.47                 | 0.406           |
| 150            | 86.72                 | 0.398           |
| 180            | 112.34                | 0.515           |

| Temperature °C | Flexural Modulus MPa | Normalised Data |
|----------------|----------------------|-----------------|
| 21             | 14285.4              | 1               |
| 35             | 14648.8              | 1.025           |
| 50             | 14282.2              | 0.999           |
| 65             | 14474.6              | 1.0132          |
| 80             | 14129.8              | 0.9891          |
| 100            | 12919                | 0.9043          |
| 120            | 11777.6              | 0.8245          |
| 150            | 12447.8              | 0.8714          |
| 180            | 13828.31             | 0.9680          |

## Appendix C2 Excel results for the Core Strength and the Modulus

| <b>Temperature °C</b> | <b>Flexural Modulus<br/>MPa</b> | <b>Normalised Data</b> | <b>Flexural Strength</b> |
|-----------------------|---------------------------------|------------------------|--------------------------|
| 21                    | 1330                            | 1                      | 14.32                    |
| 35                    | 1310.51                         | 0.985                  | 14.110                   |
| 50                    | 1298.268                        | 0.976                  | 13.978                   |
| 65                    | 1202.671                        | 0.904                  | 12.949                   |
| 80                    | 1045.56                         | 0.786                  | 11.258                   |
| 100                   | 778.167                         | 0.585                  | 8.378                    |
| 120                   | 492.045                         | 0.370                  | 5.298                    |
| 150                   | 141.019                         | 0.106                  | 1.518                    |
| 180                   | 39.13                           | 0.029                  | 0.421                    |